INFORMATION TO USERS

This manuscript has been reproduced from the microfilm master. UMI films the text directly from the original or copy submitted. Thus, some thesis and dissertation copies are in typewriter face, while others may be from any type of computer printer.

The quality of this reproduction is dependent upon the quality of the copy submitted. Broken or indistinct print, colored or poor quality illustrations and photographs, print bleedthrough, substandard margins, and improper alignment can adversely affect reproduction.

In the unlikely event that the author did not send UMI a complete manuscript and there are missing pages, these will be noted. Also, if unauthorized copyright material had to be removed, a note will indicate the deletion.

Oversize materials (e.g., maps, drawings, charts) are reproduced by sectioning the original, beginning at the upper left-hand corner and continuing from left to right in equal sections with small overlaps. Each original is also photographed in one exposure and is included in reduced form at the back of the book.

Photographs included in the original manuscript have been reproduced xerographically in this copy. Higher quality 6" x 9" black and white photographic prints are available for any photographs or illustrations appearing in this copy for an additional charge. Contact UMI directly to order.

UMI

A Bell & Howell Information Company
300 North Zeeb Road, Ann Arbor MI 48106-1346 USA
313/761-4700 800/521-0600

Multiple quantum magic-angle spinning NMR with cross-polarization: Spectral editing of high-resolution spectra of half-integer quadrupolar nuclei

by

David Patrick Lang

A dissertation submitted to the graduate faculty

in partial fulfillment of the requirements for the degree of

DOCTOR OF PHILOSOPHY

Major: Physical Chemistry

Major Professors: Dr. Bernard C. Gerstein and Dr. Robert A. Jacobson

Iowa State University

Ames, Iowa

1998

Graduate College
Iowa State University

This is to certify that the Doctoral dissertation of

David Patrick Lang

has met the dissertation requirements of Iowa State University

Signature was redacted for privacy.

Committee Member

Signature was redacted for privacy.

Committee Member

Signature was redacted for privacy.

Committee Member

Signature was redacted for privacy.

Committee Member

Signature was redacted for privacy.

Co-major Professor

Signature was redacted for privacy.

Co-major Professor

Signature was redacted for privacy.

For the Major Program

Signature was redacted for privacy.

For the Graduate College

TABLE OF CONTENTS

GENERAL INTRODUCTION 1
Cross Polarization to Quadrupolar Nuclei from Spin-1/2 Nuclei 6
Dissertation Organization 7

CHAPTER 1. SPIN INTERACTIONS AND AVERAGING TECHNIQUES 9
The External Interactions 10
The Chemical Shift Interaction 12
The Dipole-Dipole Interaction 15
The Quadrupolar Interaction 17
The Scalar Interaction 18
Magic-Angle Spinning (MAS) 19
Radio-Frequency Decoupling 21

CHAPTER 2. CROSS-POLARIZATION MAGIC-ANGLE SPINNING (CP/MAS) OF HALF-INTEGER QUADRUPOLAR NUCLEI 22
The Cross-Polarization Experiment 23
Cross-Polarization under Sample Rotation 26
Cross-Polarization of Quadrupolar Nuclei 28
Conclusions 32

CHAPTER 3. COHERENCE AND THE EXISTENCE OF MULTIPLE-QUANTUM COHERENCES 34
Coherence and Multiple-Quantum Coherences 34
Selection Rule of NMR 37
Phase Cycling Procedures in Multiple Pulse NMR Spectroscopy 38
Selection of Coherence Pathways Using Phase Cycling 39

CHAPTER 4. MULTIPLE QUANTUM MAGIC-ANGLE SPINNING NMR (MQMAS) 48
The MQMAS Experiment 49
Optimizing the Multiple-Quantum Experiment 58
Excitation of 3Q Coherences 61
Evolution of the Coherences 63
Conversion and Observation of Multiple-Quantum Coherences 64
Experimental Results 66
Pure Absorption Mode Spectrum in 2D NMR 68
Shearing and Extracting the Isotropic Information from the MQMAS Spectrum 73
Conclusions 78

CHAPTER 5. MULTIPLE-QUANTUM MAGIC-ANGLE SPINNING NMR WITH CROSS POLARIZATION: SPECTRAL EDITING OF HIGH-RESOLUTION SPECTRA OF QUADRUPOLAR NUCLEI 79

Abstract 79
Short Communication 80
Acknowledgements 85
References 85

CHAPTER 6. $^{27}Al\{^{1}H\}$ CROSS POLARIZATION TRIPLE-QUANTUM MAGIC-ANGLE SPINNING NMR 91

Abstract 91
Introduction 92
The High-Resolution MQMAS Experiment 93
The CP MQMAS Experiment 95
Experimental 98
Results and Discussion 99
Conclusions 102
Acknowledgements 102
References 102

GENERAL CONCLUSIONS 111

REFERENCES CITED 114

ACKNOWLEDGEMENTS 120

ABSTRACT

An experiment is presented that combines the techniques of multiple-quantum magic-angle spinning (MQMAS) and cross-polarization (CP) between spin-1/2 and half-integer quadrupolar spin nuclei. This technique, referred to as CP MQMAS, allows the coordination of the spin-1/2 nuclei within a quadrupole system to be determined, which demonstrates its usefulness for spectral editing. The radio-frequency (rf) pulse sequences and necessary phase-cycling are developed and examined. A novel approach of incorporating a 'z-filter' between the two techniques allowed us to optimize our new procedure, CP MQMAS, as two unique experiments prior to their coupling. Experimental details concerning the manipulations necessary to produce and detect multiple-quantum (MQ) NMR spectra of half-integer quadrupole nuclei are presented. Additionally, the spin dynamics of CP from a spin-1/2 nucleus to the central transition of a quadrupolar nucleus during magic-angle spinning (MAS) are examined. For quadrupolar systems the CP process operates most efficiently using very low rf field strengths, which is markedly different than that used in conventional CP between spin-1/2 nuclei. When low rf field strengths are used, no longer can the Hamiltonians from the second-order quadrupolar interaction, MAS speed and carrier frequency(s) offset be treated as negligible. Finally, as the MQMAS technique requires very high rf field strengths, and CP very low rf field strengths, it can be seen that the CP MQMAS technique demands high-quality linear power amplifiers.

As a preliminary test of the CP MQMAS experiment, we chose $^{19}F \rightarrow {}^{27}Al$ cross-polarization in a fluorinated triclinic, chabazite-like $AlPO_4$ aluminophosphate sample. This

material contains three equally populated crystallographic sites for aluminum: one site octahedrally coordinated to four oxygen and two fluorine atoms, and two sites that are tetrahedrally coordinated as AlO_4. The results displayed that while all three aluminum environments were resolved in the MQMAS experiment, only that Al coordinated to the fluorine atoms was resolved in the CP MQMAS experiment.

Our second CP MQMAS experiment was accomplished using $^{1}H \rightarrow {}^{27}Al$ cross-polarization to the study of a calcined and fully rehydrated $AlPO_4$-11 aluminophosphate sample. This is a much more complicated system as it involves five unique aluminum environments that can only be resolved if MQMAS NMR is employed. The application of the CP MQMAS technique allows one to determine the positions of the water molecules within the $AlPO_4$-11 framework.

GENERAL INTRODUCTION

Nuclear Magnetic Resonance (NMR) is the resonant absorption of energy by a nucleus with a magnetic moment in a magnetic field, B_0 (1). The resolving power and site specificity inherent in NMR spectroscopy have made it a powerful analytic technique for use in physics, chemistry, biology, material sciences and medicine. Using NMR one hopes to obtain a detailed knowledge of the structure of a nucleus' Hamiltonian thereby being able to determine its physical and chemical environment. While both solid and liquid systems can be studied using this technique, a key concern is always resolution. How well separated and how narrow can the resonances be made? If a spectrum cannot be well-resolved, then the information from the various internal interactions has not been separated and the understanding of the system is incomplete.

High-resolution is a common feature in the NMR spectra of liquid samples. This is a result of "rapid" molecular tumbling which leads to motional averaging of the anisotropic internal interactions. The principal anisotropic (orientation dependent) internal spin interactions are the chemical shift, dipole-dipole coupling, spin-spin scalar (or J) coupling, electric quadrupole coupling and interaction with unpaired electrons, all of which transform as tensors under rotation (2-4). In liquids, rapid molecular reorientation allows the spin systems to sample all possible positions on a sufficiently short time scale that only the average, or isotropic value, of each of the internal interactions is revealed in the NMR spectrum. In most solids, however, molecular tumbling is anisotropic, and generally not fast enough to average

the anisotropic spin interactions. The result is that nuclear resonances in solids are usually relatively broad and featureless.

Since most solids exhibit relatively broad spectral lines, much effort over the last 35 years has focused on developing ways to average the anisotropic broadening artificially, either by manipulating the space of the nuclear spins or the overall coordinate space of the sample. Presently, using techniques like magic-angle spinning (MAS), rf decoupling, cross-polarization (CP), and multi-pulse excitation schemes, one can obtain highly-resolved spectra of spin-1/2 nuclei in solids (1,3-9).

Of the nearly 120 atomic nuclei which are magnetically NMR active, over seventy percent are quadrupolar ($S > 1/2$) (1). In addition to the anisotropic interactions present in spin-1/2 nuclei, these nuclei also possess a quadrupole moment. The quadrupolar interaction can be thought of as arising from the coupling of the nonspherical charge distribution in a nucleus with the electric field gradients (EFG) produced by its surrounding electrons (2,10). Quadrupolar broadening can be orders of magnitude greater than that of the other internal interactions.

All of the experimental techniques for contending with anisotropic broadening are based in time-dependent perturbation theory or coherent averaging theory (3,11). The first-order expansion of all these anisotropic interactions expresses their perturbative influence upon a system as a function of both their orientation relative to the static magnetic field, B_0, and the energy (or magnitude) of the interaction, i.e., ω_λ where λ represents a particular interaction. In NMR, we generally consider the splitting of the energy levels via the Zeeman interaction ($H_z = \omega_0 S_z$ where S_z is the spin angular momentum) to be dominant and the

other interactions to act as perturbations upon its eigenstates (1,2,4,9,12). Thus, $\omega_0 > \omega_\lambda$, where ω_0 is referred to as the Larmor frequency of a nucleus precessing in a static magnetic field, B_0. As the anisotropic broadenings of all of the internal interactions other than quadrupolar are relatively small compared to the Zeeman splitting, their perturbative influence can usually be suppressed by treating only their first-order effects. This can be accomplished by manipulating the spatial and/or spin components of an interaction's Hamiltonian.

The broadening due to the quadrupolar interaction is such that its influence must be addressed to at least second-order even in the most favorable cases. In the least favorable cases, the use of perturbation theory is not sufficient, and one must diagonalize the entire Hamiltonian. The second-order perturbative expansion has dependence upon two unique spatial components, $P_2(\cos\beta)$ and $P_4(\cos\beta)$, simultaneously, which means that two degrees of freedom will be necessary to average it. For half-integer quadrupolar nuclei, however, the substantial first-order quadrupolar effects can be avoided if only the central transition, $+1/2 \leftrightarrow -1/2$, is observed (2,10). Although the second-order effects are 10^2 or 10^3 times smaller, their influence can still broaden a spectrum by several tens of kilohertz. Although magic-angle spinning, or rotation of the sample about other angles, can scale the second-order quadrupolar effects (SOQE) (12-14), their bi-spatial dependence makes averaging by rotation about a single axis impossible (14-16). As no techniques existed for complete averaging of the SOQE, experiments were developed only for systems having negligible quadrupolar interaction. In these experiments, the values of the chemical shift, σ, asymmetry parameter, η, and quadrupolar frequency, ν_Q, are extracted from the spectrum as a function of its width and

lineshape versus the spinning speed, ν_{rot}, spinning angle, β, and the rf power (17,18). The accuracy of these values can then be checked by using them to help simulate the observed lineshapes (19).

Several other strategies were also developed for improving the resolution of quadrupolar NMR spectra. These include static and MAS two-dimensional nutation experiments (20-23) that utilize the correlation between the quadrupolar parameters and the precession frequencies induced by rf pulses of different lengths and intensities. For moderate ν_Q values (<7 MHz), SATRAS (Satellite TRAnsition Spectroscopy) can be used to determine the quadrupole and chemical shift (24-27), or quadrupole and dipolar parameters (28). The problem of overlapping spinning sidebands in the MAS spectra of quadrupolar nuclei can be overcome using the recently proposed QPASS (Quadrupolar Phase Alternated Sideband Suppression) sequence (29). The technique of VAS (Variable Angle Spinning) can be used to reduce the width of the central transition spectra (30), however, complete narrowing cannot be obtained with this method. Finally, several MAS-based techniques were developed that allow for studies of dipolar interactions between quadrupolar and spin-1/2 nuclei. These include CP experiments (Cross Polarization) (31-33), REDOR (Rotational Echo Double Resonance) (34,35), TEDOR (Transferred Echo Double Resonance) (35,36), TRAPDOR (TRAnsfer of Populations Double Resonance) (37,38), REAPDOR (Rotational Echo Adiabatic Passage Double Resonance) (39) and DEAR (Dipolar Exchange Assisted Recoupling) (40).

Although the inability of obtaining isotropic spectra for quadrupolar systems using rotation about a single axis was known for many years, it was not until the relevant

Hamiltonians were drawn out in multi-rank formalism that solutions appeared (15,16). The fundamental concept in all second-order averaging techniques is that an additional degree of freedom needs to be brought to bear on the interaction. In the techniques of double rotation (DOR) and dynamic-angle spinning (DAS) (16,41,42) the additional degree of freedom comes from making the spinning angle, β, time dependent. This time dependence is exploited such that the evolution of the second- and fourth-order Legendre polynomial spatial terms, $P_2(\cos\beta)$ and $P_4(\cos\beta)$, cancel out. This removes the SOQE and thus allows acquisition of high-resolution isotropic NMR spectra of quadrupolar systems. Unfortunately, both the DAS and DOR techniques suffer from mechanical and experimental shortcomings that have prevented them from being widely accepted and used (13).

Most recently, Frydman et al. showed that the SOQE can be removed using a fixed rotation axis if the second degree of freedom manipulated is the spin coherence order, 'p', rather than another spatial angle (43,44). This technique is known as two-dimensional multiple-quantum magic-angle spinning (MQMAS). Normally for half-integer quadrupolar nuclei, only the $p = \pm 1$ coherence order corresponding to the $m = +1/2 \leftrightarrow -1/2$ central transition is studied. As the central transition is already devoid of first-order quadrupolar broadening due to its quadratic dependence on the S_z angular momentum (2,10,43,45), this has always seemed the logical starting point. In the MQMAS experiment, Frydman and Harwood took advantage of the fact that all of the symmetric coherence orders, $p = \pm m$, are devoid of first-order broadening effects and, more importantly, that distinct p-coherence orders evolve differently during the same time period. Thus, coherence order 'p' can be used as the necessary second degree of freedom required to void the spectra of SOQE. The

MQMAS experiment utilizes coherent mixing to remove the fourth-rank spin-dependent terms of the second-order multi-rank expansion, and couples it with MAS which removes the second-rank terms. As this technique uses MAS, it also offers the advantage that the smaller anisotropic terms, e.g., weak dipole-dipole and chemical shift anisotropies, are averaged as well. Note that multiple-quantum coherences alone cannot remove the SOQE and that simultaneous MAS is essential.

Cross Polarization to Quadrupolar Nuclei from Spin-1/2 Nuclei

The matching conditions and dynamics of cross-polarization from a spin-1/2 nucleus to the central transition (+1/2 $\leftrightarrow$ -1/2) of a half-integer quadrupolar nucleus are fairly complicated (32,33,46). No longer do the familiar conditions for efficient CP between two spin-1/2 nuclei, e.g., ^{1}H and ^{13}C, hold; namely, that the system can be treated as a fictitious spin-1/2 system, and that the matching condition is the dominant perturbation acting on the system during CP. Instead, we find out that during these CP experiments the quadrupolar splitting causes the manifold's energy levels to cross-over up to four times per rotation under MAS (32,33,46). This behavior complicates establishing and maintaining the necessary 'spin-locked' state during CP transfer. If low rf fields are used during the CP energy transfer step, however, efficient CP may be accomplished. Unfortunately, however, when low rf fields are used, no longer are they necessarily the dominant interaction. Rather, now the MAS speed, ω_{rot}, second-order quadrupole interaction, $\nu_Q^{(2)}$, and carrier frequency offset(s), $\delta_{I \text{ or } S}$, all have the possibility of being dominant or equal perturbations to the spin Hamiltonian.

In this report, we demonstrate how the combination of the CP and MQMAS techniques provides a new tool for spectral editing of half-integer quadrupolar systems. In the first paper we are able to show, for the first time, how solid-state NMR was used on a complex quadrupolar system to determine the coordination of fluorine within an $AlPO_4$ chabazite-like lattice. The second paper expands this technique to a more complicated system and shows how it was used to determine the position of water molecules within an $AlPO_4$-11 framework.

The development and theory of an experiment that combines the techniques of multiple-quantum magic-angle spinning (MQMAS) with cross-polarization (CP) will be presented. The ability to highly-resolve various quadrupolar sites within a solid sample using MQMAS and then ascertain their coordination with respect to other unique spin systems using CP, e.g., ^{1}H and ^{19}F, is a powerful addendum to the arsenal of tools available to study solids by NMR. The utility of this technique is demonstrated on two unique spin systems: (1) a fluorinated $AlPO_4$ aluminophosphate in which CP MQMAS is performed on $^{19}F \rightarrow {}^{27}Al$ nuclei, and (2) an $AlPO_4$-11 aluminophosphate where CP MQMAS is accomplished using $^{1}H \rightarrow {}^{27}Al$ nuclei.

Dissertation Organization

Two papers are included in this dissertation. The first paper, "Multiple-quantum magic-angle spinning NMR with cross-polarization: Spectral editing of high-resolution spectra of quadrupolar nuclei", appears in Volume 7 of Solid State Nuclear Magnetic Resonance on pages 327-331, 1997. The second paper, "27Al{1H} Cross Polarization Triple-Quantum

Magic Angle Spinning NMR", appears in Volume 119 of Journal of the American Chemical Society pages 6858-6862, 1997. These articles were published in collaboration with our colleagues at the Laboratoire de Dynamique et Structure des Materiaux Moleculaires in Lille, France. The papers are preceeded by a lengthy discussion on the theory and development of the technique that they present: CP MQMAS. In Chapter 1, the principal spin interactions affecting solid-state NMR, and some techniques for averaging them to their isotropic value are discussed. Chapter 2 describes the cross-polarization process and its dynamics. The technique is first explained using spin-1/2 systems and is then expanded to include quadrupolar nuclei. In Chapter 3, the concept of 'coherence' in a NMR experiment is described. The description is then expanded to show how multiple-quantum coherences can be generated, isolated and then observed in a two-dimensional (2D) NMR experiment - both mathematical and experimental results are presented. In Chapter 4, the theory of the multiple-quantum (MQ) magic-angle spinning (MAS) experiment is discussed, and an attempt is made to fully describe its optimization and processing. The two published articles follow in Chapters 5 and 6, respectively. A general conclusion is given after Chapter 6, and all of the references cited for Chapters 1-4, and the General Introduction, are listed thereafter.

It is necessary to recognize at this point that the work described here was suggested by Dr. Marek Pruski, who has been my effective Research Advisor during the course of these studies.

CHAPTER 1. SPIN INTERACTIONS AND AVERAGING TECHNIQUES

An NMR experiment involves the study of a collection of interacting nuclear spins placed within an external magnetic field, B_0. Each spin interaction, λ, can be expressed by a spin Hamiltonian, H_λ. By applying a particular spin Hamiltonian to a spin system's wave functions, the energy attributable to that interaction can be determined. The total energy of the overall spin system then is ascertained by summing the energies of the individual spin Hamiltonians present. Once the influence of all of the spin interactions is established, then a rather complete description of a nucleus' physico-chemical environment may be achieved. While numerous spin interactions exist (9), only the most prominent ones necessary to describe this study are presented. These interactions are: [1] the Zeeman and rf-field Hamiltonians, H_Z and H_{rf} respectively; [2] the chemical shift Hamiltonian, H_{CS}; [3] the dipole-dipole Hamiltonian, H_D; [4] the scalar coupling Hamiltonian, H_J; and [5] the quadrupole Hamiltonian, H_Q. In a strong magnetic field B_0, for nuclei appropriate to the present work, the Zeeman Hamiltonian is dominant. Throughout this study their hierarchy is assumed to be

$$H_Z >> H_Q >> H_{rf}, H_D >> H_{CS} >> H_J. \qquad [1.1]$$

The energies measured in NMR are due to interaction between nuclear spin operators, or between a nuclear spin operator and a magnetic field. The general expression for a Hamiltonian is (3,4):

$$H_\lambda = C\ \vec{I}\cdot\hat{T}\cdot\vec{S} \qquad [1.2]$$

where C is a constant specific to each interaction, $\vec{I}$ and $\vec{S}$ are vector operators and $\hat{T}$ is a second-rank tensor containing the orientational dependence of the interaction between the two operators. Hamiltonians H_Z and H_{rf} correspond to the interaction between the nuclear spin system and a static or oscillating (rf) magnetic field, respectively. These two interactions are external, or experimentally-supplied, while all of the other interactions are internal. H_Q and H_{CS} correspond to interactions of the nuclear spin system with its surrounding electrical environment. Interactions between nuclear spins either through-space or through the bonding electrons are expressed in the H_D and H_J Hamiltonians, respectively. A number of treatises and textbooks do an excellent and extensive job of describing the theory and phenomena of NMR couplings (1-4,9,47,48). We shall therefore only briefly describe those interactions listed above

The External Interactions

The Zeeman interaction is the coupling of a nuclear spin's angular momentum with an external magnetic field, B_0. Throughout this report, this will always be considered the dominant interaction with the effects of the other couplings being treated as perturbations upon the Zeeman states (1,2,4,9,12). With the magnetic field to lie along the z-axis of the laboratory frame, the Zeeman Hamiltonian is

$$H_Z = -\gamma_I I_Z B_0 . \qquad [1.3]$$

In this equation, $-\gamma_I I_Z$ represents the quantized spin angular momentum of the nucleus in the presence of the external magnetic field, B_0. Precession of the spin angular momentum about

the z-axis is referred to as the Larmor frequency, $\omega_0 = \gamma_I B_0$. With the Hamiltonian expressed in units of angular frequency, $2\pi\nu = \omega$, Eq. [1.3] can be reduced to

$$H_Z = -\omega_0 I_Z. \qquad [1.4]$$

The excitation of a spin system can be accomplished using a pulse of rf energy applied in a direction perpendicular to B_0. An rf pulse involves applying a time-dependent magnetic field to the sample that is oscillating with an rf frequency, ω_{rf}, sufficiently close to the Larmor frequency of the nuclei under investigation, placing it within the bandwidth of excitation (1). The oscillating rf field couples with the nuclear spin interactions and creates a transverse magnetization component whose relaxation process, free-induction decay (FID), can then be monitored. The rf field strength, $B_1(t)$, and Hamiltonian describing such an rf interaction are (48)

$$B_1(t) = 2B_1 \cos(\omega_{rf} t + \varphi) \qquad [1.5]$$

and

$$H_{rf} = -2\gamma_I B_1 \cos(\omega_{rf} t + \varphi) \cdot I_x, \qquad [1.6]$$

respectively, for a pulse applied along the x-axis with phase φ and frequency ω_{rf}. This time-dependent Hamiltonian, coupled with the time-independent Zeeman Hamiltonian yields an overall external interaction Hamiltonian of the form:

$$H = H_Z + H_{rf} = \omega_0 I_z + 2\omega_1 \cos(\omega_{rf} t + \varphi) \cdot I_x \qquad [1.7]$$

where $\omega_1 = -\gamma_I B_1$.

By transforming into an interaction frame that is rotating about the z-axis with frequency ω_{rf}, the time-dependence of the rf Hamiltonian is reduced (1,49). Transformation

into this "rotating frame", in which the rf field appears on resonance, is accomplished using the exponential operator $U_{rf} = \exp(-i I_z \omega_{rf} t)$. The effect this transformation has upon both the spin operator I_x and the overall Hamiltonian is (1,49)

$$H_{rot} = U_{rf}^{-1} H U_{rf} - i U_{rf}^{-1} \frac{dU_{rf}}{dt} \qquad [1.8]$$

therefore

$$\begin{aligned} H_{rot} &= (\omega_0 - \omega_{rf}) I_z + 2\omega_1 \cos(\omega_{rf} t + \varphi) \cdot U^{-1} I_x U \\ &= (\omega_0 - \omega_{rf}) I_z + \omega_1 (I_x \cos\varphi + I_y \sin\varphi) \\ &\quad + \omega_1 [I_x \cos(2\omega_{rf} t + \varphi) - I_y \sin(2\omega_{rf} t + \varphi)] . \end{aligned} \qquad [1.9]$$

The component of H_{rot} remaining time-dependent after transformation can be neglected since its rapid oscillation, $2\omega_{rf}$, tends to average its effect to zero (48). Thus, the overall external, time-independent Hamiltonian can be expressed as

$$H_{rot} = (\omega_0 - \omega_{rf}) I_z + \omega_1 (I_x \cos\varphi + I_y \sin\varphi) . \qquad [1.10]$$

The Chemical Shift Interaction

The chemical shift results from the coupling of a nuclear spin with the induced local magnetic field generated by the electrons that surround it. Under the influence of B_0, the electron cloud's angular momentum is modified and creates an additional magnetic field that couples with the nuclear spin moment. This secondary magnetic field, while proportional to B_0, is opposed to it, and thus tends to reduce the effects of B_0 upon the nucleus. In other words, the nucleus is "shielded" from the static external field by the molecular electronic cloud

about it. This shielding depends upon the chemical environment of the nucleus, and can be described as

$$H_{CS} = \gamma_I \vec{I} \cdot \hat{\sigma} \cdot \vec{B_0} \qquad [1.11]$$

where $\hat{\sigma}$ denotes the shielding tensor.

The chemical shift is an anisotropic interaction whose magnitude changes depending on the nucleus' orientation relative to B_0. These changes are reflected in the shielding tensor which can have a variety of values for its matrix elements, except when within the principal axis system (PAS) of the interaction. In the PAS, the shielding tensor is diagonal with nonzero elements, σ_{zz}, σ_{xx} and σ_{yy}. By convention, $\sigma_{zz} > \sigma_{xx} > \sigma_{yy}$. The dominant secular interaction, which corresponds with the magnitude of that component of the shielding tensor that lies parallel to B_0 (commutes with I_z or S_z), is most significant. Using polar angles θ and ϕ to define the orientation of the external magnetic field within the PAS of the chemical shift tensor as depicted in Figure 1.1, the secular component of the PAS is related to the σ_{ZZ} component of the laboratory frame by the transformation

$$\sigma_{ZZ} = \sigma_{iso} + \sigma_{zz}\left[1/2\left(3\cos^2\theta - 1\right) + 1/2\left(\eta \sin^2\theta \cos 2\phi\right)\right] \qquad [1.12]$$

where η is the asymmetry parameter (deviation from cylindrical symmetry)

$$\eta = \frac{\sigma_{xx} - \sigma_{yy}}{\sigma_{zz}} \qquad [1.13]$$

and σ_{iso} is the isotropic value of the shielding tensor

$$\sigma_{iso} = \frac{1}{3}\left(\sigma_{xx} + \sigma_{yy} + \sigma_{zz}\right). \qquad [1.14]$$

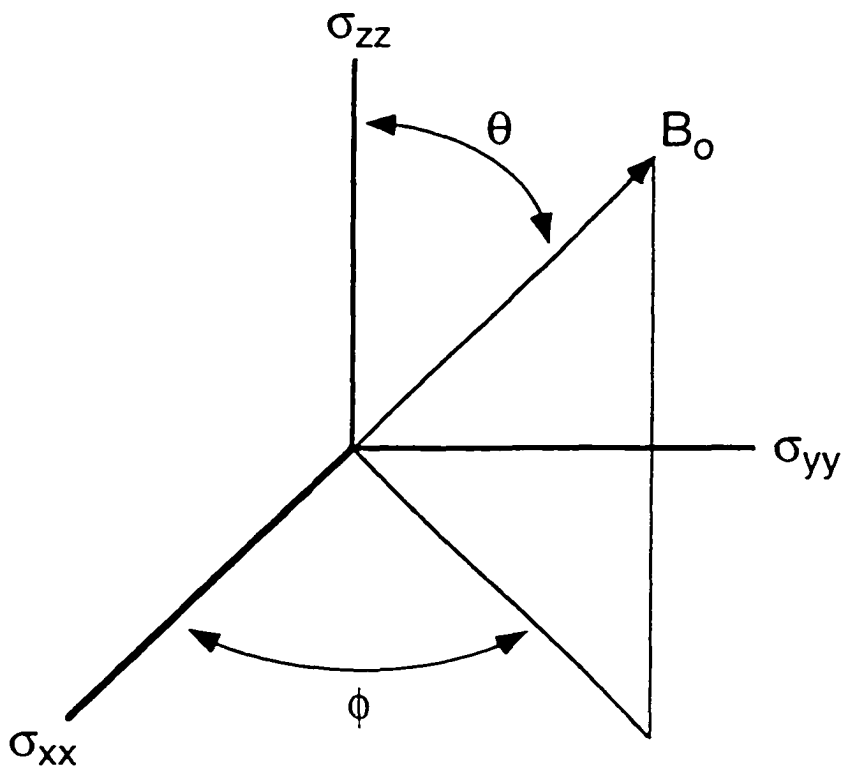

Figure 1.1: Coordinates of the external field as viewed in the principal axis system (PAS) of the chemical shift, or any other, internal spin interaction.

In liquid-state NMR of half-integer nuclei, the isotropic component of the chemical shift is the dominant internal interaction displayed in the spectrum. The anisotropic components of the dipolar (vide infra) and shielding interactions are averaged to their isotropic values by "rapid" molecular tumbling, which allows a nucleus to experience all possible orientations on a short time scale relative to the chemical shift anisotropy (CSA) and dipolar couplings. In solid-state NMR, however, where the orientation of the nuclei is fixed within the lattice, no complete averaging of this anisotropy usually occurs, naturally. Thus, the NMR spectrum will display a broad powder pattern reflecting all of the various nucleus orientations.

The Dipole-Dipole Interaction

The dipole-dipole interaction results from the classical through-space coupling of a nuclear magnetic moment with other nuclear magnetic moments. These couplings establish additional local fields at the nucleus in question. Its magnitude depends primarily on the internuclear distance, r_{IS}, between the coupled spins, but its influence on the NMR spectrum also depends on the orientation of this internuclear vector with respect to B_0. The Hamiltonian for a two spin, I and S, dipolar-coupled system can be expressed as

$$H_D^{IS} = 2\gamma_I\gamma_S\hbar\ \vec{I}\cdot\hat{D}\cdot\vec{S} \qquad [1.15]$$

where $\hat{D}$ is the dipolar coupling tensor. This interaction is anisotropic. The tensor is traceless, with principal values of $1/r_{IS}^3$, $-1/2\,r_{IS}^3$, and $-1/2\,r_{IS}^3$ within its PAS.

For a homonuclear dipole coupled system, the secular part of the dipolar Hamiltonian can be written as

$$H_D^{IS} = \frac{\gamma_I \gamma_S \hbar}{r_{IS}^3} \frac{1}{2}\left(3\cos^2\theta - 1\right)\left[\underbrace{2I_z S_z}_{\text{static}} - \frac{1}{2}\underbrace{\left(I_+ S_- + I_- S_+\right)}_{\text{flip-flop}}\right]. \qquad [1.16]$$

In this equation, θ corresponds to the angle that the internuclear vector connecting the two spins makes with respect to the magnetic field B_0. The "static" spin term corresponds to the interaction between the component of each nuclear spin that aligns with the z-axis, B_0. This dipolar contribution adds to or subtracts from the magnitude of the external field felt at the nucleus, thereby affecting its local precession frequency. The "flip-flop" spin term represents the interaction occurring between the transverse magnetization components of the two spin system. This interaction affects the reorientation of the nuclear spin when the two angular frequencies are sufficiently close, which is a condition that can only be readily met when the system is homonuclear. Since each nucleus will establish its own rotating field within B_0, the energy exchange occurring via flip-flop can only be effective when it is conserved, e.g., when it commutes with H_Z (1,48).

The secular component of the interaction Hamiltonian for a heteronuclear dipole coupled spin system takes the form

$$H_D^{IS} = \frac{\gamma_I \gamma_S \hbar}{r_{IS}^3} \left(3\cos^2\theta - 1\right) I_z S_z. \qquad [1.17]$$

This is completely analogous to the homonuclear dipolar Hamiltonian, however, no longer does the flip-flop term commute with I_z. The difference in the Larmor frequency of two

unique spins, e.g. I and S, is usually much greater than the frequency of the dipolar interaction H_D^{IS}, therefore, the possibility of an energy conserving exchange occurring is negligible.

The Quadrupolar Interaction

The quadrupole interaction may be thought of as arising from the coupling of the nonspherical charge distribution in a nucleus with the electric field gradient (EFG) of its surrounding charges (1-4,9,10). Only nuclei with a spin number greater than 1/2 possess a quadrupole moment. This, however, accounts for over 70% of all magnetically active nuclei. For quadrupolar nuclei in which $\omega_0 > \omega_Q > \omega_1$, perturbation theory may still be applied, but first-order effects can be several megahertz (MHz), and it is generally necessary to carry the calculation to second-order. The second-order quadrupolar effects (SOQE) are responsible for broadening the central, +1/2 $\leftrightarrow$ -1/2, transition, the removal of which is the subject of the current work.

For half-integer quadrupole nuclei, the central transition (+1/2 $\leftrightarrow$ -1/2) does not undergo first-order broadening due to its quadratic dependence on the S_z angular momentum (2,10,43). The Hamiltonian can be expressed as

$$H_Q^{(1)} = \omega_Q^{(1)}(\theta,\phi)\left[3\,S_z^2 - S(S+1)\right]. \qquad [1.18]$$

In this equation, $\omega_Q^{(1)}(\theta,\phi)$ is the first-order quadrupolar frequency and has dependence upon the nuclear quadrupole coupling constant, the asymmetry parameter of the EFG, and the orientation of the magnetic field B_0 within the PAS of the quadrupolar tensor, (θ,ϕ). Even with the first-order Hamiltonian's effects truncated, however, the central transition can still be

tens of kHz wide due to the SOQE. While the first-order interactions are purely anisotropic, the SOQE have bi-spatial dependence and contain both isotropic and anisotropic components. The angular frequency of this effect can be expressed in the multirank formalism to be discussed later as

$$\omega_Q^{(2)} = \underbrace{\omega_Q^{(2)}}_{\text{isotropic}} + \underbrace{\omega_{Q,2}^{(2)} P_2(\cos\beta) + \omega_{Q,4}^{(2)} P_4(\cos\beta)}_{\text{anisotropic}} \qquad [1.19]$$

The isotropic component is inversely proportional to B_0 and introduces a quadrupole induced shift (QIS) into the spectrum. Thus the observed frequency of the transition is due both to the isotropic chemical shift and the second-order quadrupole shift. Because of the bi-spatial dependence of the SOQE, any averaging technique of the anisotropic component would require manipulation by two independent degrees of freedom, either simultaneously or in succession. Three such techniques have been developed, DOR (16), DAS (41), and MQMAS (43,44) and will be presented more fully later within this report.

The Scalar Interaction

The scalar interaction involves the indirect coupling of nuclear spins via the electrons they share in an intervening chemical bond. The Hamiltonian for the scalar interaction can be expressed as

$$H_J = \vec{I} \cdot \hat{J} \cdot \vec{S} \qquad [1.20]$$

where $\hat{J}$ is the scalar coupling constant. This "through-bond" interaction is orders of magnitude smaller than the through-space coupling of the dipole-dipole interaction which it

mirrors. In contrast to the dipolar couplings, however, the isotropic value of the scalar interaction is not zero. As the anisotropic component of the dipolar interaction will eclipse those of the scalar interaction, usually the only component of the scalar coupling that can be extracted from an NMR spectrum is the isotropic one. This scalar interaction is usually too small to be distinguished in solid-state NMR where the dipolar couplings dominate, however, in liquid-state NMR it allows a distinction of modes of bonding to be determined that are not revealed by chemical shifts alone (1,48,50).

Magic-Angle Spinning (MAS)

Magic-angle spinning (MAS) is an averaging technique used to suppress the anisotropic interactions of the internal Hamiltonians (5,51). This process involves the "rapid" rotation of a sample about an axis inclined at the "magic angle" relative to B_0 such that the angular dependent component of an anisotropic interaction becomes time-dependent, and may be partially or fully removed from observation. All of the internal interactions, H_Q, H_D, H_{CS}, and H_J, contain to first-order an anisotropic component having similar angular dependence. Haeberlen showed that this similarity could be conveniently expressed by breaking down each interaction in terms of its irreducible tensor operators (3,5)

$$H_\lambda = C^\lambda \sum_{l} \sum_{m=-l}^{+l} (-1)^m R^\lambda_{l,-m} T^\lambda_{l,m} \qquad [1.21]$$

where C^λ consists of constants pertinent to a specific λ interaction, the $R^\lambda_{l,-m}$ terms are angular functions in coordinate space, and the $T^\lambda_{l,m}$ terms describe spin products. The

transformation from an anisotropic interaction's PAS into the laboratory frame is accomplished using Wigner rotation matrices (52), $D^{l}_{m',m}(\alpha, \theta, \gamma)$ and $D^{l}_{m,n}(0, \beta, \omega_r t)$, respectively. In the first matrix, α, θ, and γ are the Euler angles that bring the PAS frame of the anisotropic tensor into the spinning rotor frame, while the second matrix transforms the interaction into the laboratory frame (3,5,46). The only nonzero and secular ($l = 2,\ m = 0$) rotation matrix $D^{l}_{m,n}(0, \beta, \omega_r t)$ remaining after this second transformation is (5)

$$D^{2}_{0\,0}(0, \beta, \omega_r t) = \frac{1}{2}\left(3\cos^2\beta - 1\right) \qquad [1.22]$$

where β is the angle of the rotation axis relative to the external magnetic field, B_0. This second-order Legendre polynomial is common to all of the anisotropic Hamiltonians and can be annulled by "rapidly" rotating the sample about an axis inclined at $\beta = 54.7^{\circ}$ relative to B_0. This is the so-called "magic-angle" given the title because of its apparent magical properties (53). The spinning speed required to bring about complete nullification must be greater than the anisotropic interactions that it averages. Generally, the static sample NMR linewidth is an indication of how strong the interactions are. With this anisotropy removed, high-resolution NMR spectra of solid materials can be acquired that are comparable to those obtained in liquid-state NMR experiments. While liquids average out the anisotropic interactions naturally with their rapid isotropic tumbling, in solids such an intrinsic motion is usually absent. Thus, we can try and emulate nature by imposing an angular motion upon the nuclei within the solid samples using MAS.

Radio-Frequency Decoupling

The application of rf pulses to a spin system to perturb and negate an anisotropic broadening is another common experimental technique in solid-state NMR (54). As the rf pulse is time-dependent, it causes the coupling of the nuclear spins it perturbs to become time-dependent and, therefore, fluctuate continuously. These fluctuations may be used to average the spin-dependent terms, $T_{l,m}^{\lambda}$, in Eq. [1.21] to zero. Like MAS, the frequency of the rf decoupling interaction has to be greater than that of the anisotropic interaction's frequency which it is trying to remove. For heteronuclear systems, the application of a continuous pulse to the nuclei not being observed does a sufficient job of decoupling the dipole-dipole interaction. For strong homonuclear dipolar couplings, however, complex multi-pulse sequences are needed such as WAHUHA (6), MREV-8 (55), and BR-24 (56). These sequences may then be combined with MAS to remove chemical shift anisotropy (8) in the Combined Rotation And Multiple Pulse Spectroscopy (CRAMPS) experiment (1).

CHAPTER 2. CROSS-POLARIZATION / MAGIC-ANGLE SPINNING (CP/MAS) OF HALF-INTEGER QUADRUPOLAR NUCLEI

In solids, the technique of cross-polarization (CP) utilizes the heteronuclear dipole-dipole coupling existing between two unique spin systems, e.g. I and S, as a means to transfer magnetization. When this polarization transfer is done from a system of high abundance, e.g. ^{1}H, to one of low natural abundance, e.g. ^{13}C, it (i) enhances the sensitivity of the low magnetogyric ratio nuclei thereby improving the signal-to-noise (S/N), and (ii) provides a direct inference of the connectivities between the nuclear spins, i.e., spectral editing (4,57,58). While the I-S dipolar coupling makes the CP experiment possible, anisotropic interactions as a whole tend to dominate and broaden the spectra of solids severely.

Magic-angle-spinning (MAS) is a technique in which the angular dependent part of these anisotropic interactions are manipulated via "rapid" rotation about a fixed angle such that the first-order anisotropies are completely or partially averaged. It is experimentally possible then to use CP in conjunction with MAS to obtain relatively accurate quantitative information for spin-1/2 systems, and for this reason the CP/MAS experiment has found wide application in the area of solid-state NMR (33,59). In contrast to CP between two spin-1/2 nuclei, the CP dynamics between a spin-1/2 nucleus and a half-integer quadrupole nucleus are more complex. This process was systematically analyzed recently by Vega and by Sun et al. (32,33,46) who showed that both the matching condition which allows the polarization transfer to occur and the ability to maintain spin-locking during the CP mixing time, τ_{CP}, are significantly different than those between two spin-1/2 nuclei.

In this section, a brief overview of the classical CP process and its dynamics will be presented using a fictitious spin-1/2 system in which the dipole-dipole interaction is the dominant perturbation. Next, the influence of sample rotation, MAS, upon this process will be addressed. Finally, the conditions for accomplishing efficient CP and CP/MAS between a half-integer quadrupole spin system and a spin-1/2 system will be discussed.

The Cross-Polarization Experiment

Figure 2.1 shows the standard pulse sequence used in a CP experiment (4,58). In a system where the dipole-dipole interactions dominate, the Hamiltonian of the spin system can be expressed as

$$H_{tot} = H_I + H_S + H_D^{II} + H_D^{SS} + H_D^{IS} \qquad [2.1]$$

where H_I and H_S represent the chemical shift and resonance offset terms corresponding to spin system I and S, respectively, H_D^{II} and H_D^{SS} represent homonuclear dipole-dipole coupling, and H_D^{IS} corresponds to the heteronuclear dipolar coupling.

The cross-polarization experiment begins with a 90° pulse at frequency $\omega_{0I} = \gamma_I B_0$ applied to the I spins with magnetogyric ratio γ_I thereby creating transverse magnetization, e.g., I_x and I_y. Next, the I spin magnetization is 'spin-locked' by applying a pulse with rf strength B_{1I} and which is phase shifted by 90° relative to the first pulse. Simultaneously during mixing time τ_{CP}, a pulse of rf strength B_{1S} is applied to the S spins with magnetogyric ratio γ_S. Initially, the transverse magnetization on the S spins is zero, however, if during time τ_{CP} the Hartmann-Hahn (HH) matching condition (57)

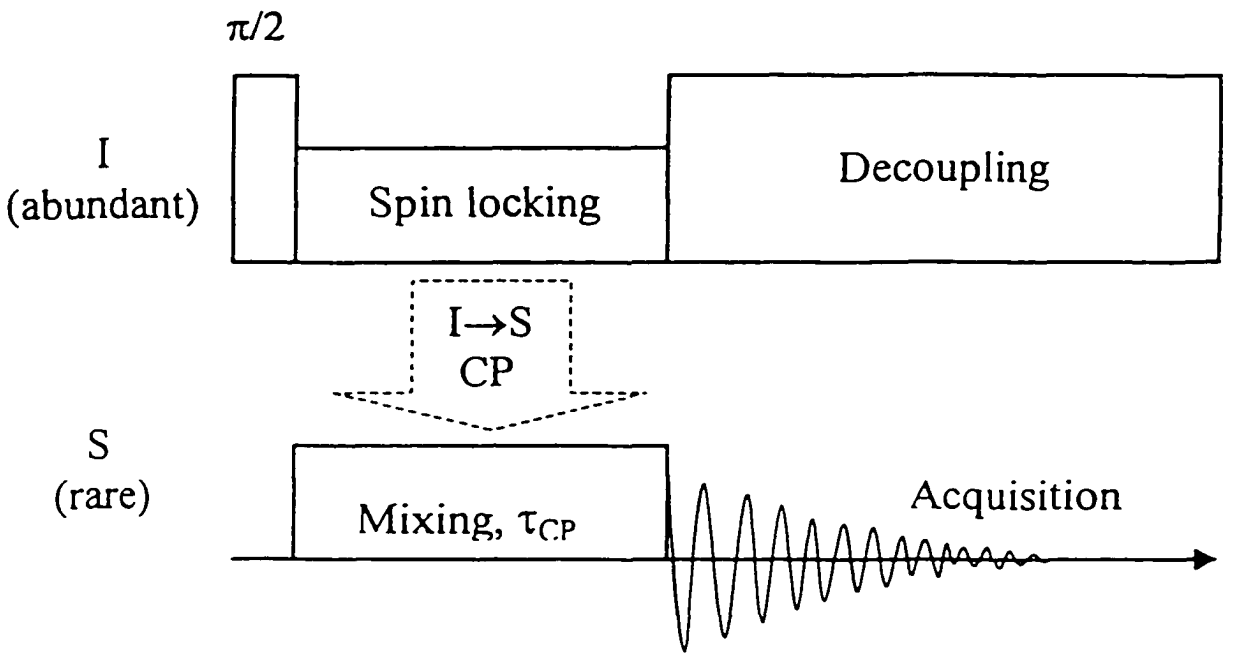

Figure 2.1: Pulse sequence for a standard cross polarization experiment. During mixing time τ_{CP}, radio-frequency irradiation occurs at the Larmor frequencies ν_{0I} and ν_{0S} for I and S spins simultaneously.

$$\omega_I = \gamma_I B_{1I} = \gamma_S B_{1S} = \omega_S \qquad [2.2]$$

is satisfied, polarization transfer between the two spin-1/2 systems can occur. Thereafter, the built-up transverse magnetization on the S spins due to CP is recorded, and, during the acquisition of the S spins free-induction decay (FID), the two spin systems are decoupled by applying continuous rf irradiation to the I spins (4,6,54).

The Hartmann-Hahn matching condition reveals that only when the angular frequency, $\omega = \gamma B$, of the two spin systems are made equal can efficient cross-polarization energy transfer occur. If these spin systems are subjected only to B_0, the difference between their Larmor frequencies, $\omega_0 = \gamma B_0$, is usually so great that there is no possibility of energy transfer from I to S. Within an experiment, however, although γ has a fixed value, the rf variables B_{1I} and B_{1S} can be manipulated in order to satisfy the Hartmann-Hahn condition. With this established, polarization transfer can occur and the benefits of the CP technique can be realized. For example, in a typical organic molecule where the ^1H to ^{13}C ratio is ~100:1 an enhancement factor of $\gamma_H/\gamma_C \sim 4$ is made to the ^{13}C (S spin) magnetization using the CP technique. This enhancement factor, along with the faster spin-lattice relaxation time, T_1, of the ^1H nuclei relative to ^{13}C nuclei, allow improvements to a spectrum's S/N of greater than 1000 to be achieved without increasing the experimental time relative to a standard ^{13}C Bloch decay experiment. Additionally, since ^{13}C nuclei are rare, the H_D^{SS} interaction is negligible, and by maintaining an rf pulse on the ^1H nuclei during the acquisition of the FID, the influence of the H_{IS} interaction is removed, too. Thus, the recorded FID only contains information regarding the system's chemical shift and the smaller second-order effects (1).

Cross-Polarization under Sample Rotation

The magnitude of the heteronuclear dipolar coupling existing between two spins, e.g., I and S, depends on (i) their internuclear distance r_{IS}, (ii) the angle of orientation ϑ_{IS} between r_{IS} and the static magnetic field B_0, and (iii) the product of their magnetogyric ratios, $\gamma_I\gamma_S$. Using polar coordinates, the secular components of the dipolar Hamiltonian can be expressed as

$$H_D^{IS} = \frac{\gamma_I\gamma_S\hbar}{r_{IS}^3}\left(3\cos^2\vartheta_{IS} - 1\right)I_zS_z . \qquad [2.3]$$

Upon rotation of the sample with angular frequency ω_{rot} at an angle β relative to the static magnetic field B_0, the angular component $\left(3\cos^2\vartheta_{IS} - 1\right)$ becomes periodically time-dependent, and can now be expressed in the laboratory frame as(97)

$$\begin{aligned}\left(3\cos^2\vartheta_{IS}(t) - 1\right) = \frac{1}{2}&\left(3\cos^2\beta - 1\right)\left(3\cos^2\theta_{IS} - 1\right)\\ &+\frac{3}{2}\sin 2\beta \sin 2\theta_{IS}\cos(\omega_{rot}\, t)\\ &+\frac{3}{2}\sin^2\beta \sin^2\theta_{IS}\cos(2\omega_{rot}\, t)\end{aligned} \qquad [2.4]$$

Figure 2.2 illustrates the coordinate frame for a rotating sample with the relevant angles and vectors shown.

If the angle of rotation β is set at 54.7° relative to B_0, the "magic angle", then the first term in Eq. [2.4] equals zero and the other two terms are modulated as a function of the frequency of angular rotation, ω_{rot}. Since the time-independent part of Eq. [2.4] is zero under magic-angle spinning (MAS), no longer does the matching condition of Eq. [2.2]

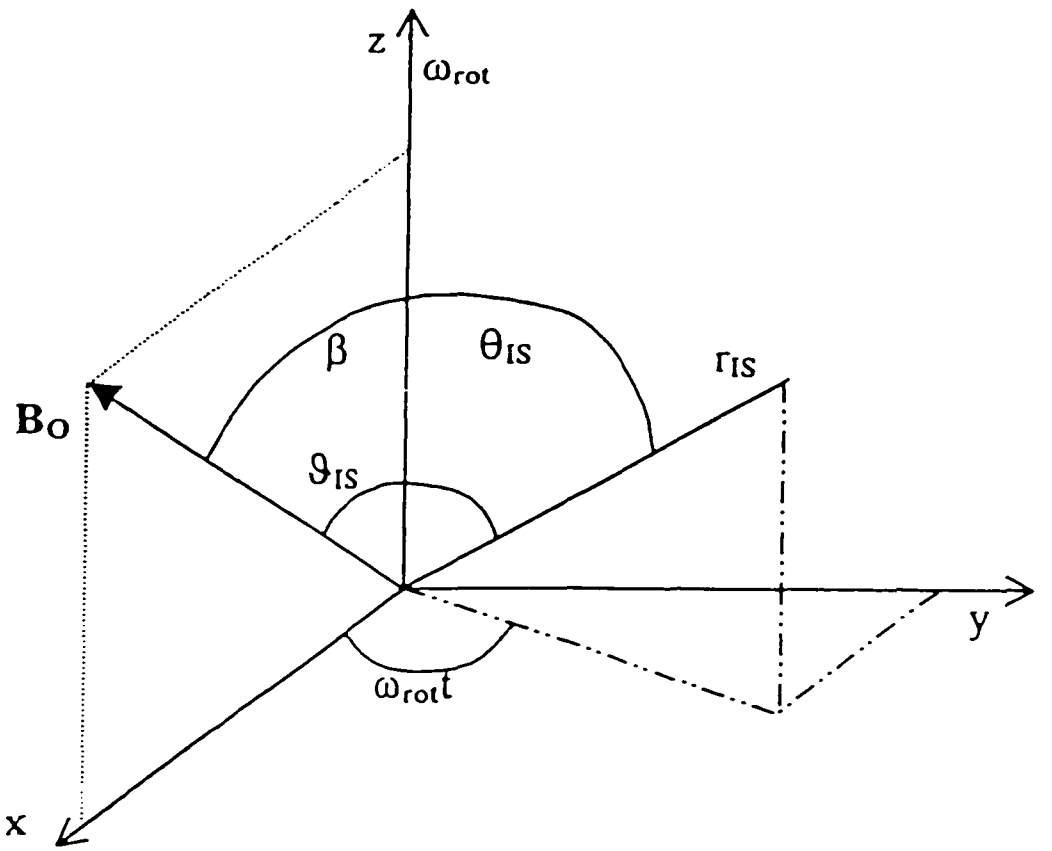

Figure 2.2: Coordinate frame of reference for a sample spinning around an axis, Z, tilted at angle β relative to B_0. The angle of vector r_{IS} is made time dependent, and the $(3\cos^2 \vartheta_{IS} - 1)$ term of Eq. [2.3] is now expressed as a function of β, θ_{IS} and $\omega_{rot}t$ (see Eq. [2.4]).

express the necessary state required for efficient cross-polarization between the spin systems. Rather, as the frequency of rotation ω_{rot} becomes comparable to that of H_D^{IS}, the matching condition will reflect its influence upon the spin systems, too. Under MAS, the best HH matching conditions are found to be close to either the first or second-order sideband frequencies (60)

$$\gamma_I B_{1I} = \gamma_S B_{1S} + n\omega_{rot}$$
$$\text{or} \qquad [2.5]$$
$$\omega_{1I} = \omega_{1S} + n\omega_{rot} \qquad n = \pm 1, \pm 2$$

Cross-Polarization of Quadrupolar Nuclei

Cross-polarization from a spin-1/2 nucleus to the central transition of a half-integer quadrupole nucleus can be accomplished using a pulse sequence analogous to that shown in Figure 1.1. Although several researchers have been successful in obtaining satisfactory CP of such systems (61-65), only recently were the theoretical and experimental aspects of the spin dynamics reported (32,33,46). These investigations revealed that significant differences exist in both the CP matching and spin-locking dynamics of quadrupolar systems versus those of spin-1/2 systems. For our discussion here, only those systems in which the quadrupolar interaction is dominant ($\omega_Q >> \omega_{1S}$ or ω_D^{IS}) will be addressed. Systems having small quadrupolar interaction, e.g. $\omega_Q << \omega_{1S}$, behave similar to the spin-1/2 systems already discussed.

The HH matching condition for CP between a spin-1/2 nucleus and the central transition of a half-integer quadrupolar nucleus in a static sample is (2,66-68)

$$\omega_{1I} = (S+1/2)\omega_{1S} = \omega_{nut}. \qquad [2.6]$$

This equation is more general than Eq. [2.2], and states that for polarization transfer to occur to a particular transition level of a quadrupole split system, ω_{1I} must be set equal to the nutation frequency ω_{nut} of that transition. If $\omega_Q >> \omega_{1S}$, no longer does the nutation behavior depend solely upon the relative magnitude of ω_{1S}, but also upon the quadrupole splitting (11,33)

$$Q^{(1)}(\theta,\phi) = \frac{1}{2}\omega_Q\left(3\cos^2\theta - 1 + \eta\sin^2\theta\cos 2\phi\right) \qquad [2.7]$$

where ω_Q is the quadrupole frequency which depends on the nuclear quadrupole coupling constant and the spin's quantum number (33,46,67,69,70). Similar to the other anisotropic interactions, the first-order quadrupole splitting is made periodically time-dependent under MAS. This dependence affects the CP process in two significant ways: [1] it severely affects the spin-locking dynamics, and [2] it rapidly modulates the interaction under which the CP transfer occurs. These effects are explained below.

Attempts at averaging the quadrupolar interaction are obscured by the fact that $Q^{(1)}(\theta,\phi,t)$ crosses through zero and changes sign two or four times per rotor cycle. Such crossover changes complicate the spin-locking dynamics and thus the efficiency of the CP experiment. What happens to a spin-locked state during and after these crossings can be classified according to the magnitude of the passage parameter, α, which is defined as (32,33,46),

$$\alpha = \omega_{1S}^2/\left(\omega_Q\omega_{rot}\right). \qquad [2.8]$$

Three distinct passage regimes exist, (i) adiabatic; $\alpha >> 1$, (ii) intermediate; $\alpha \approx 0.4$, and (iii) sudden; $\alpha << 1$. Since the magnitude of ω_Q cannot be modified within an experiment, only the speed of rotation ω_{rot}, and the rf power ω_{1S} can be manipulated in order to modify the passage parameter, α.

Efficient spin-locking can be achieved in both the adiabatic ($\alpha >> 1$) and sudden ($\alpha << 1$) passage regimes. In the adiabatic regime, high rf power and a slow spinning speed are used in order to maximize α. While a high α value provides a favorable condition for spin-locking, the slow spinning speeds required will introduce multiple spinning sidebands (SSB) into the spectrum and will not nullify the smaller anisotropic interactions effectively. The resulting spectra will therefore be poorly resolved and difficult to interpret. For this reason, operation within the adiabatic regime is avoided. In contrast to the adiabatic settings, low rf power and a high spinning speed are utilized in the sudden regime in order to minimize α (32,33,46). Higher rotation speeds improve the spacing of the SSB and the averaging of the other anisotropic interactions. However, by using lower rf power the dominance of the B_{II} or B_{1S} perturbations are potentially forfeited. In this scenario, the magnitude of the second-order quadrupole effects (SOQE), offset terms δ_I and δ_S, and MAS speed could all be comparable to the B_{II} or B_{1S} rf strength and thus their influence upon the spin-locked state must be considered. If the frequency of the SOQE is comparable to that of the spin-locking rf field, $\omega_Q^2/\omega_L \approx \omega_{1S}$, the evolution of the locked magnetization will be adversely affected. This was confirmed by numeric and experimental studies which showed that the SOQE can induce large oscillations in the spin-locked signal depending on the crystallite's orientation and

the size of α (46). The best spin-locking is maintained when ω_{1S} is greater than the SOQE and α is made sufficiently small, i.e., $\alpha \leq 0.0005$. Additionally it should be noted that since the SOQE is inversely proportional to ω_0, its influence is minimized by operating with the highest external field B_0 available. It was also found (46) that the spin-locking efficiency reduces significantly when the resonance condition $\omega_{1S} \cong \omega_{rot}$ is matched, regardless of the magnitude of α. This reduction occurs due to an increased probability of single-quantum between the central transition and the satellite transitions, e.g. $(\pm 1/2 \leftrightarrow \pm 3/2)$ which disrupts the eigenstates of the central transition thereby decaying the spin-lock condition. Since the sudden regime utilizes low rf power, this resonance condition can be avoided by keeping $\omega_{rot} > \omega_{1S}$. Finally, the influence of any possible offset effects δ are minimized by positioning the carrier frequencies close to the resonance frequencies of the two nuclei, I and S.

Similar to CP between two spin-1/2 nuclei, sample rotation modifies the matching condition for effective polarization transfer between a spin-1/2 nucleus and a half-integer quadrupolar nucleus, too. In these systems, however, both the quadrupole and dipole-dipole interactions are periodically time-dependent under MAS, and each affects the matching condition. This time dependence is most dramatic within the adiabatic regime. As the quadrupolar splitting, $Q^{(1)}(\theta,\phi,t)$, changes sign due to the sample rotation, no longer do the spin-locked eigenstates necessarily remain fixed. Rather, as the Hamiltonian of the eigenstate is modulated under rotation, it will follow the Hamiltonian through the eigenstates which is passes (2,32). Thus, the populations within the density matrix are continuously changing. Such alternations frustrate the Hartmann-Hahn matching process. The effects this alternating

populations phenomena has on the spin-locked state has been studied numerically and experimentally by Vega (32,33). As stated previously though, the poor spectral resolution that occurs in the adiabatic regime due to slow MAS makes operation here unfavorable. In contrast to the adiabatic regime, the passage of the Hamiltonian occurs so "rapidly' within the sudden regime that the eigenstates do not change. For this reason, more efficient spin-locking can be accomplished and therefore better Hartmann-Hahn matching. However, since the eigenstates remained fixed, only those nuclei located within the central transition can take part in polarization transfer. As the size of the quadrupolar interaction is strongly dependent on orientation, even establishing a well-defined Hartmann-Hahn match with these nuclei is difficult. Additionally, as the rf power is reduced to improve the matching conditions, the resonance offset frequency, δ, becomes more significant, and all properly coordinated nuclei may not undergo cross-polarization. The matching conditions within the sudden regime are similar to those in the a CP/MAS experiment condition between two spin-1/2 systems already discussed (see Eq. [2.5])

$$\omega_{1I} = \pm(S+1/2)\omega_{1S} + n\,\omega_{rot} \qquad n = \pm 1, \pm 2 \qquad [2.9]$$

Under these settings, efficient spin-locking can occur, but all of the previous rf power and sample rotation conditions need to be fulfilled, too.

Conclusions

A CP/MAS experiment involving two spin-1/2 systems is usually performed in order to improve a spectrum's S/N ratio, and to determine the connectivities between differing spins. This process, however, is more complex when one on the two spin systems involved is

a half-integer quadrupole nucleus. If the quadrupolar interaction is dominant, compared to the sizes of the rf fields, i.e., $\omega_Q >> \omega_{1S}$ or ω_{IS}^D, it strongly alters both the matching and spin-lock conditions of the CP experiment. Under MAS, the effects of these conditions can be characterized by the magnitude of the passage parameter $\alpha = \omega_{IS}^2/(\omega_Q \omega_{rot})$. While a spin-locked condition can be established in both the adiabatic ($\alpha >> 1$), and sudden ($\alpha << 1$) regimes, only the sudden regime is favorable for solid-state NMR experiments since the slow spinning speeds used in the adiabatic regime result in spectra having low resolution. In the sudden regime, low rf power and a high spinning speed are used in order to minimize α. The best CP conditions occur when [1] α is made as small as possible, [2] $\omega_{rot} > \omega_{1S}$, [3] $\omega_{1S} > \omega_Q^2/\omega_0$, and [4] when the frequency offset δ is minimal.

CHAPTER 3. COHERENCE AND THE EXISTENCE OF MULTIPLE-QUANTUM COHERENCES

Multiple-quantum magic-angle spinning (MQMAS) is a two-dimensional (2D) NMR technique that allows for the acquisition of high-resolution spectra of solid phase half-integer quadrupolar systems. How multiple-quantum (MQ) coherences can be generated, isolated and then observed in NMR, a technique that theoretically only provides for single-quantum visibility, warrants explanation. To this end, we shall briefly review some of the fundamentals of NMR and the 2D technique as they pertain to the MQMAS experiment. While a great deal of literature already exists describing the fundamental principles of one- and two-dimensional NMR (1-4,9,47,48,71,72), we will rely primarily on the books of Ernst et al. (47), Goldman (71), and Munowitz (48) for help in our discussion here.

Coherence and Multiple-Quantum Coherences

A state $|\psi\rangle$ describing N non-interacting spins is a superposition of $(2S+1)^N$ basis states in Hilbert space, each state corresponding to a specific magnetic energy level. The density matrix $\rho = \overline{|\psi\rangle\langle\psi|}$, which carries the statistical information relevant to the measurement of observables, is a superposition of $(2S+1)^N \times (2S+1)^N$ orthogonal basis operators. The superposed bar implies an ensemble average. The basis operators, or cells within the matrix, represent the non-interacting elements into which the density matrix may be decomposed. Implicit in each element of this matrix is the statistical property of coherence,

the net interference between two basis states over the ensemble (48). For a pure state, expressed in a given basis under the form

$$|\psi_i\rangle = \sum_i a_i \exp(i\varphi_i)\,|i\rangle \qquad [3.1]$$

where the coefficients a_i are positive real numbers, and φ_i the phase of the ith state. The elements of the density matrix for such a state are

$$\begin{aligned} \langle i|\rho|i\rangle &= a_i^2 \\ \langle j|\rho|j\rangle &= a_j^2 \\ \langle i|\rho|j\rangle &= a_i a_j \exp\{i(\varphi_j - \varphi_i)\}, \end{aligned} \qquad [3.2]$$

so that if neither $\langle i|\rho|i\rangle$ or $\langle j|\rho|j\rangle$ vanishes, neither does $\langle i|\rho|j\rangle$. This is a consequence of the fact that $|\psi_i\rangle$ is a superposition of the basis states, and implies that the phase of these two states, e.g. φ_i and φ_j, are not random but exhibit some "coherence". For a mixed state at equilibrium, however, coherent superpositions are not inherently present even when the diagonal elements, e.g. $\langle j|\rho|j\rangle$, do not vanish, since the phases of the states can be randomly distributed (71). Viewed as a mode of coherence, a given element of a density matrix will evolve independent from the rest when no propagator is applied. Its transformation into other components of the density matrix is prescribed by the Hamiltonian according to the Liouville-von Neumann equation of motion (48),

$$\frac{d}{dt}\rho = i\,[\rho(t),\, H(t)] \qquad [3.3]$$

Under Zeeman splitting, a mode of coherence may be classified according to its order, 'p', which is the difference in magnetic quantum numbers, $|m_i\rangle$, between the states it

connects, $p=(m_1 - m_2)$. There may be many modes of coherence present at the same time, but each pair of coherently superimposed states, represented by a basis operator such as $\rho^p = |m_1\rangle\langle m_2|$, remains an autonomous two-level system when no propagator is applied (48).

The simultaneous existence of various orders of coherence can readily be shown even in the simplest of experiments. Imagine a homonuclear two spin system (71), α and β, whose interaction Hamiltonian can be expressed as:

$$H_z = \sum_{\alpha} \sigma_\alpha S_z^\alpha + \sum_{\alpha,\beta} J_{\alpha\beta} S_z^\alpha S_z^\beta \qquad [3.4]$$

where σ_α represents the chemical shift interaction, J represents the indirect scalar coupling tensor between the two spins and $S_z^{\alpha,\beta}$ refers to the spin magnetization that aligns along the z-axis.

If this system is subjected to two $\pi/2$ pulses of similar phase that are separated by a time interval 't_1', the resulting operator-dependent part of the density matrix after the second pulse is proportional to (71):

$$H_x = \underbrace{\frac{1}{2}\sum_{\alpha} \sigma_\alpha \left(S_+^\alpha + S_-^\alpha\right)}_{p=1} + \underbrace{\frac{1}{4}\sum_{\alpha,\beta} J_{\alpha\beta}\left(S_+^\alpha S_+^\beta + S_-^\alpha S_-^\beta + S_+^\alpha S_-^\beta + S_-^\alpha S_+^\beta\right)}_{p=0 \text{ or } \pm 2} \qquad [3.5]$$

where $S_+^{\alpha,\beta}$ raises the magnetic quantum number by one level and $S_-^{\alpha,\beta}$ lowers its level by one. By adding the raising and lowering operators in each component of Eq. [3.5], the coherence order attributed by that operator can be determined, e.g. $S_+^\alpha S_+^\beta$ gives a p = +2 coherence order. In Eq. [3.5], the time evolution of the system has been expressed using a Taylor's expansion:

$$\rho(t) = \rho(0) + \sum_n \frac{1}{n!} \frac{d^n}{dt^n} \rho(t) \Big|_{t=0} \qquad [3.6]$$

which yields

$$\rho(t) = \rho(0) - it[H_x, \rho(0)] - i\frac{t^2}{2!}[H_x, [H_x, \rho(0)]] + \cdots\cdots \qquad [3.7]$$

The effect of the first commutator, $[H_x, \rho(0)]$, gives rise to coherences of order p = 0, ± 1, ± 2 (see Eq. [3.5]). Providing 't_1' is sufficiently long, the effects of the second and third commutators become significant and even higher orders of coherence result.

Selection Rule of NMR

In a pulsed NMR experiment, only the transverse nuclear magnetization that is the expectation value of the operator $S_\pm$ is observable:

$$\langle S_\pm \rangle = Tr\{S_\pm \rho\}. \qquad [3.8]$$

A non-vanishing expectation value of such an operator implies that the density matrix must contain operators S_x and S_y since

$$S_\pm = (S_x \pm iS_y). \qquad [3.9]$$

Thus only when the Zeeman quantum numbers differ by one, $\Delta m = \pm 1$, is the coherence amplitude $\langle m_1 | S_\pm | m_2 \rangle$ between the two states observable. Only single quantum coherences ($p = \pm 1$) are reflected directly in the observed response of the NMR experiment. However, as Eq. [3.5] shows, this does not mean that multiple coherences ($p > 1$) are not generated as well. When $p \neq 1$, the associated multiple-quantum coherence is no less real, but the

oscillations of such coherent states do not involve observable magnetization and thus can only be detected indirectly by conversion to observable single-quantum coherence in a two-dimensional experiment (48).

Phase Cycling Procedures in Multiple Pulse NMR Spectroscopy

The idea of indirect multiple-quantum spectroscopy, as applied to 2D NMR, was first proposed by Jeener, and then systematically analyzed by Aue et al. on systems of coupled spin-1/2 nuclei (73,74). It is accomplished using a three-step process (71):

(1) Excitation of multiple quantum (MQ) coherence;

(2) Free evolution of these coherences during a time 't_1'; and

(3) Conversion of the multiple quantum coherence into observable single-quantum coherence which is subsequently detected during 't_2'.

The simplest type of MQ experiment is a two pulse sequence in which the phases of both the rf pulses and of the receiver can be adjusted (67,68,75,76). Our previous discussion on a homonuclear two spin system, α and β, is an example of such an experiment, and it utilizes the above three step process. As we saw in the description of that experiment, several orders of coherence can exist simultaneously. However, in order to detect a multiple-quantum coherence, one must convert it back to the single-quantum state for observation. Thus, what is ultimately detected in a 2D experiment is the behavior of the spin system in the evolution period monitored indirectly through the modulation imposed upon the initial system at $t_2 = 0$ by the systematic variation of t_1 from experiment to experiment (47). How a

particular coherence order pathway is selected and brought to detection, while other pathways are excluded, will now be presented.

Selection of Coherence Pathways using Phase Cycling

We begin by reiterating the fact that the basis operators at equilibrium in the density matrix at time t = 0, $\rho(0)$, represent the non-interacting components into which the whole matrix may be separated. These basis operators, however, can be brought into coherence with one another through the use of propagators, U_i (47)

$$\rho(0) \xrightarrow{U_1} \xrightarrow{U_2} \cdots\cdots \xrightarrow{U_n} \rho(t). \qquad [3.10]$$

After a strong rf pulse, the density matrix is propagated into various orders of coherence

$$U_i \rho^p\left(t_i^-\right) U_i^{-1} = \sum_p \rho^{p'}\left(t_i^+\right) \qquad [3.11]$$

where t_i^- and t_i^+ refer to the states just prior to and just after the rf pulse, respectively. The separation of these various orders is accomplished by noting that each coherently superimposed state oscillates independently with a characteristic phase. By manipulating this phase coherence via rotation around the z-axis, specific orders of coherence can be separated and isolated from the others. For example, let F_p correspond to a p-quantum coherence state. When we perform a rotation of this state about the z-axis it transforms as

$$\exp(-i\varphi I_z)\, F_p\, \exp(i\varphi I_z) = \exp(-i\, p\varphi)\, F_p \qquad [3.12]$$

The proof of such a transformation follows: With

$$F_p = \sum_{m,\alpha,\beta} |m+p,\, \alpha\rangle\langle m+p,\, \alpha\, |F_p|\, m,\, \beta\rangle\langle m,\, \beta| \qquad [3.13]$$

then a rotation by an angle φ around the z-axis is represented by

$$e^{-i\varphi I_z}F_p e^{i\varphi I_z} = \sum_{m,\alpha,\beta} \exp(-i\varphi I_z)|m+p,\alpha\rangle\langle m+p,\alpha|F_p|m,\beta\rangle\langle m,\beta|\exp(i\varphi I_z)$$

$$= \sum_{m,\alpha,\beta} \exp(-i(m+p)\varphi)|m+p,\alpha\rangle\langle m+p,\alpha|F_p|m,\beta\rangle\langle m,\beta|\exp(i\, m\varphi)$$

$$= \sum_{m,\alpha,\beta} |m+p,\alpha\rangle\langle m+p,\alpha|F_p|m,\beta\rangle\langle m,\beta|\exp(-i\,(m+p)\varphi + i\, m\varphi)$$

$$= F_p \exp(-i\, p\, \varphi) \qquad [3.14]$$

This implies that when the phase is shifted by φ, the p-quantum coherence state, F_p, sees an apparent phase shift of $p\varphi$.

The above property is the key to coherence separation. By using the propagators that are shifted in phase

$$U_i(\varphi_i) = \exp\{-i\varphi_i\, I_z\}U_i(0)\exp\{i\varphi_i\, I_z\} \qquad [3.15]$$

rather than $U_i(0)$, as in Eq. [3.11], we obtain

$$U_i(\varphi_i)\rho^p(t_i^-)U_i(\varphi_i)^{-1} = \sum_{p'}\rho^{p'}(t_i^+)\exp\{-i\Delta p_i\varphi_i\} \qquad [3.16]$$

where $\Delta p_i = p'(t_i^+) - p(t_i^-)$ corresponds to the change in the order of coherence. The phase shift of a coherence component undergoing this $p \rightarrow p'$ change of order is expressed as

$$\rho(\Delta p_i,\ \varphi_i) = \rho(\Delta p_i,\ \varphi_i = 0)\exp(-i\Delta p_i\varphi_i). \qquad [3.17]$$

This phase shift is inscribed in the coherence state, and carried over to detection, p = -1

$$s(\Delta p_i, \varphi_i, t) = s(\Delta p_i, \varphi_i = 0, t)\exp(-i\Delta p_i\varphi_i). \qquad [3.18]$$

Since the total signal will contain information from all allowed coherence pathways

$$S(\varphi_i, t) = \sum_{\Delta p_i} s\,(\Delta p_i, \varphi_i, t), \qquad [3.19]$$

in order to restrict the transfer to a particular order, Δp_i, one must perform N_i experiments using systematic increments of the rf phase φ_i in the propagator

$$\varphi_i = k_i 2\pi / N_i \quad \text{where} \quad k_i = 0,\ 1,\ \ldots,\ N_i - 1\,. \qquad [3.20]$$

Then using discrete Fourier analysis with respect to phase φ_i, the superposition of all the allowed coherence pathways can be unraveled to yield the desired signal, $S\,(\Delta p_i, t)$

$$S\,(\Delta p_i, t) = \frac{1}{N_i} \sum_{k_i=0}^{N_i-1} S\,(\varphi_i, t)\ \exp(i\ \Delta p_i\ \varphi_i)\,. \qquad [3.21]$$

This equation is a linear combination of only the N_i signals that have undergone the desired Δp_i change brought about by the U_i propagator. However, not all of the undesired pathways are rejected. By performing N_i experiments a series of values are selected

$$\Delta p_i^{\text{selected}} = \Delta p_i^{\text{desired}} \pm n N_i \quad \text{with} \quad n = 0,\ 1,\ 2,\ \ldots. \qquad [3.22]$$

How to properly combine or weight these signals then is essential to the selection process. One means of accomplishing this is by shifting the phase of the receiver by

$$\varphi^{\text{rcvr}} = -\Delta p_i \varphi_i\,. \qquad [3.23]$$

We now illustrate the concepts of phase cycling in a hypothetical one pulse experiment (47,72). Figure 3.1 shows two possible coherence transfer pathways to the single-quantum coherence state p = -1. Assume the "desired" coherence pathway is p = -2 → p = -1. By applying appropriate phase cycling to both the applied rf pulse and the receiver the desired transients can be monitored and those from the undesired pathway, p = 0 → p = -1, disregarded. Figures 3.2 and 3.3 show the transients gathered for each of these pathways

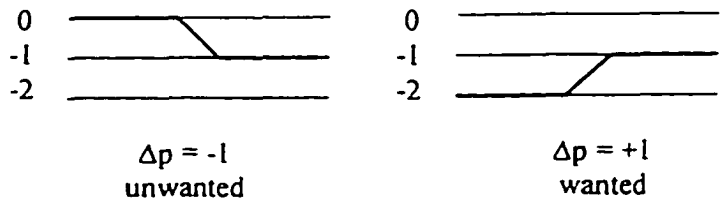

Figure 3.1: Conversion of two coherence pathways to the single-quantum detection state p = -1.

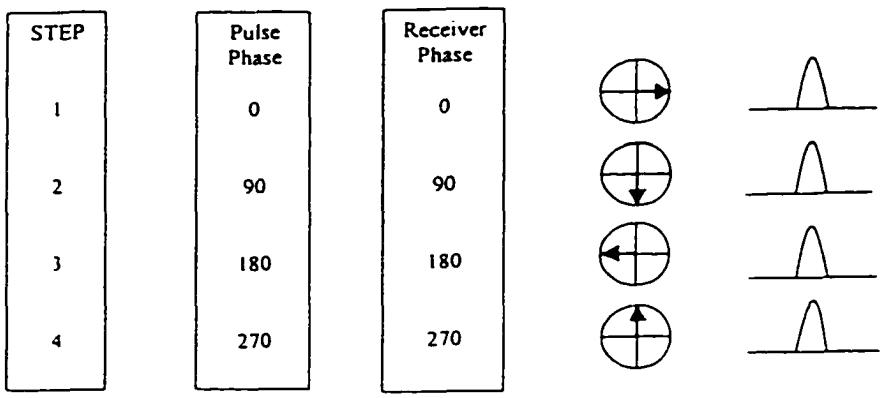

Figure 3.2: Selection of the coherence pathway Δp = +1 using a four step cycle. Note how the final spectra all have lines with the same phase.

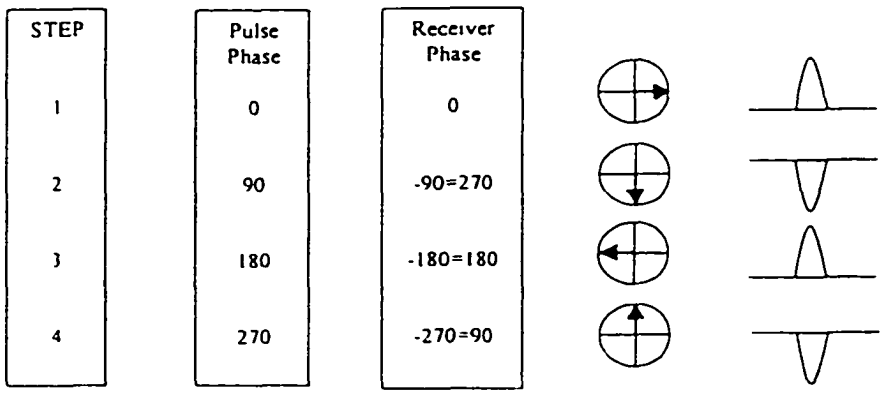

Figure 3.3: Rejection of the pathway Δp = -1 by the phase cycle used in Fig. [3.3]. Note how the final spectra will cancel one another upon summation.

using a single pulse experiment repeated four times, $N_i = 4$, each time with the phase of the pulse and the receiver being shifted through 90°. By combining the resulting transients of each four step experiment, the desired coherence pathway's signal is isolated. Note that all of the transients of the desired pathway, $-2 \rightarrow -1$, are of the same phase and will thus add constructively, while those of the undesired pathway will cancel out upon addition. This shows how essential being able to adjust the receiver reference phase is to the overall selection process. If the four transients of either pathway were collected using a fixed receiver reference phase, both pathway's transients would cancel out completely.

We now consider multiple coherence transfer pathways, which can be followed by introducing successive propagators, U_i, into the NMR experiment. A **bold font** vector notation is used to depict their combined, Total, effect, e.g., $\mathbf{\Delta p}^{\mathbf{T}}$, $\mathbf{\Delta \varphi}^{\mathbf{T}}$, $\boldsymbol{\varphi}^{\mathbf{rcvr}}$.

$$\mathbf{\Delta p}^{\mathbf{T}} = \{\Delta p_1,\ \Delta p_2,\ \cdots,\ \Delta p_n\} \qquad [3.24]$$

$$\boldsymbol{\varphi}^{\mathbf{T}} = \{\varphi_1,\ \varphi_2,\ \ldots,\ \varphi_n\} \qquad [3.25]$$

To separate the various coherence pathways created, it is necessary to cycle the phases of the propagators independently

$$\varphi_1 = k_1\, 2\pi / N_1,\ \ldots\ldots,\ \varphi_n = k_n\, 2\pi / N_n \qquad [3.26]$$

for

$$k_1 = 0,\ 1,\ \ldots,\ N_1 - 1;\ \ldots;\ k_n = 0,\ 1,\ \ldots,\ N_n - 1\ . \qquad [3.27]$$

The total number of experiments to be performed is then $N = N_1 \cdot N_2 \cdot N_3 \cdot \ldots \cdot N_n$.

Under our new notation, equations [3.21]-[3.23] can be expressed, respectively, as

$$S\left(\Delta \mathbf{p}^{\mathbf{T}}, t\right) = \frac{1}{N} \sum_{k_1=0}^{N_1-1} \sum_{k_2=0}^{N_2-1} \cdots \sum_{k_n=0}^{N_n-1} S\left(\boldsymbol{\varphi}^{\mathbf{T}}, t\right) \exp\left(i\, \Delta \mathbf{p}^{\mathbf{T}} \boldsymbol{\varphi}^{\mathbf{T}}\right) \qquad [3.28]$$

$$\Delta \mathbf{p}^{\mathbf{T,\ selected}} = \left\{\Delta p_1 \pm n_1 N_1,\ \Delta p_2 \pm n_2 N_2,\ \cdots,\ \Delta p_n \pm n_n N_n\right\} \qquad [3.29]$$

$$\varphi^{\mathbf{rcvr}} = -\Delta \mathbf{p}^{\mathbf{T}} \cdot \boldsymbol{\varphi}^{\mathbf{T}} = -\sum_i \Delta p_i \varphi_i \qquad [3.30]$$

We now illustrate the concepts of multiple propagators in a triple-quantum (3Q) experiment that requires the use of three rf pulses with phases $(\varphi_1,\ \varphi_2,\ \varphi_3)$. The overall experiment is shown in Figure 3.4 with the desired coherence pathways $(0 \rightarrow \pm 3 \rightarrow 0 \rightarrow -1)$ illustrated as bold lines. The branching or fanning out of pathways that are retained in this experiment according to Eq. [3.29] are depicted as dashed lines. For our example, the number of phases used for each of the three pulses are, respectively, $N_1 = 1$, $N_2 = 6$ and $N_3 = 4$. Table 3.1 shows the phase cycle for the selection of the coherence transfer pathway $p = 0 \rightarrow \pm 3 \rightarrow 0 \rightarrow -1$. One complete experiment consists of 24, three pulse sequences with final weighting of the signals done by the positioning of the receiver reference phase, $\varphi^{\mathbf{rcvr}}$.

In this example, the first two pulses in the experiment with phases φ_1 and φ_2, respectively are applied using high (hard), non-selective rf fields while the third pulse, with phase φ_3, is applied using a much softer, more selective rf field. The technique of bringing the coherences back to $p = 0$ prior to the final observation pulse is referred to as "z-" filtering (77,78). This technique helps in removing undesired transients from the observed signal, and coupled with the technique CYCLOPS provides an easy and robust method for obtaining pure-absorption spectra. In order to obtain a pure-absorption 2D spectrum, signals from both the echo and anti-echo pathways need to be obtained with equal intensity. Using z-filtering,

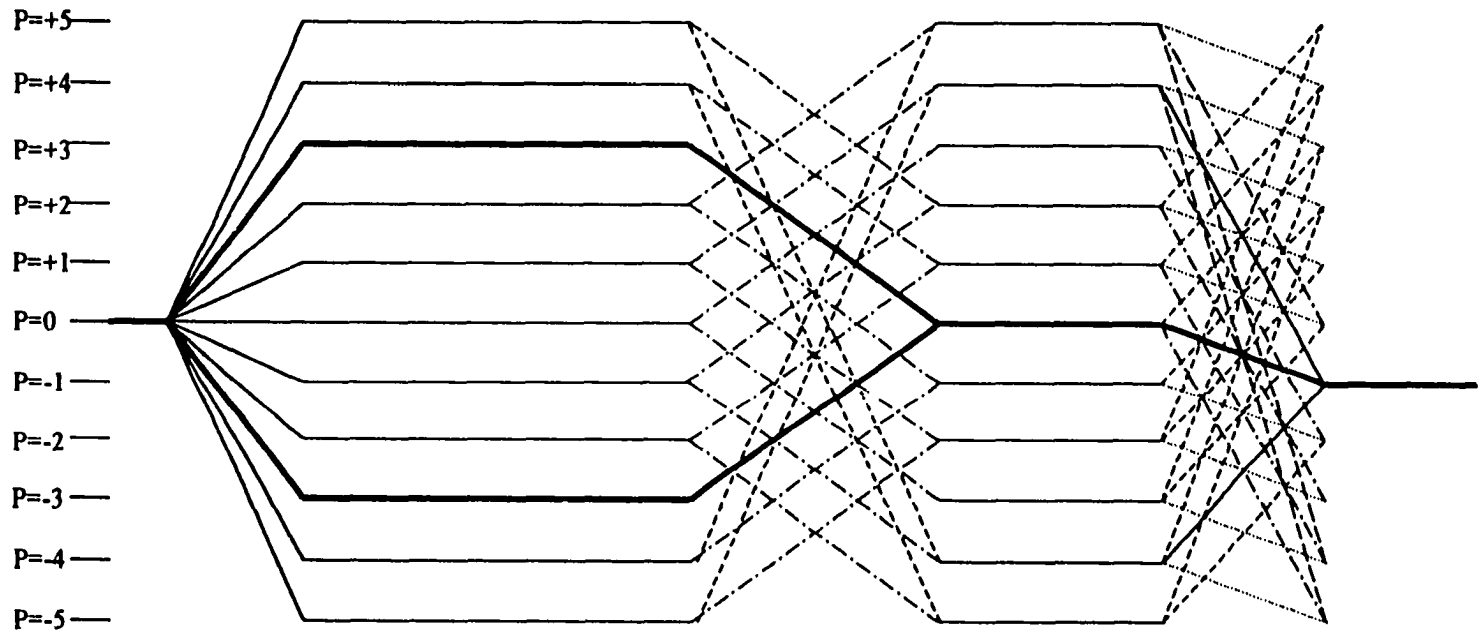

Figure 3.4: Branching of the pathways that occurs in an experiment whose desired coherence pathway is $(0 \rightarrow \pm 3 \rightarrow 0 \rightarrow -1)$, shown in bold lines. The experiment uses three pulses with phase cycles $N_1=1$, $N_2=6$, and $N_3=4$. The use of a z-filter, in conjunction with a 'soft' selective third pulse, φ_3, minimizes the possibility of the coherences from the undesired, yet still allowed, pathways to influence the signal observed.

Table 3.1: Selection of the coherence pathway ($0 \rightarrow \pm 3 \rightarrow 0 \rightarrow -1$) using a 24 phase cycle three pulses sequence. The influence of the undesired coherence pathways is negated by the use of the 'soft' selective third pulse.

PULSE 1 PHASE φ_1 +/-3 Q	PULSE 2 PHASE φ_2 -/+3 Q	PULSE 3 PHASE φ_3 -1 Q	RECEIVER PHASE φ_{RCVR}
0	0	0	0
0	60	180	0
0	120	0	0
0	180	180	0
0	240	0	0
0	300	180	0
0	0	180	180
0	60	0	180
0	120	180	180
0	180	0	180
0	240	180	180
0	300	0	180
0	0	90	90
0	60	270	90
0	120	90	90
0	180	270	90
0	240	90	90
0	300	270	90
0	0	270	270
0	60	90	270
0	120	270	270
0	180	90	270
0	240	270	270
0	300	90	270

by bringing the coherences of the $p = \pm 3$ quantum states back to $p = 0$, the symmetry of the pathways is assured and their amplitudes will be equal. More will be presented on this, later. Finally, it should be noted that magnetization from the ± 4 quantum states are still allowed coherence pathways according to this phase cycling scheme (see Figure 3.4). However, by using 'soft', selective rf power on the third pulse, leakage from the coherence pathways ($-4 \xrightarrow{\Delta p=3} -1$ and $+4 \xrightarrow{\Delta p=5} -1$) is minimized.

CHAPTER 4. MULTIPLE QUANTUM MAGIC-ANGLE SPINNING NMR (MQMAS)

To infer the isotropic chemical shifts of a compound using NMR requires that one be able to obtain a high-resolution spectrum. With this information, a detailed understanding of the local chemical and physical perturbations occurring at an atomic site can be surmised. Such resolution can be readily obtained for liquid samples. Solids, however, are a different matter. No longer are the anisotropic internal interactions of the moments averaged by inherent isotropic motional processes. Rather, only by the advent of averaging techniques such as magic-angle spinning (MAS), rf decoupling, cross polarization (CP), and multi-pulse schemes has the field of solid-state NMR been opened (5-8). Presently the advancements in NMR theory and experimental techniques, in conjunction with those to software and hardware, have made it possible to manipulate the Hamiltonians that governs the spin system almost at will. Some of these techniques were described earlier in this work. Although the linewidths in solid phase spectra are still greater than those in liquid spectra, the additional information they provide cannot readily be garnered from solution.

As we already discussed in Chapter 1, for quadrupole nuclei the anisotropy of this internal interaction is sufficiently large that it requires extending perturbation or coherent averaging theory to higher orders (3,11,30). These extensions describe the quadrupolar interaction using higher orientational terms and, thus, require that one be able to manipulate either the coordinate space and/or spin space of the sample in a more complex fashion in order to achieve isotropic line narrowing. Only recently have experimental techniques been

developed that are capable of performing such manipulations. We describe these new techniques in detail, below.

The MQMAS Experiment

The evolution of a spin system placed in a static magnetic field, B_0, is governed by a Hamiltonian composed of its principle spin interactions

$$H_{total} = H_Z + H_Q + H_D + H_{CS}. \qquad [4.1]$$

In strong magnetic fields, the Zeeman interaction $(H_Z = -\omega_0 S_Z)$ usually dominates and the other internal spin interactions can be treated as first- and second-order perturbative effects acting upon its eigenstates (1-4,9). While all of these interactions will lead to anisotropic line broadening in the NMR spectrum, we will confine our discussion here to an ensemble of spins subjected to the combined effects of the Zeeman and quadrupolar interactions.

Figure 4.1 shows the energy level diagram of a dominant Zeeman interaction being perturbed by the cumulative effects of first- and second-order quadrupolar splitting. The energy of the static first-order quadrupole splitting can be expressed by the Hamiltonian:

$$H_Q^{(1)} = \omega_Q^{(1)}(\theta,\phi)\left[3S_Z^2 - S(S+1)\right] \qquad [4.2]$$

with quadrupolar frequency,

$$\omega_Q^{(1)}(\theta,\phi) = \frac{e^2qQ/\hbar}{4S(2S-1)}\left[3\cos^2\theta - 1 + \eta\sin^2\theta\cos 2\phi\right]. \qquad [4.3]$$

where e^2qQ/h is the nuclear quadrupole coupling constant (C_Q), η is the asymmetry parameter, and θ and ϕ are the angles between the principal axis system (PAS) of the

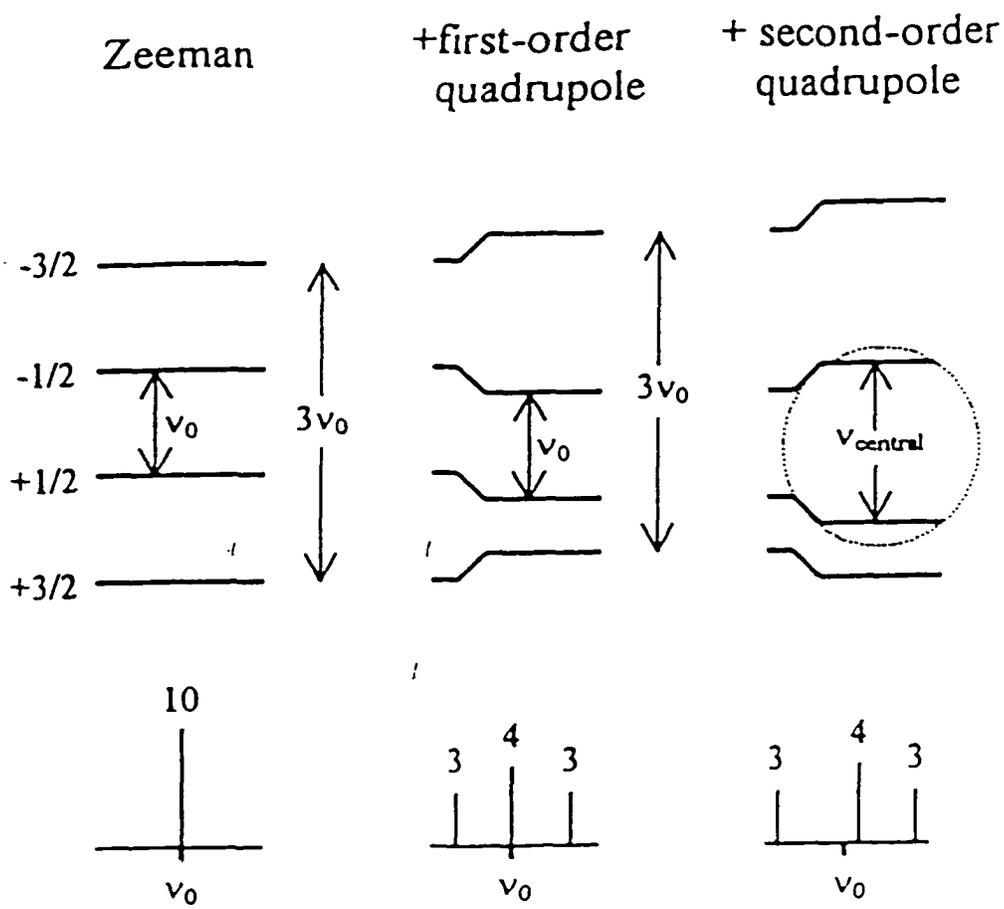

Figure 4.1: Zeeman and quadrupolar splitting of a spin-3/2 nucleus in a strong magnetic field. The top shows the energy level splittings due to: Zeeman effects only (left); Zeeman plus first-order quadrupolar splitting effects (middle); and Zeeman plus first- and second- order quadrupolar splitting effects (right). The bottom of the Figure shows the NMR spectrum of a single crystal subject to the effects above. Note that the all of the symmetric transitions (+m ↔ -m) are unaffected by first-order quadrupolar effects. Additionally, note that the second-order effects induce an isotropic shift to the central transition away from ν_0.

quadrupolar interaction tensor and the external magnetic field, B_0. The effects of the first-order quadrupolar interaction perturbs all of the Zeeman energy levels, however, it keeps the spacing between the symmetric transitions $(+m \leftrightarrow -m)$ unchanged (see Figure 4.1). It is the Hamiltonian's quadratic dependence on the S_z angular momentum (see Eq. [4.2]) that accounts for this effect. The absence of first-order broadening, which is typically in the MHz range, makes observation of the central transition (+1/2 ↔ -1/2) with some degree of resolution possible. However, the second-order quadrupolar effects (SOQE) can still broaden this transition by tens of kHz. This second-order quadrupolar shift can be expressed as (2)

$$\nu_{Q,\,1/2\leftrightarrow -1/2}^{(2)} = \frac{-\nu_Q^2}{16\nu_0}\left[S(S+1)-\frac{3}{4}\right]\left(1-\cos^2\theta\right)\left(9\cos^2\theta-1\right) \qquad [4.4]$$

where ν_Q is the quadrupolar frequency, $\nu_Q = 2\pi C_Q / 2S(2S-1)$, θ is the angle between the crystal's interaction tensor and the magnetic field, B_0 and S is the spin number. This equation shows that the second-order quadrupolar effect (SOQE): (i) broadens the spectral resonance by an amount proportional to ν_Q^2 / ν_0; (ii) is inversely proportional to B_0 $(1/\nu_0)$; and (iii) has dependence upon two unique spatial components.

As described previously, a standard NMR procedure for reducing anisotropic effects is to rapidly rotate a sample about an axis inclined at an angle, β, with respect to the static magnetic field, B_0. Within this 'rotating frame' each of the spin interaction Hamiltonians are made time-dependent, and thus the anisotropies get averaged over the rotor period (50,85). Expanding Eq. [4.4] to account for amorphous samples, the frequency of the SOQE

corresponding to any of the symmetrical transition in the sample rotating at angle β with respect to B0 can be expressed as (13,30,43,79,86):

$$\nu_{Q,p}^{(2)} = \frac{pC_Q^2}{4S(S-1)\nu_0}\left[A_0(S,p)B_0^Q(\eta_Q) + A_2(S,p)B_2^Q(\eta_Q,\alpha_Q,\beta_Q)P_2(\cos\beta) + A_4(S,p)B_4^Q(\eta_Q,\alpha_Q,\beta_Q)P_4(\cos\beta)\right] \quad [4.5]$$

where p = 2m is the order of the coherence, and S, C_Q and η_Q have been previously defined. The $A_i(S,p)$ terms

$$A_0(S,p) = p\left[S(S+1) - \frac{3}{4}p^2\right] \quad [4.6]$$

$$A_2(S,p) = p\left[8S(S+1) - 3p^2 - 3\right] \quad [4.7]$$

$$A_4(S,p) = p\left[18S(S+1) - \frac{17}{2}p^2 - 5\right] \quad [4.8]$$

are the zero-, second- and fourth-rank coefficients depending on the spin number S and the order p of the transition. $B_0^Q(\eta_Q)$ is the zero-rank (isotropic) quadrupolar shift component, and the $B_i^Q(\eta_Q,\alpha_Q,\beta_Q)$, i = 2, 4, terms are orientation dependent functions relating the quadrupole tensor with respect to the rotor axis (13,86). Finally, the dependence of the rotor orientation with respect to B_0 is accounted for in the second- and fourth-order Legendre polynomials. The functional form of these two polynomials are

$$P_2(\cos\beta) = \frac{1}{2}\left(3\cos^2\beta - 1\right) \quad [4.9]$$

$$P_4(\cos\beta) = \frac{1}{8}\left(35\cos^4\beta - 30\cos^2\beta + 3\right), \qquad [4.10]$$

and are illustrated in Figure 4.2. Note in this Figure , that the zero points of the second- and fourth order Legendre polynomials do not occur at the same angle(s). Therefore, rotation about any one fixed axis can, at best, only average out one of the spatial terms in the second-order effects equation. However, if the angle of rotation, β, is made time-dependent by moving the spinning axis during the experiment, then the second-order anisotropies can be averaged out. Two techniques that accomplish this spatial manipulation are double rotation (DOR) and two-dimensional dynamic-angle spinning (2D DAS) (15,16,41).

Both DOR and 2D DAS remove second-order broadening by coherently averaging the spatial components, $P_2(\cos\beta)$ and $P_4(\cos\beta)$, of the quadrupolar interaction (see Eq. [4.5]). The second-order effect, however, also contains an isotropic component $A_0(S,p)B_0^Q(\eta_Q)$ which does not have any spatial dependence. Thus, even if the anisotropic components of the SOQE can be effectively averaged, the isotropic component will still impose a quadrupolar induced shift (QIS) in the NMR spectrum.

In 2D DAS experiments, a sample is rotated about two unique axes in succession that are at complementary angles for time lengths t_1 and t_2 such that (41)

$$P_2(\cos\beta_1)\, t_1 + P_2(\cos\beta_2)\, t_2 = 0, \qquad [4.11]$$

$$P_4(\cos\beta_1)\, t_1 + P_4(\cos\beta_2)\, t_2 = 0. \qquad [4.12]$$

These equations imply that the anisotropy that develops during (β_1, t_1) must develop during (β_2, t_2) with reverse sign, such that their cumulative effect vanishes. This is exactly what

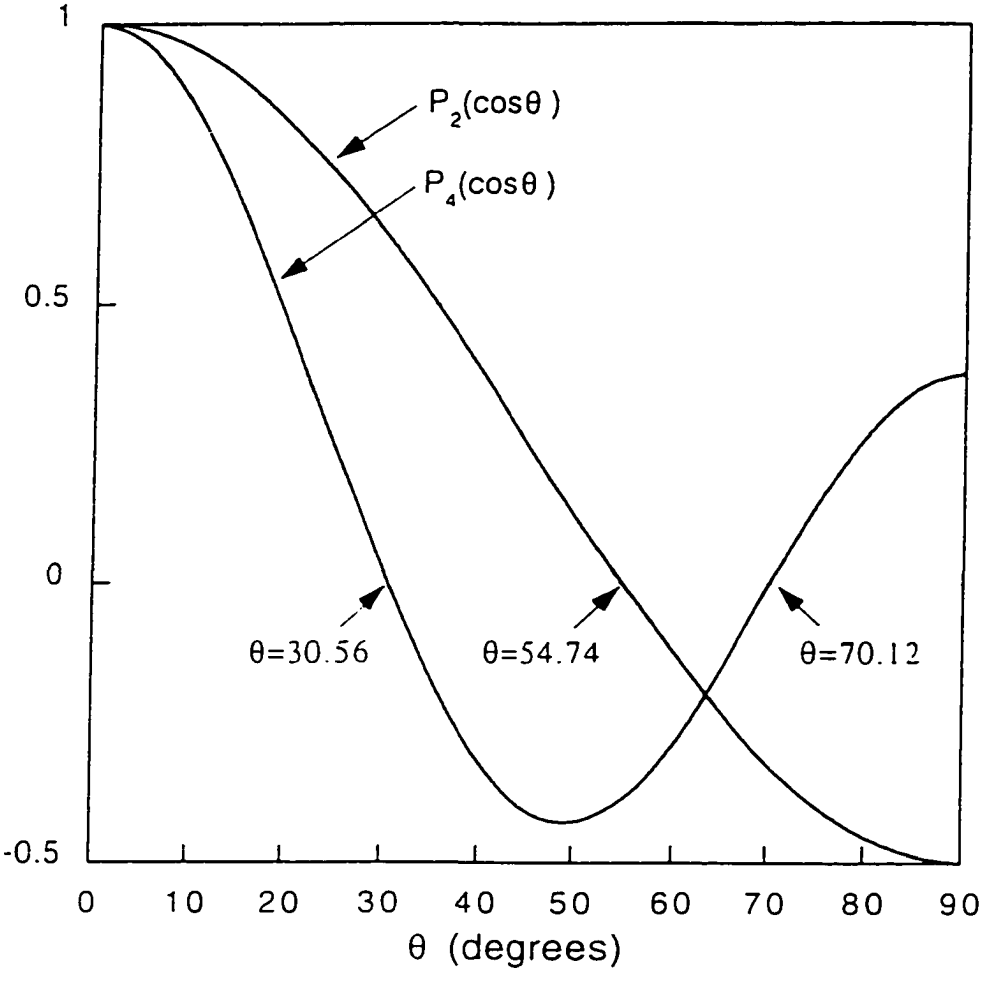

Figure 4.2: Functional forms of the second- and fourth-order Legendre polynomials. The magic angle is a root of $P_2(\cos\theta)$, however, note that there are no common roots between $P_2(\cos\theta)$ and $P_4(\cos\theta)$.

happens. If we request that the time spent at each angle during an experiment be equal, $t_1 = t_2$, then $\beta_1 = 79.19°$ and $\beta_2 = 37.38°$ are used as the complementary angles for rotation. As this experiment requires the manipulation of two degrees of freedom, β_1 and β_2, it is naturally two-dimensional. After correctly processing the data, the resulting NMR spectrum consists of one dimension containing only the information from the isotropic interactions, $\nu_{cs} + \nu_{Q,iso}^{(2)}$, and the other dimension containing the combined isotropic and anisotropic information.

In DOR, a similar averaging of the SOQE is accomplished, albeit one-dimensional since the sample is subjected to rotation about two axes simultaneously. This means that the spatial components are continuously averaged throughout the experiment. It can be shown (15,16,87) that under DOR that

$$\left\langle P_{2,4}\cos\theta(t)\right\rangle_{DOR} = P_{2,4}(\cos\beta_1)P_{2,4}(\cos\beta_2) \qquad [4.13]$$

Thus, complete averaging is achieved when

$$P_2(\cos\beta_1)\cdot P_2(\cos\beta_2) \;=\; P_4(\cos\beta_1)\cdot P_4(\cos\beta_2) \;=\; 0, \qquad [4.14]$$

i.e., when $\beta_1 = 54.7°$ and $\beta_2 = 30.56°$. Such an experiment requires the use of two rotors: an outer one that is inclined at an angle of 54.7° relative to the external magnetic field, B_0, and an inner rotor containing the sample tilted at an angle of 30.56° relative to the outer rotor. In spite of DAS and DOR's success at obtaining purely isotropic spectra for quadrupole nuclei, each method has significant shortcomings. Unless the DAS experiment utilizes the magic angle, 54.7°, as one of the angles of rotation, it cannot effectively address strongly dipole-coupled systems. Additionally, the time needed to 'jump' from one complementary angle to the next, ~30 ms, excludes its use for studying any fast-relaxing systems, which is a severe

limitation for quadrupolar spin systems. These concerns are better addressed by DOR, however, the use of two concentric rotors dramatically reduces the sample filling factor, and the low rotation speed of the outer rotor, ≤ 1.5 kHz, places the desired isotropic data within a mass of closely spaced spinning sidebands. As a result, the lineshape parameters are often difficult to ascertain from the spectra (12,13). Finally, it should also be noted that the mechanical challenge confronted by attempting to manipulate about two angles within one experiment, DAS or DOR, is a daunting task.

Recently, Frydman and Harwood introduced a multiple-quantum technique that is analogous to 2D DAS, but which accomplishes second-order averaging by keeping the angle of rotation β fixed and using the order of coherence 'p' as the necessary second degree of freedom (43,44). This two-dimensional (2D) experiment is referred to as multiple-quantum magic-angle spinning (MQMAS) (43). Like DAS and DOR, this technique relies upon the quadratic dependence of the quadrupolar Hamiltonian in order to remove the first-order broadening effects. For suppression of the SOQE, however, advantage is taken of the fact that evolution frequency has different dependences under different coherence orders. In a MQMAS experiment, the quadrupolar spins are allowed to evolve during initial and final times under the effects of the two unique orders of coherence, p_1 and p_2, chosen so as to fulfill second-order averaging. From Eq. [4.5] we obtain the following averaging condition

$$A_2(S,p_1)P_2(\cos\beta)\,t_1 + A_2(S,p_2)P_2(\cos\beta)\,t_2 = 0, \qquad [4.15]$$

$$A_4(S,p_1)P_4(\cos\beta)\,t_1 + A_4(S,p_2)P_4(\cos\beta)\,t_2 = 0. \qquad [4.16]$$

Either of the equations above can be effectively fulfilled by spinning the sample at a root value of the Legendre polynomial, $P_2(\cos\beta)$ or $P_4(\cos\beta)$ (see Fig. 4.2). By setting β at 54.7°, however, the technique of MAS is effectively employed, and all of the anisotropies that are a function of $P_2(\cos\beta)$ will be selectively averaged out, including the anisotropic effects due to chemical shift and dipole-dipole interactions. With the effects of Eq. [4.15] averaged out by MAS, only the coherence pathways capable of refocusing the anisotropies in Eq. [4.16] need yet to be addressed. This is accomplished by manipulating the coherence order, 'p'. While the selection rules dictate that the signal be single-quantum $(p = \pm 1)$ at its time of observation in t_2, manipulation of the rf excitation and demodulation phases can still allow one to choose the apparent sense of multiple-quantum precession during t_1 (43,44). Completely analogous to the (β_i, t_i) manipulations in the 2D DAS experiment, the $A_4(S,p_i)\,t_1$ and $A_4(S,-1)\,t_2$ terms in Eq. [4.16] must dephase with opposite signs in order to fulfill second-order averaging. Since all observations must be made at p = -1, and since all $A_4(S,-1)$ terms are positive, the coherence pathway that leads to refocusing, or averaging, of the anisotropy is dictated by the p-quantum term, $A_4(S,p_i)$, which can be negative for certain p_i values. Thus, the averaging of the second-order quadrupole interaction can be accomplished by correlating the phase evolution of the p-quantum coherence in t_1 with the single-quantum coherence in t_2 such that a purely isotropic 'echo' is generated at time

$$t_2 = \left|A_4(S,p)/A_4(S,-1)\right| t_1 = R(S,\ p)\ t_1 . \qquad [4.17]$$

This equation implies that the second-order quadrupole broadening will be averaged to zero along a 'ridge' in the time-domain that is a function of the ratio $\left|A_4(S,p)/A_4(S,-1)\right|$. Our experimental studies confirm this prediction. Figure 4.3 shows the time-domain data of a triple-/single-quantum correlation experiment of ^{23}Na (S =3/2) in $Na_2C_2O_4$ using the two-pulse sequence shown in Figure 4.4. A line representing where the isotropic echo is expected to refocus according to Eq. [4.16] is displayed in Figure 4.3b. As different dwell times, dw_i, were used in each dimension, the slope of the refocusing line is modified to: $R(S,p)\cdot(dw_1/dw_2)$. Additionally, only one of the two coherence pathways, $0 \rightarrow \pm 3 \rightarrow -1$, will serve as the 'echo' pathway. The other pathway is referred to as the 'antiecho' pathway as it appears to refocus the quadrupolar broadening at negative values of the acquisition time, t_2 (47). This pathway's time-domain data are shown in Figure 4.3a. While this pathway's FID is not wholly detectable in the two-pulse MQMAS experiment, the information it contains is still needed in order to obtain pure absorption spectra, as will be discussed later.

Optimizing the Multiple-Quantum (MQ) Experiment

Both the creation of MQ coherence, as well as its subsequent conversion into observable single-quantum coherence, require calculating the propagation of the density matrix under the effects of non-commuting time-dependent Hamiltonians. Analytical solutions of such systems are not straightforward, but can be calculated if all interactions but the dominant rf and first-order quadrupolar interactions are neglected (44,68,74,88). While these calculations impose many restrictions (e.g., no sample spinning, single crystal, on resonance

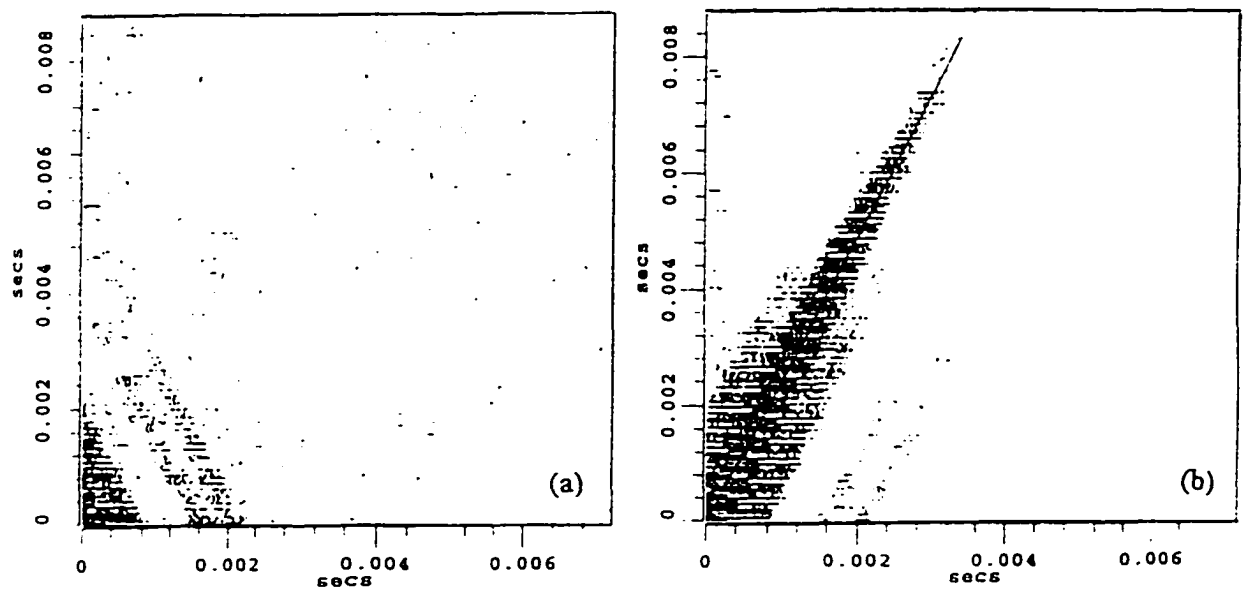

Figure 4.3: Time domain data of a triple-/single-quantum correlation experiment done on $Na_2C_2O_4$. Fig. 4.3b shows the refocusing pathway with the isotropic 'echo' formation occurring along a ridge with slope: $t_2 = |A_4(S,p)/A_4(S,-1)| \cdot t_1$. Fig. 4.3a shows the signal collected from the antiecho pathway in the experiment. Both pathways are necessary in order to acquire pure absorption-mode spectra.

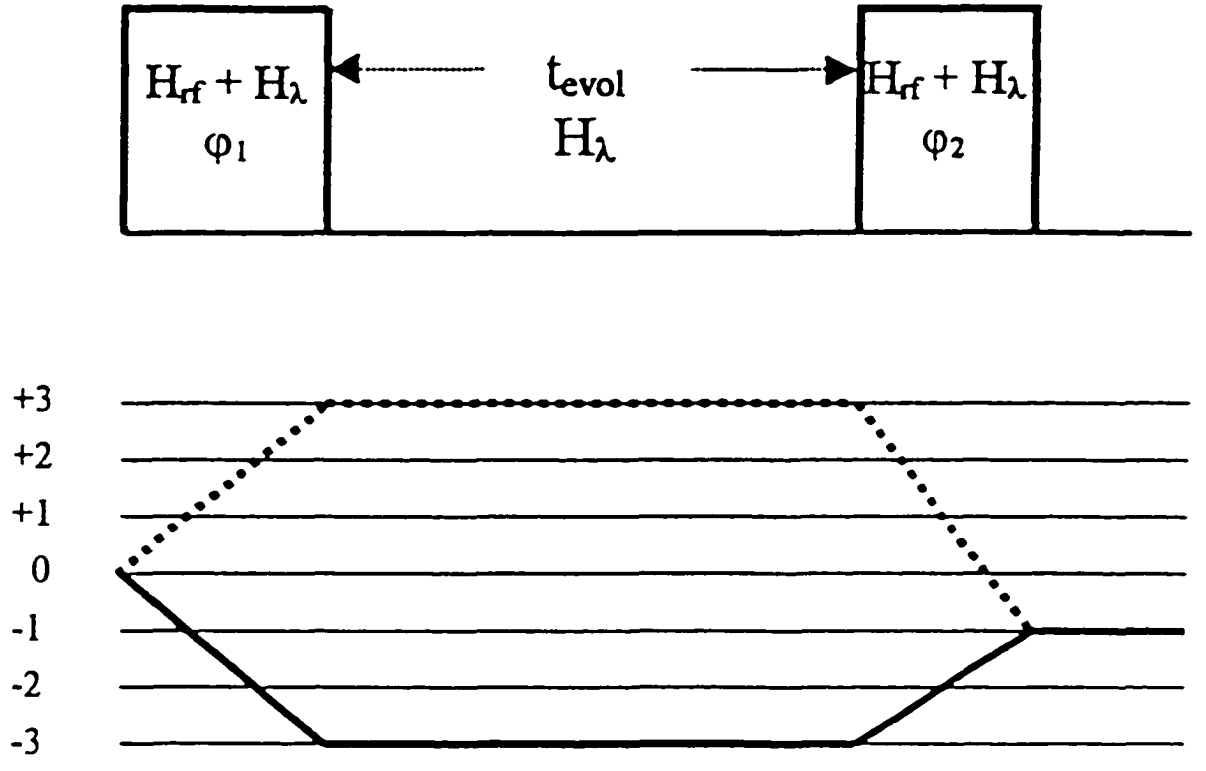

Figure 4.4: Multiple-quantum experiment using a two pulse sequence, φ_1 and φ_2. For a spin-3/2 nucleus, the echo pathway is $(0 \rightarrow -3 \rightarrow -1)$ and $(0 \rightarrow +3 \rightarrow -1)$ is the antiecho pathway. During t_{evol}, which is incremented during a 2D experiment, the spin system evolves as a function of its internal spin interactions.

irradiation, negligible second-order broadening...), their results do provide general insight regarding the behavior of the spin system. Recently, however, software capable of doing full computational simulations has been developed and applied to such systems (89). Results for a 2D MQ experiment on a quadrupolar spin system are discussed below.

Excitation of 3Q Coherences

Figure 4.5 shows signal intensity build up curves of triple-quantum, 3Q, coherence in powdered samples of quadrupolar nuclei with differing spin number, S. The intensities are plotted as a function of the excitation angle, $\theta_1 = 360^\circ \nu_{rf} t_1$ (12). The vertical scale is expressed as a percentage versus the intensity that can be obtained using a single, selective 90° pulse to the central transition (-1/2 ↔ +1/2). Notably, all of the nuclei show 3Q coherence build up in excess to that of the normalized ideal when the ratio ν_Q / ν_{rf} is made sufficiently small. Since ν_Q cannot be adjusted experimentally, this result implies that the use of a high rf field increases the efficiency of excitation. While a large value for ν_Q / ν_{rf} lowers the efficiency at the first local maximum for each spin number S (this is the point at which the experiments are to be optimized) it does not alter, substantially, the optimal angle of excitation, $\theta_1 = 360^\circ \nu_{rf} t_1$. This effect can be explained by the fact that, in solids, all nuclei with a similar spin number will have a similar nutation rate. (Keeping in mind, of course, that for different crystallographic sites a nucleus will respond differently to rf pulse excitation.) Additionally, while the efficiency of triple-quantum build up is nearly independent of the spin number, the optimum flip angle for triple-quantum excitation reduces as the spin number

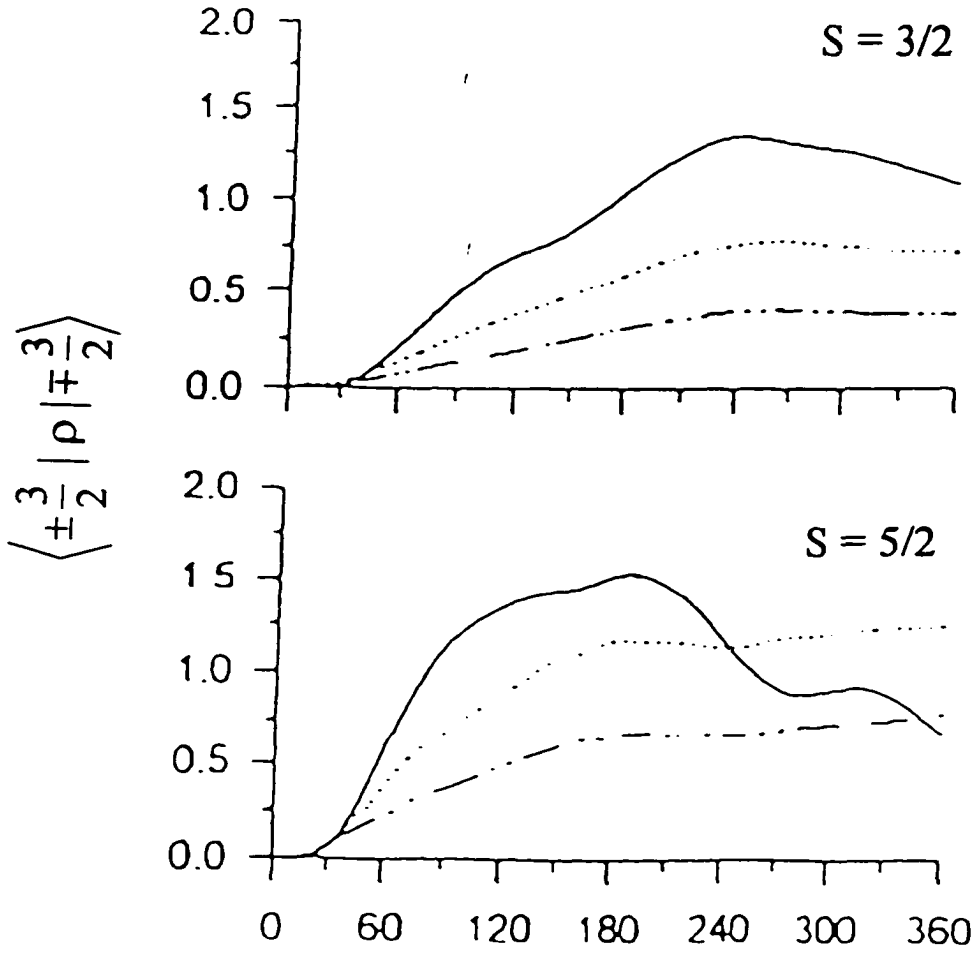

Figure 4.5: Simulated build-up curves for triple-quantum coherence in powdered samples of spin-3/2 and spin-5/2 nuclei as a function of pulse angle, θ. The vertical scale is normalized to a maximum signal intensity for -1/2 ↔ 1/2 transitions equal to 1. Computations assumed the following ratios between ν_Q and ν_{rf} ($\eta = 0$): ν_Q/ν_{rf} = 5 (–···–), ν_Q/ν_{rf} = 2.5 (···), ν_Q/ν_{rf} = 1.25 (—). The experimental data was taken using Na_2SO_4 and $KMnO_4$ for the S = 3/2 and 5/2 nuclei, respectively.

increases. It is the nutation rate which accounts for the sharpening and shifting of the local maximum towards smaller values as the spin number, S, is increased. In pulsed NMR, the precession rate of a nucleus is proportional to the magnetic dipole transition, $\sqrt{S(S+1)-m(m+1)}$. Thus, as S increases so does its rate of precession and, therefore, the length of the central transition $\pi/2$ pulse shortens according to the equation 1/(S + 1/2) (2,66-68).

Evolution of the Coherences

In the absence of relaxation processes and an applied rf field, the elements of the density matrix freely evolve under the influence of the internal Hamiltonians. The elements (m, m') describe statistical coherences between states $|m\rangle$ and $|m'\rangle$. In general, the phase evolution $\varphi_{m\,m'}$ on a coherence (m, m') under the influence of the first and second-order quadrupolar interactions during time interval $d\tau$ can be expressed as

$$d\varphi_{m\,m'}(\tau) = \underbrace{\nu_Q\left(m^2 - m'^2\right)d\tau}_{1^{st}\text{ order}} + \underbrace{\frac{1}{2}\left[A(\alpha,\beta,\eta_Q) + B(\alpha,\beta,\eta_Q)\left(m^2 + mm' + m'^2\right)\right](m-m')d\tau}_{2^{nd}\text{ order}} \quad [4.18]$$

where m and m' are the magnetic quantum numbers associated with two unique coherences and the variables α, β and η_Q have their previous meaning (90). Clearly this interaction has no effect on the zero-quantum coherences (m = m'), whereas the anti-diagonal (m = -m') and non-diagonal ($m \neq \pm m'$) elements are dephased by second-order and both first- and second-order effects, respectively (see Eq. [4.18]). We take a moment to note, once again, that first-order effects are significantly greater than those of the second-order (MHz vs. kHz). Thus, all

coherences with $m \neq \pm m'$ will decay quickly due to the quadrupole interaction. For this reason, the primary pathway by which all coherences will proceed is along the anti-diagonal where only the second-order dephasing effects are encountered. A natural consequence of Eq. [4.18] is that for all internal interactions linear in S_z, such as e.g. CSA, their MQ evolution occurs at a frequency that is enhanced by a factor of 'p'.

Conversion and Observation of Multiple-Quantum Coherences

The conversion of the MQ transitions into observable, single-quantum coherence requires manipulating the density matrix in a fashion similar to that used during the creation sequence. Figure 4.6 illustrates the efficiency of the conversion of triple-quantum coherence into single-quantum coherence for powdered samples with spin number S equal 3/2 and 5/2 as a function of the pulse angle $\theta_2 = 360^\circ \nu_{rf} t_2$ (12). In general, the curves resemble those for the triple-quantum excitation process, although the 3Q $\rightarrow$ -1Q conversion process is much less efficient. The two maxima present in some curves of Figures 4.5 and 4.6 correspond to the intensities 'arriving' via two different pathways: the more efficient pathway being along the anti-diagonal (first maximum), and the less efficient one along the non-diagonal (second maximum). Unlike the excitation pulse which has only to maximize the amount of $\pm$ 3Q coherence, the conversion pulse must simultaneously bring two unique states to the same single-quantum state for observation: $0 \rightarrow -3(t_1) \rightarrow -1(t_2)$ and $0 \rightarrow +3(t_1) \rightarrow -1(t_2)$. Note that these pathways are not symmetric, as they involve two- versus four-quantum jumps, respectively. For spin-3/2 nuclei, the first of these two pathways is the refocusing or echo

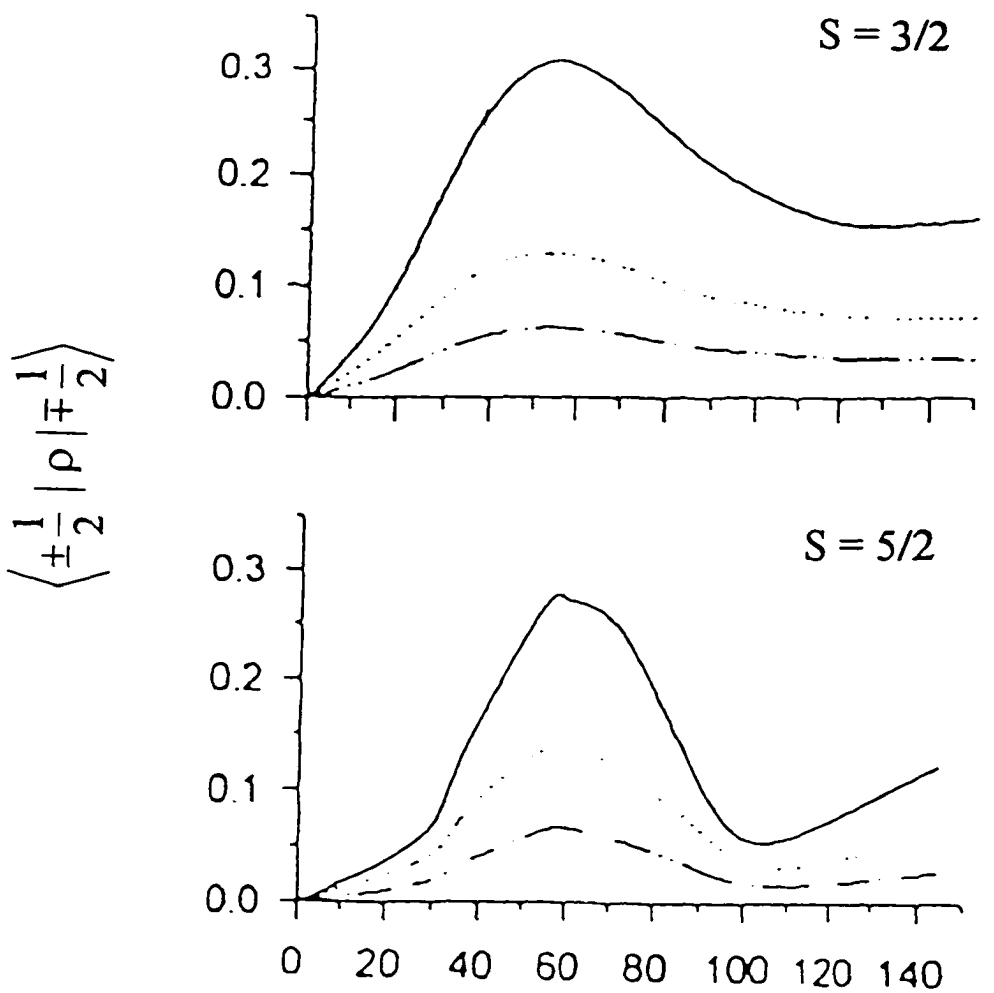

Figure 4.6: Efficiency of the conversion from triple-quantum to single-quantum coherence as a function of pulse angle, θ. Computational and experimental conditions are the same as those used in Fig. 4.5.

pathway, while the second pathway serves as the 3Q echo pathway for S = 5/2, 7/2 or 9/2 quadrupolar nuclei. While the refocused (echo) pathway possesses the desired information, signal from both the echo and anti-echo (non-refocused) pathways are needed, with equal intensity, in order to obtain pure absorption-mode two-dimensional spectra (see below).

Experimental Results

The quadrupolar and chemical shift isotropic information can be obtained from the spectra generated using this simple two-pulse MQMAS sequence. While Figures 4.5 and 4.6 show what the optimum pulse angle should be for both pulses, they do not illustrate what effects the rf field strength, ν_{rf}, and MAS speed, ν_{rot}, have on the resulting spectra. We do know from the "Excitation to 3Q Coherences" section, however, that for our experiments it is beneficial to minimize the ratio ν_Q / ν_{rf}. This suggests that one should use as high a value as possible for ν_{rf}. Our findings support this supposition. While MAS is required if one wants to average the SOQE, since it is one of the two required degrees of freedom, what effect does the magnitude of the spinning speed have on the resulting NMR spectrum? Figure 4.7 displays the isotropic projections of the 3QMAS spectra of ^{23}Na in $Na_2C_2O_4$ recorded for several values of ν_{rf}, and ν_{rot}. These sodium oxalate spectra, $Na_2C_2O_4$ (η_Q = 0.77, C_Q = 2.43 MHz), were acquired at 105.8 MHz using a 3.2 mm Chemagnetics MAS probehead (90). The spectra, denoted 100/5, 100/10 ...300/20, were acquired using three rf fields for the multiple-quantum conversions (ν_{rf} = 100, 200, and 300 kHz) and three rotation speeds (ν_{rot} = 5, 10, and 20 kHz). For a constant value of ν_{rf}, the spectra in this Figure show a strong

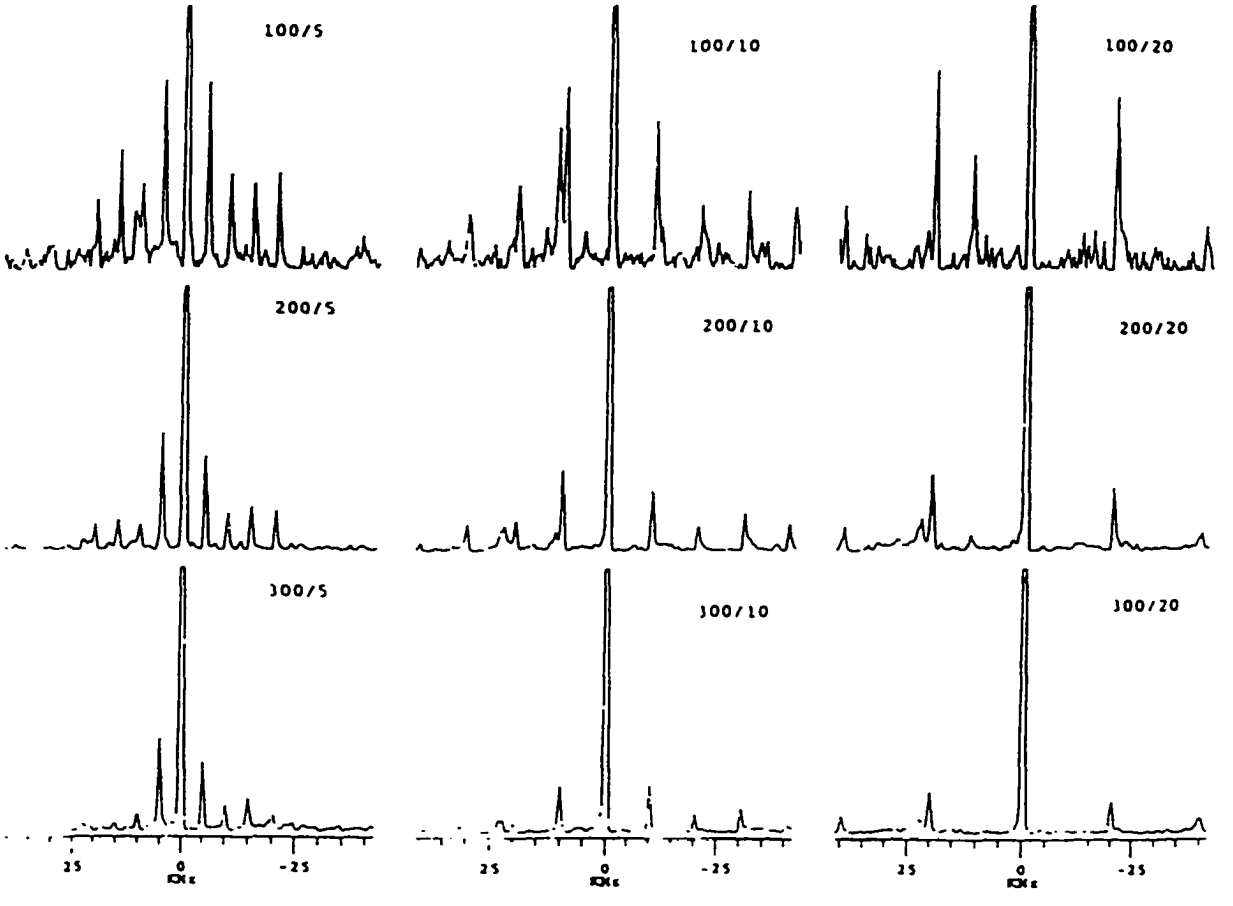

Figure 4.7: Projections of sheared 23Na 2D MQMAS spectra of Na2C2O4 onto the isotropic axis. RF field ν_{rf} = 100 (a-c), 200 (d-f) and 300 (g-i) kHz; spinning speed ν_{rot} = 5 (a,d,g), 10 (b,e,h), and 20 (c,f,i) kHz.

dependence on ν_{rot}, which is in agreement with previous work (91). More noticeable, however, are the changes in the sideband patterns obtained when ν_{rf} is varied and ν_{rot} is kept constant. Comparison of spectra a, d, and g; b, e, and h; or c, f, and i indicates that (i) for a fixed spinning speed the number and relative intensity of the sidebands decreases with increasing ν_{rf}, and (ii) the overall width of the sideband pattern increases at higher spinning speeds. As each experiment was independently optimized for each value of ν_{rf}, we conclude that the changes observed originate from (i) rotor-driven reorientations that the quadrupole tensors undergo during the evolution period, t_1, and (ii) different evolution of the spin density matrix during the first rf pulse (90,91).

The benefits of using the highest available values for ν_{rf} and ν_{rot} are apparent when comparing spectra 100/5 and 300/20 (ν_{rf} and ν_{rot}, respectively). In this case, the centerband intensity observed was increased by a factor of ~9 and the overall efficiency increased by 50% using the 300/20 kHz settings. Since signal intensity is proportional to the square root of the number of acquisitions, this 9-fold increase corresponds to a reduction of ~80 in the required experimental time. In addition, the 300/20 spectra is essentially free of spinning sidebands, which facilitates analysis of complex spectra.

Pure Absorption Mode Spectrum in 2D NMR

Only in a pure absorptive 2D NMR spectrum can one effectively extract the distribution of the quadrupolar and chemical shift parameters. To acquire such a spectrum however, it is essential that one retain signal from both the 'echo' and 'antiecho' pathways

(47). Failure to do this yields spectra consisting of 2D 'phase-twisted' lineshapes, which lower the spectrum's resolution and introduce dispersive cancellation effects. The original MQMAS data suffered these drawbacks (43). Two techniques that provide for the acquisition of pure absorption spectra are time-proportional phase incrementation (TPPI) and the hypercomplex method (92-94). Utilizing these techniques, a number of pure absorption mode procedures have recently been developed for the processing of MQMAS data (44,78,79,83,84). Although TPPI and hypercomplex both accomplish the same task, we will only describe the hypercomplex method in our discussion here.

Using quadruture detection in a 1D experiment, the procession of the transverse magnetization, $S_{\pm}(t)$, is acquired along two orthogonal axes simultaneously, i.e. x- and y-axis. This process make it possible to determine the sign, $+\omega$ or $-\omega$, of the evolving coherences. In the computer, this information is stored in separate buffers. After complex Fourier transformation (FT) into the frequency domain, the transform is evaluated as

$$S(\omega) = \int_0^{\infty} S(t) \exp(-i\omega t)\, dt = A(\omega) + iD(\omega) \qquad [4.19]$$

yielding both absorptive (A, real) and dispersive (D, imaginary) lineshapes. Using the notation of A.P.M. Kentgens (95), an illustration of these ideas are depicted below in Table 4.1 and Figure 4.8. In these, the symbols F and ω represent frequency with units of (cycles/sec) and (radians/sec), respectively.

In a 2D NMR experiment a series of complex FIDs are collected as a function of t_1. Data collection in the t_1-dimension can be either frequency- or amplitude-modulated. When the signal from the echo and antiecho pathways are combined with equal amplitude, the data

Table 4.1: Results of processing a cosine or sine signal using a cosine or sine frequency transformation. Fourier transforms are $\cos(\omega t) \pm i \sin(\omega t)$.

Signal	Fourier Transform	Result
Cos (Ft)	Cos (ωt)	A(ω)+A(-ω)
Cos (Ft)	Sin (ωt)	D(ω)-D(-ω)
Sin (Ft)	Cos (ωt)	D(ω)+D(-ω)
Sin (Ft)	Sin (ωt)	-A(ω)+A(-ω)

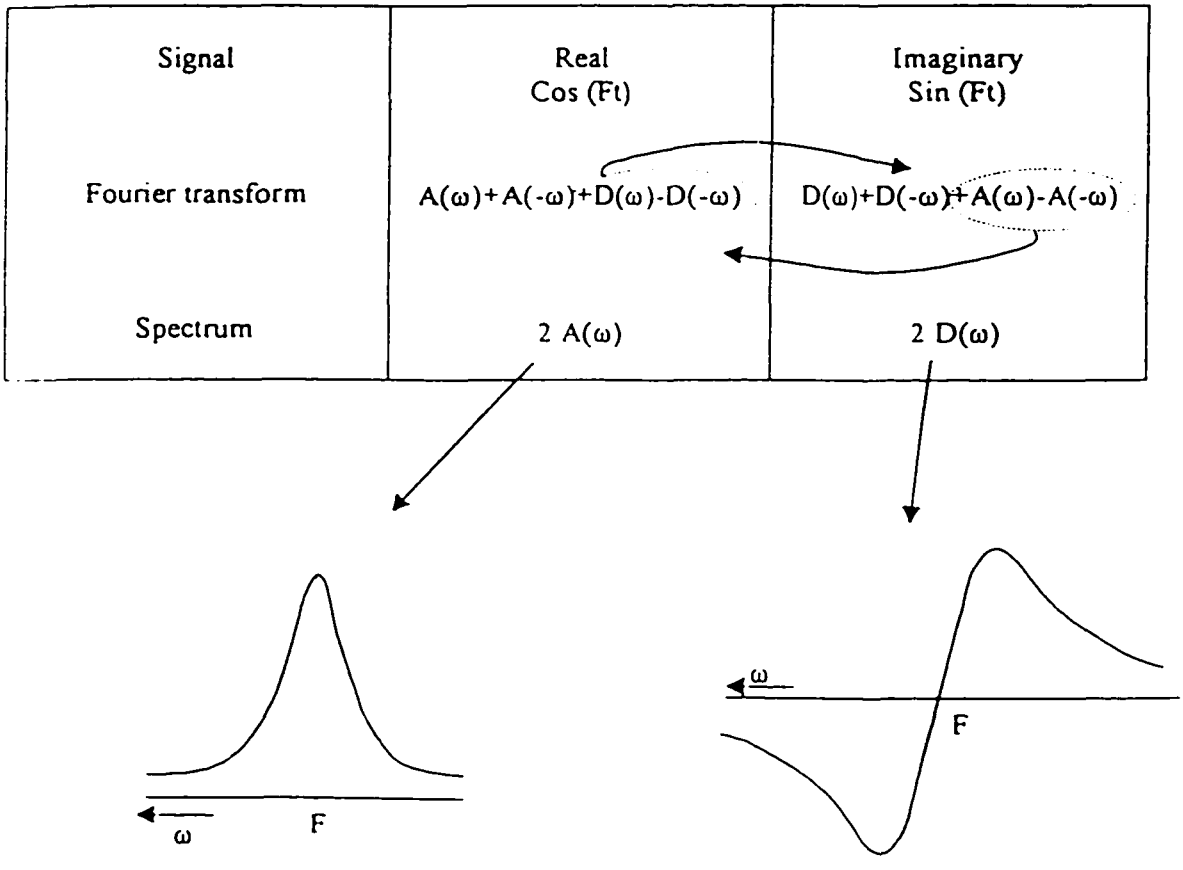

Figure 4.8: Presentation of a NMR signal obtained using quadruture detection, an d the spectra resulting after Fourier transformation (FT). 'A" and 'D' stand for absorptive and dispersive, respectively.

in the t_1-dimension will be amplitude-modulated. If each pathway is selected individually, however, then the signal in t_1 will be phase-modulated (47). The information from both pathways is required to obtain pure absorption spectra. Although either form of modulation can be used to obtain pure phase spectra, we will use the amplitude-modulated procedure for this discussion. After complex Fourier transformation (FT) of the spectrum in the t_2-dimension (Eq. [4.19]), a complex interferogram for the t_1 dimension is produced by combining the n^{th} point of the real and imaginary buffer of each FT row of data; in other words, a slice is taken through the spectrum along the t_1 dimension. Unlike the simple 1D FT experiment described above, complex FT of either the frequency- or amplitude-modulated t_1-dimension does not result in purely absorptive and dispersive lineshapes, but in a superposition of the two. The processing steps leading to these 'phase twisted' spectra are analogous to those used in the t_2-dimension. The signals they yield are

$$S_{fm}(\omega_1,\omega_2) = A_1(\omega_1)A_2(\omega_2) - D_1(\omega_1)D_2(\omega_2) \qquad [4.20]$$

and

$$S_{Am}(\omega_1,\omega_2) = [A_1(\omega_1) + A_1(-\omega_1)]A_2(\omega_2) + [-D_1(\omega_1) + D_1(-\omega_1)]D_2(\omega_2) \qquad [4.21]$$

for the frequency- and amplitude-modulated signals, respectively. If, however, the FID in t_1 is amplitude-modulated, and only a real complex FT is applied in that dimension, then a pure absorption phase spectrum can be obtained with signal (95)

$$S_{Am}(\omega_1,\omega_2) = (A_1(\omega_1) + A_1(-\omega_1))A_2(\omega_2). \qquad [4.22]$$

Unfortunately, since the transformation will be symmetric about the carrier frequency, $\omega_1 = 0$, no discrimination as to the sign of the frequency evolution will be obtained, e.g., $+\omega_1$ or $-\omega_1$.

In the hypercomplex technique, the superposition problem is addressed by acquiring separately both a cosine (S_X) and sine (S_Y) modulated signal for each t_1 data point (47). These two signals are varied in phase by 90° by shifting the preparation pulse by $\pi/(2|p|)$ where p is the order of coherence existing during the t_1 evolution period. Each FID acquired will be a linear combination of both the echo (refocusing) and antiecho (non-refocusing) signal. The collected time-domain signals can then be rearranged so as to construct the echo and anti-echo signals, exclusively. For a quadrupole spin-3/2 nucleus, the equations for these pathways are (84):

$$S_{echo} = S_X(t_1, t_2) + i\, S_Y(t_1, t_2) \qquad [4.23]$$

$$S_{anti} = S_X(t_1, t_2) - i\, S_Y(t_1, t_2). \qquad [4.24]$$

(For spins 5/2, 7/2, and 9/2, the assignment of the triple-quantum pathways is reversed.) Each pathway's signal can be complex Fourier transformed and phase corrected in both dimensions and their absorption spectrum combined, $S(\omega)_{echo} + S(\omega)_{anti\text{-}echo}$, to yield a pure-absorption spectrum. Similarly, one can complex FT the cosine or sine modulated signals directly, and combine them prior to the second FT. In this scenario, each signal is FT in the t_2 (ω_2) dimension (84).

$$S(0,0)\cos(\omega_1 t_1)\exp(i\omega_2 t_2) \xrightarrow{FT} S(0,\omega_2)\cos(\omega_1 t_1)[A(\omega_2) + iD_2(\omega_2)] \qquad [4.25]$$

$$S(0,0)\sin(\omega_1 t_1)\exp(i\omega_2 t_2) \xrightarrow{FT} S(0,\omega_2)\sin(\omega_1 t_1)\left[A(\omega_2)+iD_2(\omega_2)\right]. \quad [4.26]$$

Then, after proper phase correction in the ω_2 dimension, the imaginary component of each signal is eliminated and the real components combined to form one set of 2D complex data

$$S(t_1,\omega_2) = S(t_1,\omega_2)\left[\cos(\omega_1 t_1)+i\sin(\omega_1 t_1)\right] A_2(\omega_2). \quad [4.27]$$

Finally, a complex FT with respect to t_1 (ω_1) will yield a spectrum whose real part is pure absorption, $A(\omega_1)A(\omega_2)$.

Shearing and Extracting the Isotropic Information from the MQMAS Spectrum

It has been shown that inhomogeneous quadrupolar broadening that is spread along a ridge with slope $|A_4(S,p)|/A_4(S,-1)$ in the time-domain can be Fourier transformed into a spectrum with pure absorption. However, the main purpose of the MQMAS experiment is to obtain a spectrum from which the isotropic chemical and second-order quadrupolar isotropic shifts can be readily extracted. In the pure absorption-mode spectrum, the isotropic echo information is correlated along a gradient between the two axes with slope

$$\omega_1 = \frac{|A_4(S,p)|}{A_4(S,-1)}\,\omega_2 \quad \text{or} \quad \omega_1 = R(S,p)\,\omega_2. \quad [4.28]$$

The MQMAS experiment utilizes this correlation between the two axes as a means of separating the combined effects of the isotropic chemical and quadrupole-induced shifts (CS and QIS, respectively) into individual components. This is done by taking advantage of the fact that their shifts evolve differently in the multiple- and single-quantum dimensions, ω_1 and

ω_2, respectively. The correlation between the evolution of these two shifts in each dimension are

$$\nu_1^{cs} = p\nu_2^{cs}\ (\text{Hz}) \qquad \text{or} \qquad \delta_1^{cs} = \delta_2^{cs}\ (\text{ppm}) \qquad [4.29]$$

and

$$\nu_1^{QIS} = \frac{A_0(S,p)}{A_0(S,-1)} \cdot \nu_2^{QIS} = \xi(S,p) \cdot \nu_2^{QIS}\ (\text{Hz}) \qquad [4.30]$$

or

$$\nu_2^{QIS} = \frac{\xi(S,p)}{p} \cdot \nu_2^{QIS}\ (\text{ppm})\,. \qquad [4.31]$$

Thus MQMAS makes possible the separation of resonances that share a similar CS but differ in their QIS.

While MQMAS allows for separation of the isotropic shifts, each resonance will still be skewed relative to the ω_1 axis along a line with slope R(S,p) (see Eq. [4.28]). In order to isolate the isotropic shift, one must project the 2D spectrum onto an axis that is orthogonal to the resonance ridges (44,47). Rather than calculating a skew projection, however, an easier process is to perform a shearing transformation on the data such that the resonance ridges lie parallel to the ω_2-axis. After shearing, the isotropic spectrum can be easily obtained from a simple projection of the final 2D spectrum onto the ω_1-axis. Although shearing can be applied after the spectrum is fully transformed, e.g. $S(\omega_1,\omega_2)$, to avoid interpolation problems, it is best to apply the shearing transformation while in the mixed time-frequency-domain, $S(t_1,\omega_2)$ (47). Massiot et al. (84,92) have shown that this shearing transformation corresponds to the application of a t_1-dependent first-order phase correction of form (47)

$$S'(t_1',\omega_2') = \exp[-i\,R(S,p)\omega_2 t_1]\cdot S(t_1,\omega_2)\,. \qquad [4.32]$$

Note that this phase correction reduces the spectral widths in the ω_1-dimension by a factor of $[R(S,p)+1]^{-1}$ (84,92,96). Additionally, the shearing transformation requires that the data be complex. Thus, if amplitude-modulation was used to acquire the data, then sign discrimination has to be restored and the echo and antiecho pathways fully separated before the shearing transformation can be performed. The shearing equations take the form (84)

$$S'_{echo}(t_1',\omega_2') = \exp[-i\,R(S,p)\omega_2 t_1]\cdot S_{echo}(t_1,\omega_2) \qquad [4.33]$$

$$.S'_{anti}(t_1',\omega_2') = \exp[-i\,R(S,p)\omega_2 t_1]\cdot S_{anti}(t_1,\omega_2)\,. \qquad [4.34]$$

After each pathway is Fourier transformed in t_1', the signals are then combined according to

$$S(\omega_1',\omega_2') = S'_{echo}(\omega_1',\omega_2') + S'_{anti}(-\omega_1',\omega_2')\,. \qquad [4.35]$$

An isotropic projection onto the ω_1'-axis of the data now contains only information from the isotropic shifts. For a spin-3/2 and spin-5/2 nucleus, the positions of the resonances (in ppm) in the isotropic projections are given by, respectively,

$$\delta_{iso} = \frac{17}{8}\delta + \frac{1x10^6}{8}\cdot\frac{\omega_Q^2}{\omega_0^2}\left(\frac{\eta^2}{3}+1\right) \qquad [4.36]$$

$$\delta_{iso} = -\frac{17}{31}\delta + \frac{8x10^6}{93}\cdot\frac{\omega_Q^2}{\omega_0^2}\left(\frac{\eta^2}{3}+1\right) \qquad [4.37]$$

where δ is the difference between the chemical shift and the reference frequency. Note that the fractions prior to the δ terms in the equations above show that reference offsets in the

single-quantum dimension need to be multiplied by (-p+R(S,p)) / (1+R(S,p)) when used in the isotropic δ_{iso} dimension.

The purely isotropic data of the ω_1-dimension can now be teamed with the single-quantum MAS data of the ω_2-dimension to solve for the exact isotropic chemical- and quadrupolar shifts. For spin-3/2 nuclei these terms will be:

$$\delta_{iso} = \frac{17}{8}\delta + \frac{1x10^6}{8}\cdot\frac{\omega_Q^2}{\omega_0^2}\left(\frac{\eta^2}{3}+1\right) \qquad [4.38]$$

$$\delta_2 = \delta + 3\cdot\frac{\omega_Q^2}{\omega_0^2}\left(\frac{\eta^2}{3}+1\right) + A_4(S,p)B(\theta,\varphi,\eta)P_4(\cos\beta) \qquad [4.39]$$

Although the data for δ_2-dimension still contains the fourth-rank anisotropic functions, its functional form shows that in a random powder distribution, its center of mass is identically zero; a model-free first moment analysis of a site's centerband along the δ_{iso} and δ_2 dimensions then breaks down to a straightforward calculation of two equations and two unknowns (44).

Figure 4.9 displays the transformation steps as applied to the two-dimensional ^{27}Al MQMAS NMR of an $AlPO_4$ chabazite-like aluminophosphate sample. Note in Figure 4.9b that the first FT with respect to t_2, e.g. $S(t_1,\omega_2)$, leaves the data skewed along the t_1-axis. Application of a first-order t_1-dependent phase correction, $\exp[-i\,R(S,p)\omega_2 t_1]\cdot S(t_1,\omega_2)$, to the mixed time-frequency data, aligns the skewed data parallel to the ω_2-axis (see Fig. 4.9c). Completion of the data processing is accomplished by transforming the 'sheared' data, $S'(t_1',\omega_2')$, with respect to the t_1' isotropic axis. For this sample, the following values for the isotropic chemical shift and isotropic second-order quadrupolar shift, δ_{cs}^{iso} and ν_Q^{iso}, were

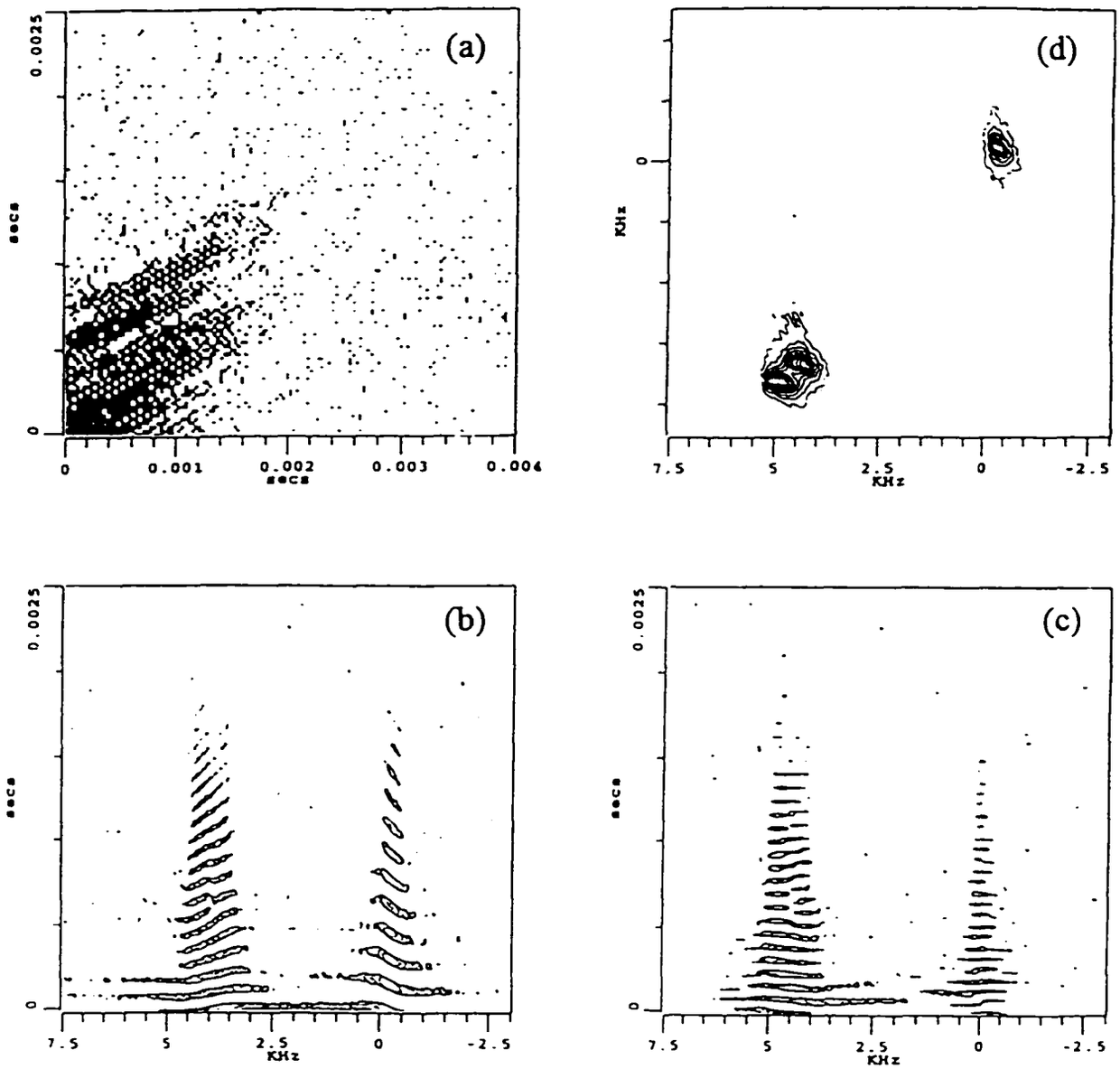

Figure 4.9: 2D ^{27}Al MQMAS spectrum of an $AlPO_4$ sample. Fig. 4.9a shows the time domain data. Fig. 4.9b shows the data after FT in the t_2-dimension. Fig. 4.9c shows the data after shearing in the mixed frequency-time domain. Shearing uses a first-order t_1 dependent phase correction. $\exp[i\nu_2 t_1 |A_4(S,p)| / A_4 S,-1)|$ Fig. 4.9d shows the final pure absorption spectrum.

measured to be: δ_{cs}^{iso} of -4.5, 43.9 and 47.6 ppm, and ν_Q^{iso} of 0.9, 2.0, and 2.6 MHz for sites Al_1, Al_2, and Al_3, respectively. It is worth noting that previous single-quantum approaches require variable magnetic field measurements, B_0, or iterative computational lineshape fits for achieving a similar distinction among the isotropic quadrupolar and shielding contributions.

Conclusions

In Chapter 4, we presented a detailed discussion regarding the acquisition of high-resolution quadrupolar NMR spectra using the MQMAS technique. Using MQMAS, inequivalent atomic sites can be resolved and their isotropic chemical and quadrupolar shifts determined directly from the spectrum. With this data known, other quadrupolar parameters, e.g. e^2qQ/h and η, can be extracted using anisotropic 1D spectra and computer simulations. The MQMAS technique is remarkably straightforward and, unlike DAS and DOR, can be readily performed on any modern spectrometer using only a conventional MAS probe. Pulse lengths used in the MQMAS experiment are optimized primarily according to the spin number S, and the ν_Q / ν_{rf} ratio. Additional advantages are gained by using high spinning speeds and by incorporating a z-filter within the experiment. The benefits of using the high spinning speed and optimized pulse lengths of the highest rf power available are shown in Figure 4.7.

CHAPTER 5. MULTIPLE-QUANTUM MAGIC-ANGLE SPINNING NMR WITH CROSS POLARIZATION: SPECTRAL EDITING OF HIGH-RESOLUTION SPECTRA OF QUADRUPOLAR NUCLEI

A paper published in Solid State NMR

M. Pruski[1], D.P. Lang[1], C. Fernandez[2], and J.P. Amoureux[2]

[1]Ames Laboratory, 230 Spedding Hall, Ames, IA 50011, USA

[2]Laboratoire de Dynamique et Structure des Matériaux Moléculaires, CNRS URA 801, Université des Sciences et Technologies de Lille, F-59655 Villeneuve d'Ascq Cedex, France

Abstract

An experiment is presented that combines the multiple-quantum magic angle spinning (MQMAS) technique with cross polarization (CP). As a preliminary test of this new method, we measured and compared the ^{27}Al 3QMAS and ^{19}F$\rightarrow$^{27}Al CP 3QMAS spectra of a fluorinated $AlPO_4$ aluminophosphate. A complete discrimination between the fluorinated and nonfluorinated Al sites was easily achieved, which demonstrates the usefulness of CP MQMAS for spectral editing. Future applications of this experiment will include other spin pairs and heteronuclear correlation NMR spectroscopy.

Keywords: multiple-quantum MAS NMR of quadrupolar nuclei; cross polarization; aluminophosphate

Short Communication

Several techniques have recently been proposed to overcome the anisotropic line broadening in the NMR spectra of half-integer quadrupolar nuclei in solids.[1-5] This broadening arises from the interaction of the nonspherical charge distribution of a nucleus with the gradient of the surrounding electric field. The first order corrections to the Zeeman energy levels are comparable to the quadrupolar frequency and are typically in the MHz range. However, the central -1/2 ↔ 1/2 transition remains unaffected to first order by quadrupolar broadening, and thus has attracted most of the research interest.[6-8]

The time averaged quadrupolar frequency corresponding to any symmetrical (-m ↔ m) transition in a fast rotating sample can be calculated following second order perturbation theory. According to Amoureux,[3] this frequency is written as

$$\nu_p^Q = \frac{Q_{cc}^2}{\nu_0}\left[A_0(I,p)B_0^Q(\eta_Q) + A_2(I,p)B_2^Q(\eta_Q,\alpha_Q,\beta_Q)P_2(\cos\theta) + A_4(I,p)B_4^Q(\eta_Q,\alpha_Q,\beta_Q)P_4(\cos\theta)\right]. \quad (1)$$

The resonance frequency also includes the chemical shift

$$\nu_p = \nu_p^{CS} + \nu_p^Q, \quad (2)$$

with

$$\nu_p^{CS} = p\nu_0\left[\sigma_{iso} + B_2^{CS}(\eta_{CS},\alpha_{CS},\beta_{CS})P_2(\cos\theta)\right]. \quad (3)$$

In the above equations $p = 2m$, ν_0 is the Larmor frequency, and I, Q_{cc}, η_Q, η_{CS} and σ_{iso} have their usual meaning. The terms $A_i(I,p)$, $i = 0,\ 2,\ 4$, are known functions of the quantum numbers I and p, whereas $B_2^{CS}(\eta_{CS},\alpha_{CS},\beta_{CS})$, $B_0^Q(\eta_Q)$, $B_2^Q(\eta_Q,\alpha_Q,\beta_Q)$ and $B_4^Q(\eta_Q,\alpha_Q,\beta_Q)$ depend on the orientation of the chemical shift and quadrupole tensors with respect to the

rotor axis.[3] Finally, $P_2(\cos\theta)$ and $P_4(\cos\theta)$ are the second- and fourth-order Legendre polynomials of $\cos\theta$, with θ being the angle between the static field $\vec{B}_0$ and the rotation axis.

It is well known that $P_2(\cos\theta)$ and $P_4(\cos\theta)$ do not have a common root. Therefore, the second order broadening of the -1/2 ↔ 1/2 transition can only be scaled, but not completely removed, by rotating the sample around a single axis. However, complete line narrowing can be achieved by making the spinning angle θ time dependent. Such experimental capabilities were developed in the late 1980's and involved sample rotation around two axes: either simultaneously in a one-dimensional technique called double rotation (DOR),[1] or in succession using a two-dimensional dynamic angle spinning (DAS) method.[2]

Most recently, Frydman et al. have performed a novel multiple-quantum experiment in which the second order averaging was achieved by keeping θ fixed and using p as an independent variable.[4,5] The most favorable choice of the rotation axis for this technique is the magic angle, $\theta = 54.7°$. Magic angle spinning (MAS) nullifies the $P_2(\cos\theta)$ term thereby eliminating the chemical shift anisotropy (CSA), and has the additional effect of reducing the dipolar interactions.[3-5] In such a case, only the last term in Eq. (1) contributes to the anisotropic line broadening. However, the phase evolutions of the p-quantum coherence in t_1 and the single quantum coherence in t_2 can be correlated by generating a purely isotropic echo at

$$t_2 = \left| A_4(I,p) / A_4(I,-1) \right| t_1 . \qquad (4)$$

This two-dimensional experiment is referred to as multiple-quantum magic angle spinning (MQMAS).[4] Being technically straightforward, the MQMAS experiment offers an attractive

method for the study of a variety of important groups of materials, including catalysts,[9-11] glasses,[12] and other amorphous and crystalline inorganic solids.[12-14] Several experimental strategies aimed at increasing the efficiency of multiple-quantum coherence excitation,[13-17] and obtaining the pure-phase 2D spectra,[13,14,17] have recently been proposed. It should be noted, however, that the efficiency of multiple-quantum excitation and conversion strongly depends on the quadrupole coupling constant, therefore, caution must be exercised when analyzing the intensities in the MQMAS spectra. One proposed strategy relies upon the MQMAS experiment in order to obtain the isotropic chemical shifts and quadrupolar induced shifts. This information can then be utilized in the computer simulations of one-dimensional, quantitative MAS spectra in order to obtain the remaining line shape parameters, including their relative intensities.[12]

In this paper we introduce a complementary experiment that produces the high resolution spectra of half-integer quadrupolar nuclei by combining MQMAS with cross polarization (CP) from spin-1/2 nuclei. This technique will be referred to as CP MQMAS. While MQMAS mainly provides information about the electronic environment of the observed nuclei as revealed by the quadrupolar and chemical shifts, the dipolar interaction with other nuclear spins is not reflected in the spectra. We propose to recover this information by utilizing the dipolar coupling between two spins, I and S, to produce nuclear magnetization of spins S via CP transfer. This polarization can then be further employed to produce high resolution spectra of spins S using the MQMAS scheme. An immediate advantage of this new approach is that it allows spectral editing of the MQMAS spectra and the direct inference of connectivities between nuclear spins.

As a preliminary test of CP MQMAS experiment, we chose the ^{19}F-^{27}Al cross polarization in a fluorinated triclinic chabazite-like $AlPO_4$ aluminophosphate. This material contains three equally populated crystallographic sites for aluminum: an Al(1) site octahedrally coordinated to four oxygen and two fluorine atoms, and two sites labeled Al(2) and Al(3) representing aluminum in AlO_4 tetrahedra. The two tetrahedral sites could not be distinguished in the ^{27}Al MAS spectra, but were clearly resolved by using 5QMAS NMR.[10] The following values were determined for the chemical shift and the second order quadrupolar effect parameter, $SOQE = C_Q\sqrt{1+\eta^2/3}$: σ_{iso} of -4.5 ppm, 43.9 ppm and 47.6 ppm, and SOQE of 0.9 MHz, 2.0 MHz and 2.6 MHz for sites Al(1), Al(2) and Al(3), respectively.[10]

The schematic diagrams of the pulse sequence and the coherence transfer pathways are shown in Figure 1. In the first step of the experiment, magnetic spin polarization is transferred from ^{19}F nuclei to the -1/2 $\leftrightarrow$ 1/2 transition coherence of the ^{27}Al nuclei using a conventional CP pulse sequence. The dynamics and efficiency of spin locking and polarization transfer in quadrupolar nuclei under MAS have recently been studied by Vega[18,19] and by Sun et al.[20] In short, for $\nu_Q >> \nu_{1S}$ the matching condition for CP is $\nu_{1I} = \left(S+\frac{1}{2}\right)\nu_{1S}$, where ν_Q, ν_{1I} and ν_{1S} denote the quadrupole frequency and the strengths of the rf fields applied to the I and S spins, respectively. The best spin locking efficiency is achieved using very weak rf fields, such that $\nu_{1S} < \nu_r$, with ν_r being the MAS rotation frequency.[19,20] Our experiment relies upon optimization of the CP conditions in order to maximize the nondiagonal elements $\rho_{+1/2,-1/2}$ and $\rho_{-1/2,+1/2}$ of the Al spins density matrix, ρ, at the end of the CP transfer. We note

that these coherences also include contributions from the direct polarization of the ^{27}Al spins, but these can be easily filtered out by alternating the phase of the ^{19}F excitation pulse. A pair of 'hard' rf pulses (labeled H in Fig. 1) of ~150 kHz were used to excite the ±3Q coherences and to transfer them back to p = 0 after the t_1 evolution period. The hard pulses were preceded and followed by 'soft' (selective) pulses (labeled S, in Fig. 1) to produce a pair of z filters. It has recently been shown that the use of z filters facilitates the maximizing and matching of the efficiencies of the symmetrical coherence pathways, and thus leads to a pure-phase observable signal.[17,21]

The 3QMAS and CP 3QMAS spectra of the fluorinated $AlPO_4$ sample were taken at 9.4 T on a Chemagnetics Infinity spectrometer using a 5 mm MAS probehead. The Hartmann-Hahn condition was established with an rf field ν_{1S} of ~5 kHz under a MAS speed of 10 kHz. The 3QMAS spectrum (Fig. 2a) was acquired using a three pulse sequence with z filtering and a 24-phase cycling scheme. This scheme consisted of 6-phase cycling for simultaneous selection of the ±3Q coherence pathways, and included CYCLOPS to eliminate the receiver artifacts. Several phase cycling schemes were successfully combined with the CP 3QMAS experiment. The spectrum of Fig. 2b was acquired using a 48-phase cycling scheme, which consists of 2-phase cycling of the ^{19}F pulse, 2-phase cycling of ϕ_1, 6-phase cycling of ϕ_3 and 2-phase cycling of ϕ_4. In both experiments the hypercomplex method was used to produce pure-phase 2D spectra.

The results of Figure 2 demonstrate the spectral editing capability offered by CP MQMAS: while three resolved resonance lines representing Al(1), Al(2) and Al(3) were

detected using 3QMAS, the CP 3QMAS method produced a single resonance representing Al(1), the only aluminum site that is coordinated to fluorine. Further extensions of this work will include: (i) other pairs of nuclei, and (ii) heteronuclear correlation experiments, similar to those performed earlier with MAS[22] and DAS.[23] A gain in signal to noise should not, however, be expected from this experiment, as in most cases the polarized spins will relax faster than the polarization source.

ACKNOWLEDGEMENTS

This research was supported at Ames Laboratory by the U.S. Department of Energy, Office of Basic Energy Sciences, Division of Chemical Sciences, under Contract W-7405-Eng-82.

REFERENCES

1. A. Samoson, E. Lippmaa, and A. Pines, *Mol. Phys.*, 65 (1988) 1013.
2. K.T. Mueller, B.Q. Sun, G.C. Chingas, J.W. Zwanziger, T. Terao, and A. Pines, *J. Magn. Reson.*, 86 (1990) 470.
3. J. P. Amoureux, *Solid State Nucl. Magn. Reson.*, 2 (1993) 83.
4. L. Frydman and J.S. Harwood, *J. Am. Chem. Soc.*, 117 (1995) 5367.
5. A. Medek, J.S. Harwood and L. Frydman, *J. Am. Chem. Soc.*, 117 (1995) 12779.
6. M.H. Cohen and F. Reif, in 'Solid State Physics', ed. F. Seitz and D. Turnbull, Academic Press, New York, 1957, vol 5, p. 321.

7. A. Abragam, 'The Principles of Nuclear Magnetism', Clarendon Press, Oxford, 1961, Chaps. 6,7.

8. D. Freude and J. Haase, in 'NMR Basic Principles and Progress', ed. P. Diehl, E. Fluck and R. Kosfeld, Springer-Verlag, 1993, Vol. 29, p. 1.

9. C. Fernandez and J.P. Amoureux, *Chem. Phys. Lett.*, 242 (1995) 449.

10. C. Fernandez, J.P. Amoureux, L. Delmotte, and H. Kessler, *Microporous Materials*, 6 (1996) 125.

11. C. Fernandez, J.P. Amoureux, J.M. Chezeau, L. Delmotte, and H. Kessler, *Microporous Materials*, 6 (1996) 331.

12. S.-J. Hwang, C. Fernandez, J.P. Amoureux, J. Cho, S.W. Martin, and M. Pruski, *Solid State Nucl. Magn. Reson.*, in press.

13. C. Fernandez and J.P. Amoureux, *Solid State Nucl. Magn. Reson.*, 5 (1996) 315.

14. D. Massiot, B. Touzo, D. Trumeau, J.P. Coutures, J. Virlet, P. Florian, P.J. Grandinetti, *Solid State Nucl. Magn. Reson.*, 6 (1996) 73.

15. J.P. Amoureux, C. Fernandez and L. Frydman, *Chem. Phys. Lett.*, 259 (1996) 347.

16. G. Wu, D. Rovnyank, B. Sun and R.G. Griffin, *Chem. Phys. Lett.*, 249 (1996) 210.

17. J.P. Amoureux, C. Fernandez and S. Steuernagel, *J. Magn. Reson.*, in press.

18. A.J. Vega, *J. Magn. Reson.*, 96 (1992) 50.

19. A.J. Vega, *Solid State Nucl. Magn. Reson.*, 1 (1992) 17.

20. W. Sun, J.T. Stephen, L.D. Porter, and Y. Wu, *J. Magn. Reson.*, A116 (1995) 181.

21. S.P. Brown, S.J. Heyes, and S. Wimperis, *J. Magn. Reson.*, A119 (1996) 280.

22. C.A. Fyfe, K.C. Wong-Moon, Y. Huang, H. Grondey, and K.T. Mueller, *J. Phys. Chem.*, 99 (1995) 8707.

T.P. Jarvie, R.M. Wenslow and K.T. Mueller, *J. Am. Chem. Soc.*, 117 (1995) 570.

FIGURE CAPTIONS

Fig. 1. Pulse sequence used in the CP 3QMAS experiment.

Fig. 2. Comparison between ^{27}Al 3QMAS (a) and ^{19}F-^{27}Al CP 3QMAS (b) spectra of $AlPO_4$. Spectrum (a) was acquired using 24 scans (one phase cycle) for each of 128 experiments in t_1 and 0.3 s recycle delay. Spectrum (b) results from twice as many scans (due to 48-phase cycle used), and was taken with 5 s recycle delay. The spectra were not sheared; 'ss' denotes a spinning sideband.

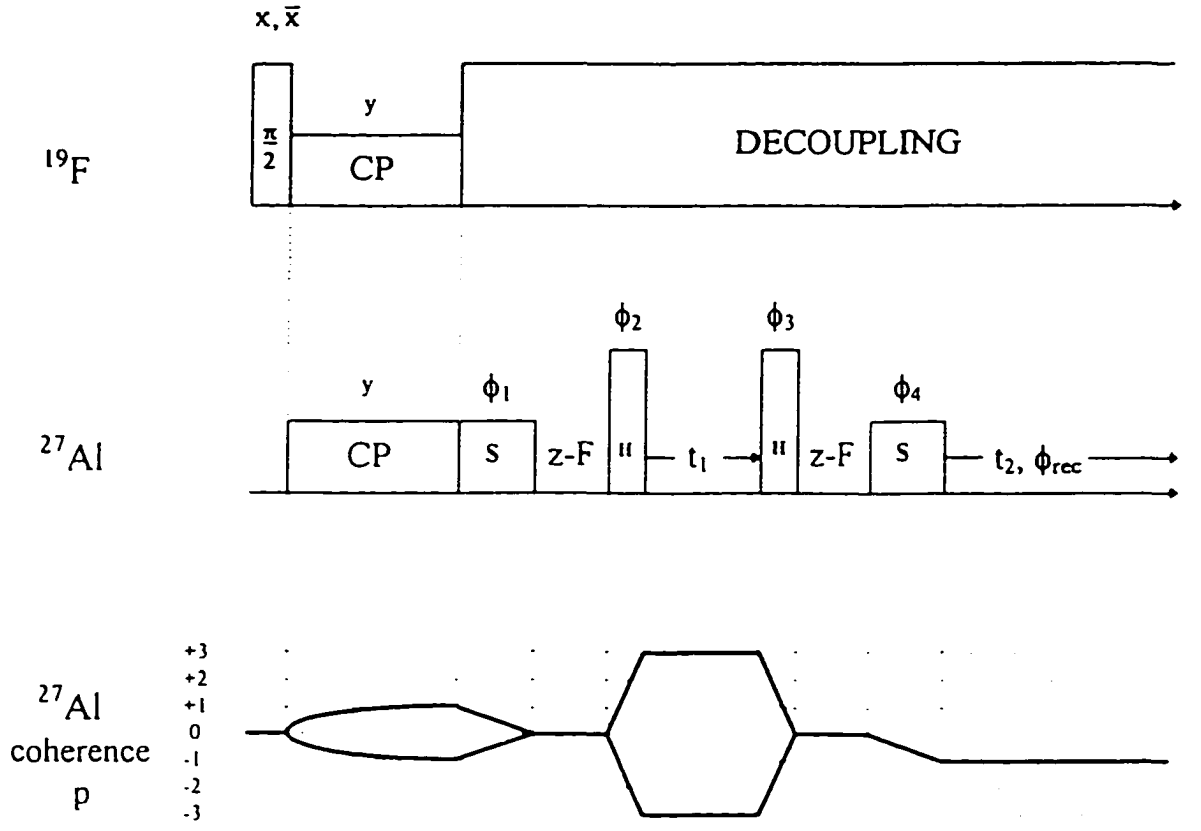
x, x̄
^{19}F
π/2
y
CP
DECOUPLING
^{27}Al
y
CP
ϕ_1
S
z-F
ϕ_2
II
t_1
ϕ_3
II
z-F
ϕ_4
S
t_2, ϕ_{rec}
^{27}Al
coherence
p
+3
+2
+1
0
-1
-2
-3

Figure 1

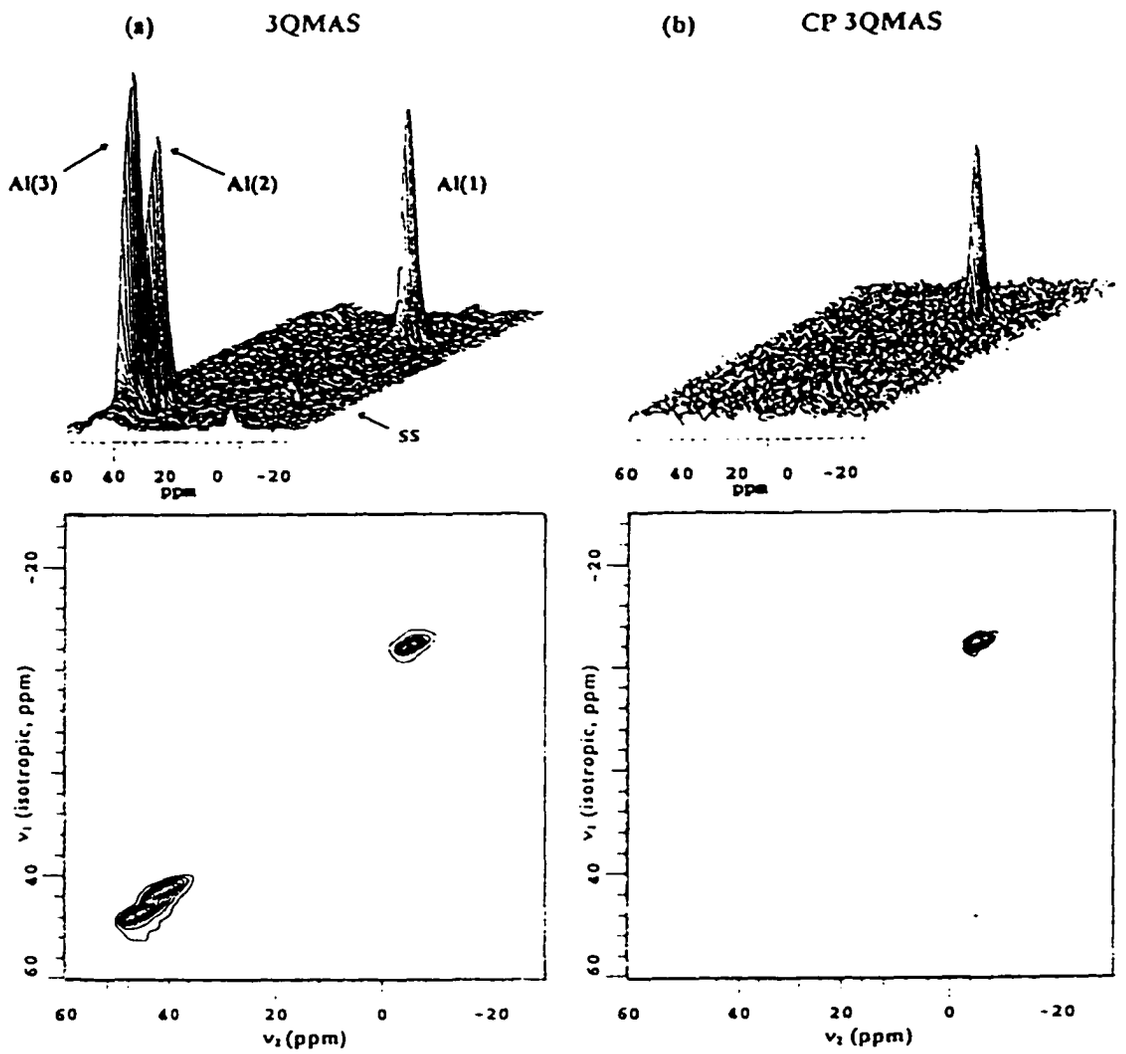
(a) 3QMAS
(b) CP 3QMAS
Al(3)
Al(2)
Al(1)
SS
60 40 20 0 -20
ppm
ν_1 (isotropic, ppm)
ν_2 (ppm)

Figure 2.

CHAPTER 6. $^{27}Al\{^{1}H\}$ CROSS POLARIZATION TRIPLE QUANTUM MAGIC-ANGLE SPINNING NMR

A paper published in Journal of the American Chemical Society

C. Fernandez, L. Delevoye, J.-P. Amoureux

Laboratoire de Dynamique et Structure des Materiaux Moleculaires,
CNRS URA 801, 59655 Villeneuve d'Ascq Cedex France

D. P. Lang and M. Pruski

Ames Laboratory, 230 Spedding Hall, Ames, Iowa 50011, USA

Abstract

An experiment is described that produces multiple quantum magic angle spinning (MQMAS) NMR spectrum of ^{27}Al via ^{1}H cross polarization (CP). An application of this new technique to the study of a fully hydrated $AlPO_4$-11 aluminophosphate is presented. It is shown that a combination of MQMAS and CP MQMAS provides new insight into the structure of this sample. While MQMAS alone can be used to obtain high-resolution spectra and quantitative information on the distribution of Al sites, CP MQMAS allows one to establish the positions of water molecules within the $AlPO_4$-11 framework.

Introduction

Spectral resolution for solid state NMR of quadrupolar nuclei has recently been enhanced with the development of the multiple quantum magic angle spinning (MQMAS) method by L. Frydman and J. S. Harwood.[1] Several improvements have been made to this technique during the last year. These include optimization of the conditions for excitation of multiple quantum (MQ) coherences,[2,3] the development of different methods to produce pure-absorption spectra,[4-8] and the elimination of spinning sidebands in the MQ dimension using synchronization of the dwell time with the rotor period.[9] The sensitivity of the triple quantum (3Q) MQMAS technique has proved to be excellent for many applications dealing with several important quadrupolar nuclei, e.g., ^{23}Na,[5,6,8,10] ^{11}B,[11] ^{87}Rb,[4,5] and ^{27}Al.[5,6,12-14] For ^{27}Al, quintuple quantum (5Q) MQMAS spectra have also been obtained,[15-18] leading to significant improvement in resolution. Compared to other high resolution techniques such as double rotation (DOR) and dynamic angle spinning (DAS),[19-21] which suffer from mechanical limitations, the MQMAS method is relatively easy to use. The basic MQMAS technique can be further enhanced by incorporating it with cross polarization (CP).[22,23] The authors have shown recently that such a CP MQMAS experiment is possible between ^{19}F and ^{27}Al in a fluorinated triclinic chabazite-like $AlPO_4$ aluminophosphate.[24] A clear discrimination between the fluorinated and nonfluorinated Al sites was achieved, which demonstrated the utility of CP MQMAS for spectral editing. In this paper, we show the first CP MQMAS experiment between ^{1}H and ^{27}Al spins and provide a detailed description of the experimental method used. Furthermore, we show that MQMAS can be used to obtain quantitative determination

of the distribution of aluminum sites in a sample. The experiments were performed using a fully rehydrated form of $AlPO_4$-11 aluminophosphate[25] and their results will be compared with those obtained earlier using MAS,[26] DOR,[26-28] and CPDOR[29,30] techniques.

The High-Resolution MQMAS Experiment

The MQMAS method is a two-dimensional (2D) experiment capable of averaging the second-order quadrupolar interaction of half-integer nuclear spins (S>1/2).[1] Briefly, in the fast MAS speed limit, the lineshape of the MQ powder spectrum of quadrupolar nuclei is governed by the expression[31]

$$\delta(\alpha,\beta) = \delta_{CS} + \delta_{QIS}(S,p,C_Q,\eta) + A_4(S,p)B_4(\alpha,\beta,C_Q,\eta) \qquad [1]$$

where $\delta(\alpha,\beta)$ represents the resonance shift (in ppm), as a function of the polar angles α and β describing the orientation of the rotor axis with respect to the quadrupolar tensor, δ_{CS} is the isotropic chemical shift, δ_{QIS} is the quadrupolar induced shift, p is the order of the MQ coherence corresponding to the non-diagonal elements (+p/2,-p/2) of the density matrix, while C_Q and η are the quadrupolar coupling constant and asymmetry parameter, respectively. A_4 and B_4 terms were given explicitly in ref. (31). The ppm scale is defined with respect to the apparent Larmor frequency $-p\nu_0$. The MQMAS experiment is designed to refocus the anisotropy of the quadrupolar interaction, which is represented by the third term in eq. 1. This refocusing is achieved by correlating the evolution of the MQ coherences $(\pm p/2, \mp p/2)$

during t_1 and the observable single-quantum central transition coherence (-1/2,+1/2) during t_2. Using the pulse sequence shown in Figure 1a, an echo is observed at

$$t_{2e} = |A_4(S,p) / A_4(S,-1)| t_1 = Rt_1 \qquad [2]$$

Echoes are generated in a two-dimensional way by incrementing t_1. A 2D Fourier transformation with respect to t_1 and t_2 leads to the MQMAS spectrum. Among the different procedures used to obtain pure-absorption 2D spectra,[4-8] we found the z-filter method[7] to be the most advantageous (see below)..

The typical MQMAS spectra of polycrystalline samples consist of narrow two-dimensional ridges that are extended along the direction given by the R/p ratio.[15] An orthogonal projection of this 2D spectrum onto the F_2 dimension resembles the conventional MAS spectrum, although with pQ-filtered intensities. The F_1 projection corresponds to the p-quantum spectrum. The analysis of the MQMAS spectra is assisted by applying a shearing transformation that places the anisotropic direction perpendicular to the isotropic axis, F_1^{ISO}. Such a transformation can be performed either in the frequency domain or in the time domain using the phase shift theorem.[5,32]

The center of gravity of a powder spectrum of quadrupolar nuclei is not observed at the isotropic chemical shift δ_{CS}, but is displaced from it by δ_{QIS} in the F_2 dimension and by δ_{QIS}^{ISO} in the F_1^{ISO} dimension of the sheared 2D spectrum. These quadrupolar induced shifts are given in ppm by the following expressions:

$$\delta_{QIS}(S, C_Q, \eta) = -\frac{3}{10}[4S(S+1)-3]\left\{\frac{SOQE}{4S(2S-1)\nu_0}\right\}^2 \cdot 10^6 \quad [3]$$

and

$$\delta_{QIS}^{ISO}(S, C_Q, \eta) = -\frac{10}{17}\delta_{QIS}(S, C_Q, \eta) \quad [4]$$

where $SOQE = C_Q(1+\eta^2/3)^{1/2}$ defines the second-order quadrupolar effect parameter.

Thus, the center of gravity of different species with the same δ_{CS} but different SOQE parameters are located along the so-called QIS direction with a slope $\xi = -10/17$. Similarly, species experiencing the same quadrupolar interactions, but different isotropic chemical shifts, will be located along a direction parallel to the CS axis with a slope of 1 (Fig. 2a).

Note that the slopes of the CS and QIS axes do not depend on the coherence p chosen to perform the MQMAS experiment. Consequently, the 3QMAS and 5QMAS spectra of ^{27}Al should be similar in the fast spinning speed limit. However, experimental resolution between different sites can be enhanced in 5QMAS.[15-18]

The CP MQMAS Experiment

The main difference between the MQMAS and the CP MQMAS experiments is in the preparation period. In both the techniques, the preparation pulses are used to create and maximize the $\rho_{+p/2,-p/2}$ and $\rho_{-p/2,+p/2}$ elements of the density matrix of the observed spins S. In order to use the CP MQMAS experiment for spectral editing, it is essential to achieve efficient coherence transfer that proceeds via the I spins and to eliminate the effect of direct S

polarization. While a direct excitation of the multiple-quantum coherences can be conceivably achieved via cross polarization,[33,34] in this work we chose a more approachable coherence transfer scheme $(0 \rightarrow \pm 1 \rightarrow 0 \rightarrow \pm 3 \rightarrow 0 \rightarrow -1)$. The implementation of this scheme becomes relatively easy with the use of a pair of z-filters.[7] Below, we describe the experimental setup of the CP MQMAS experiment, which relies upon maximizing the transfer of S magnetization obtained using $I \rightarrow S$ cross polarization process through the selected coherence pathways.

It is well known that cross polarization of quadrupolar spins is difficult, even with conventional MAS. The major difficulty, which was systematically studied by A. Vega,[33,34] is in maintaining spin-locking of the central transition coherence under MAS. The spin-locking efficiency can be expressed in terms of the parameter

$$\alpha = \nu_{IS}^2 / (\nu_Q \nu_r) \qquad [5]$$

where ν_{IS} is the amplitude of the radio-frequency (rf) field for the S nuclei being cross polarized, $\nu_Q = 3C_Q / 2S(2S-1)$ is the quadrupolar frequency, and ν_r is the sample spinning frequency. Vega showed that the spin-locking efficiency can be preserved under adiabatic $(\alpha >> 1)$ or rapid passage conditions $(\alpha << 1)$, but becomes nearly impossible in the intermediate regime $(\alpha \approx 0.4)$. Later work by Sun et al.[30] showed that the most efficient locking is achieved when $\alpha << 1$, which is satisfied using a high spinning speed and a weak rf field during the CP transfer. Furthermore, care must be taken to avoid the resonance condition $\nu_r = k\nu_{IS}$.[30]

The first part of the CP MQMAS experiment, referred to as CP in Figure 1c, relies upon optimization of the CP conditions to maximize the $(\pm 1/2, \mp 1/2)$ elements of the density

matrix of the S spins in the same manner as in conventional CP/MAS. These coherences will, however, include contributions from the direct polarization of the S spins; thus it is important to apply a 180° phase alternation to the I spin excitation pulse.[34] For quadrupolar nuclei, a highly selective excitation of the $(\pm 1/2, \mp 1/2)$ coherences can be obtained using the Hartmann-Hahn matching condition

$$\nu_{II} \approx (S + 1/2)\nu_{IS} \pm n\nu_r \qquad [6]$$

where ν_{II} is the strength of the rf field applied to the I spins.

The second part of the sequence, the multiple-quantum evolution and excitation period, is designed to transfer the single-quantum coherences $(\pm 1/2, \mp 1/2)$ created via CP to 3Q coherences $(\pm 3/2, \mp 3/2)$ with the highest possible efficiency. This can be efficiently achieved using a z-filter followed by a strong rf pulse (see Figure 1c). The z-filter consists of a 'soft' (selective) 90° pulse which, in this case, stores the CP magnetization along the direction of the magnetic field, $\vec{B}_0$. After a suitable delay introduced in order to dephase the undesired components of the density matrix, the $(\pm 3/2, \mp 3/2)$ coherences are produced in the standard way by a strong rf pulse which is followed by the evolution period.

The last part of the sequence, referred to as the observation period, transfers the $(\pm 3/2, \mp 3/2)$ coherences to an observable single-quantum (-1/2,+1/2) coherence. Again, a z-filter scheme is used to symmetrise the coherence transfer pathway, composed of a strong rf pulse that transfers the triple-quantum coherences to zero-quantum coherences followed by a selective 90° pulse to create observable signal.[7] The phase cycling used in this experiment consisted of 24 phases, as shown in Table 1. Two-dimensional spectra were acquired using

the hypercomplex method to obtain phase separation. Other phase cycling methods, including a 48-phase scheme (with 2-phase cycling of ϕ_1) and a 96-phase scheme (CYCLOPS-based), did not result in further improvement of the observed spectra. Since the optimization of the CP process and of the multiple-quantum coherence transfer can be done independently, we found the setup of the CP MQMAS experiment to be relatively straightforward. We note, however, that the spin dynamics of the cross polarization process is very complex. In particular, the experiment is sensitive to the resonance offset of both I and S spins and the spinning speed, especially when very low rf power is used for cross polarization.

Experimental

The ^{27}Al 3QMAS spectra without and with ^{1}H dipolar decoupling (DD) were taken at 9.4T on a Bruker DSX 400 spectrometer using the pulse sequences depicted in Figures 1a and 1b, respectively. The spectrometer was equipped with a newly developed, 4 mm MAS probehead capable of producing a rf field of 300 kHz, and a MAS speed of 14 kHz. The CP MQMAS experiment (Fig. 1c) was performed on a Bruker ASX 400 using a 4 mm CP/MAS probehead working with a maximum ν_{1S} rf field of 60 kHz. The Hartmann-Hahn condition was established with a rf field ν_{1S} = 15 kHz, under a MAS speed of 12 kHz. Proton decoupling during the evolution and acquisition times was performed using ν_{1I} = 80 kHz.

The $AlPO_4$-11 sample was provided by the Laboratoire des Materiaux Mineraux (ENSCM, Mulhouse, France). It was calcined and fully rehydrated prior to the NMR experiment.

Results and Discussion

The result of a standard 3QMAS experiment performed with the hydrated $AlPO_4$-11 sample is shown in Figure 2a. Five distinct aluminum resonances are observed in the isotropic projection of the two-dimensional spectrum, which is similar to the results obtained previously using DOR.[27,28] It is known that $AlPO_4$-11 has a structure consisting of AlO_4^- and PO_4^+ tetrahedra connected by bridging oxygen atoms to form a one-dimensional, 10-membered ring pore system.[35,36] The dehydrated $AlPO_4$-11 has three distinct crystallographic Al sites with 2:2:1 occurrences, while the fully rehydrated form undergoes changes in symmetry leading to five different crystallographic Al sites[25] of equal population. In general, polar molecules such as water or ammonia can coordinate to a part of the framework aluminum sites in aluminophosphates, and change the aluminum's symmetry form tetrahedral to five- or six-coordinated. The NMR results show that in $AlPO_4$-11, only four- and six-coordinated species were observed following hydration.[27]

We note here that for a given rf field, the integrated intensities of the 2D MQMAS resonances strongly depend on the value of the quadrupolar coupling constant and on the crystallite orientation (α,β).[2] Therefore, strong lineshape distortions are possible, especially when the rf field is not large compared to the MAS linewidth. Although the use of high power MAS probes capable of producing an rf field of up to 300 kHz (such as one designed for this work) can reduce these experimental distortions, reliable spectral information can only be obtained with the aid of numerical methods. One possible strategy relies upon the MQMAS experiment to obtain high-resolution and isotropic chemical shifts and using it for

the simulation of one-dimensional, quantitative MAS spectra to obtain quadrupolar parameters and relative intensities.[11] We have recently developed another numerical method that allows quantitative determination of the distributions of δ_{CS} and SOQE parameters directly from the 2D MQMAS spectrum. The strategy utilizes a leapfrog method to compute the evolution of the density matrix under the rf power and spinning conditions used in the experiment.[37] Applying this method to the spectrum of Figure 2a leads to the canonical representation[37-39] displayed in Figure 2b. The relative intensities found using this method are in remarkably good agreement with the expected 1:1:1:1:1 Al site population in $AlPO_4$-11.[25]

The interaction of the water molecules wit the aluminophosphate framework can be probed using the 3QMAS experiment with high power (80 kHz) proton dipolar decoupling (DDMQMAS), according to the sequence shown in Figure 1b. The resulting spectrum (Fig. 3) shows that the resonances from the octahedral site Al_2 and the tetrahedral sites Al_1, Al_3, and Al_4 were visibly narrowed in the MQ isotropic dimension. On the other hand, ^1H decoupling has negligible effect on resolution in the anisotropic dimension. This effect is not surprising, because the apparent strength of the dipolar interaction in the isotropic dimension of the 3QMAS spectrum is enhanced by a factor of 3, and the resulting broadening cannot be completely removed by MAS at 14 kHz.

The CP MQMAS spectrum of the same sample is shown in Figure 4. Clearly, this technique provides more direct information about the interaction of various aluminum sites with water. It is evident that the Al_2 resonance exhibits the strongest CP intensity, while the Al_5 resonance is essentially absent. these observations are consistent with the previous ^{27}Al

DOR NMR and x-ray diffraction data of Peeters et al.[27,28] and the CPDOR results of Wu et al.,[29] which also suggested that the Al_2 and Al_5 sites are the most and the least susceptible to hydration, respectively. Furthermore, the CP MQMAS technique shows that among the remaining tetrahedral sites, Al_4 interacts with water more strongly than Al_1 and Al_3. This observation can be explained if one considers that a water molecule strongly bound to Al_2 by its oxygen atom may also have one of its hydrogens bound with one of the oxygens near Al_4.[28] In this case, the Al_1 and Al_3 atoms are the next nearest neighbors, and thus are also cross polarized, yet less efficiently. In this scenario, the Al5 is too far away to interact with this water molecule.

When we compare the CP MQMAS experiment with CPDOR,[30] we note that both methods require comparable experimental time. While the tetrahedral Al sites in hydrated $AlPO_4$-11 yielded a slightly better S/N ratio in a shorter time by CPDOR (25,000 accumulations versus a total of 38,400 in 2D CP MQMAS), the CP MQMAS method provided a better quality spectrum for the octahedral site. This effect is due to the presence of several overlapping spinning sidebands in the CPDOR spectrum, which is the common shortcoming of the DOR technique. The CP MQMAS method demands, however, the usage of a very wide range of rf fields which, in turn, requires high-quality linear power amplifiers.

Conclusions

The above results demonstrate that the ^{1}H-^{27}Al CP MQMAS method offers a tool for spectral editing of high-resolution MQMAS spectra of ^{27}Al based on the strength of the dipolar coupling with hydrogen. Further extension of this work will include (i) other pairs of nuclei, e.g., ^{31}P-^{27}Al CP MQMAS, and (ii) heteronuclear correlation experiments, similar to those performed earlier with MAS and DAS.[40,41]

Acknowledgments

C.F., L.D., and J.-P.A. are grateful to Bruker (S. Steuernagel, F. Engelke, H. Forster) for technical help and to Dr. L. Delmotte for providing the $AlPO_4$-11 sample. This research was supported, in part, by the U.S. Department of Energy, Office of Basic Energy Sciences, Division of Chemical Sciences, under Contract W-7405-Eng-82.

References

1. Frydman, L.; Harwood, J.S. *J. Am. Chem. Soc.* **1995**, *117*, 5367.

2. Amoureux, J-P.; Fernandez, C.; Frydman, L. *Chem. Phys. Letters* **1996**, *259*, 347.

3. Wu, G.; Rovnyank, D.; Sun, B.; Griffin, R.G. *Chem. Phys. Letters* **1995**, *249*, 210.

4. Fernandez, C.; Amoureux, J-P. *Solid State NMR* **1996**, *5*, 315.

5. Massiot, D.; Touzo, B.; Trumeau, D.; Coutures, J.P.; Virlet, J.; Florian P.; Grandinetti, P.J. *Solid State NMR* **1996**, *6*, 73.

6. Medek, A.; Harwood, J. S.; Frydman, L. *J. Am. Chem. Soc.* **1995**, *247*, 12779.

7. Amoureux, J-P.; Fernandez, C.; Steuernagel, S. *J. Magn. Reson.* **1996,** *A123*, 116.

8. Brown, S.P.; Heyes S.J.; Winperis, S. *J. Magn. Reson.* **1996**, *A119*, 280.

9. Massiot, D. *J. Magn. Reson.* **1996**, *A122*, 240.

10. Massiot, D.; Conanec, R.; Feldmann, W.; Marchand, R.; Laurent, Y. *Inorganic Chemistry* **1996**, *35*, 4957.

11. Hwang, S. J.; Fernandez, C.; Amoureux, J-P.; Cho, J.; Martin, S.W.; Pruski, M. *Solid State NMR*, in press.

12. Fernandez, C.; Amoureux, J-P.; Chezeau, J.M.; Delmotte, L.; Kessler, H. *Microporous Materials* **1996**, *6*, 331.

13. Rocha, J.; Esculas, A.; Fernandez, C.; Amoureux, J-P. *J. Phys. Chem.* **1996**, *100*, 17889.

14. Baltisberger, J.H.; Xu, Z.; Stebbins, J.F.; Wang S.H.; Pines, A. *J. Am. Chem. Soc.* **1996**, *118*, 7209.

15. Fernandez, C.; Amoureux, J-P. *Chem. Phys. Letters* **1995**, *242*, 449.

16. Fernandez, C.; Amoureux, J-P.; Delmotte, L.; Kessler, H. *Microporous Materials* **1996**, *6*, 125.

17. Rocha, J.; Lin, Z.; Fernandez, C.; Amoureux, J-P. *Chem. Commun.* **1996**, 2513.

18. Sarv, P.; Fernandez, C.; Amoureux, J-P.; Keskinen, K. *J. Phys. Chem.*, **1996**, 100, 19223.

19. Llor A.; Virlet, J. *Chem. Phys. Letters* **1988**, *152*, 248.

20. Samoson, A.; Lippmaa E.; Pines, A. *Mol. Phys.*, **1988**, *65*, 1013.

21. Mueller, K.T.; Sun, B.Q.; Chingas, G.C.; Zwanziger, J.W.; Terao T.; Pines, A. *J. Magn. Reson.* **1990**, *86*, 470.

22. Hartmann S. R.; Hahn, E. L. *Phys. Rev.* **1964**, *128*, 2042.

23. Pines, A.; Gibby M.G.; Waugh, J.S. *J. Chem. Phys.* **1973**, *59*, 569.

24. Pruski, M.; Lang, D. P.; Fernandez C.; Amoureux, J-P. *Solid State NMR*, in press.

25. Khouzami, R.; Coudurier, G.; Lefebvre, F.; Vedrine J.C.; Mentzen, B. *Zeolites* **1990**, *10*, 183.

26. Barrie, P.J.; Smith M.E.; Klinowski, J. *Chem. Phys. Letters* **1991**, *180*, 6.

27. Peeters, M.P.J.; De Haan, J.W.; Van de Ven, L. J. M.; Van Hooff, J.H.C. *J. Phys. Chem.* **1993**, *97*, 5363.

28. Peeters, M.P.J.; Van de Ven, L.J.M. ; De Haan, J. W.; Van Hooff, J.H.C. *J. Phys. Chem.* **1993**, *97*, 8254.

29. Wu, Y.; Lewis, D.; Frye, J.S.; Palmer A.R.; Wind, R.A. *J. Magn. Reson.* **1993**, *100*, 425.

30. Sun, W.; Stephen, J.T.; Potter L.D.; Wu, Y. *J. Magn. Reson.* **1995**, *116*, 181.

31. Amoureux, J-P. *Solid State NMR* **1993**, *2*, 83.

32. Ernst, R. R.; Bodenhausen G.; Wokaun A. *Principles of Nuclear Magnetic Resonance in One and Two Dimensions*; Clarendon Press: Oxford, 1987.

33. Vega, A.J. *J. Magn. Reson.* **1992**, *96*, 50.

34. Vega, A.J. *Solid State NMR*, **1992**, *1*, 17.

35. Bennett, J. M.; Richardson, J. W.; Pluth J J.; Smith, J. V. *Zeolites* **1987**, 7, 160.

36. Rechardson, J. W.; Pluth, J. J.; Smith, J. V. *Acta Crystallogr.* **1988**, B44, 367.

37. Fernandez, C.; Delevoye, L.; Amoureux, J. P.; Sarv, P. Manuscript in preparation.

38. Zwanziger, J. W. *Solid State NMR* **1994**, 3, 219.

39. Samoson, A. *J. Magn. Reson.* **1996**, A121, 209.

40. Fyfe, C. A.; Wong-Moon, K. C.; Huang, Y.; Grondey, H.; Mueller, K. T. *J.Phys. Chem.* **1995**, 99, 8707.

41. Jarvie, T. P.; Wenslow, R. M.; Mueller, K. T. *J. Am. Chem. Soc.* **1995**, 117, 570.

Figure Captions

Figure 1: Schematic diagram of (a) MQMAS with z-filter, (b) DDMQMAS, and (c) CP MQMAS pulse sequences.

Figure 2: (a) 3QMAS spectrum of the calcined and fully rehydrated $AlPO_4$-11; Rf field amplitude $\nu_{1S} = 300$ kHz, spinning speed $\nu_r = 14$ kHz, dwell time in t_1 set to $1/\nu_r$, number of accumulations per row of data: 24, delay for T_1 relaxation : 500 ms, number of t_1 increments: 128, approximate acquisition time: 30 min. The resonances are labeled by following the assignment given by Peeters et al.[27] (b) Canonical representation obtained from inversion of the 3QMAS spectrum.

Figure 3: ^1H DD3QMAS spectrum of the calcined and fully rehydrated $AlPO_4$-11. Experimental conditions are identical to those of Figure 2.

Figure 4: ^1H-^{27}Al CP 3QMAS spectrum of the calcined and fully rehydrated $AlPO_4$-11: Rf field amplitude during the 500 μs CP contact time $\nu_{1S} = 5$ kHz, rf field amplitude during 'soft' pulses $\nu_{1S} = 10$ kHz, rf field amplitude during 'hard' pulses $\nu_{1S} = 60$ kHz, spinning speed $\nu_r = 12$ kHz, dwell time in t1 set to $1/\nu_r$, number of accumulations per row of data: 1200, delay for T_1 relaxation : 1.5 s, approximate experimental time 16 h.

Table 1. Basic phase-cycling scheme used in the ^{1}H-^{27}Al CP3QMAS experiment. The phase notation is consistent with the scheme of Figure 1c.

$\pi/2$	x	x	-x	-x
CP (I)	y	y	y	y
CP (S)	0°	0°	0°	0°
ϕ_1	90°	90°	90°	90°
ϕ_2	0°	0°	0°	0°
ϕ_3	0°, 60°, 120°, 180°, 240°, 300°	0°, 60°, 120°, 180°, 240°, 300°	0°, 60°, 120°, 180°, 240°, 300°	0°, 60°, 120°, 180°, 240°, 300°
ϕ_4	0°	180°	0°	180°
ϕ_{rec}	0°, 180°, 0°, 180°, 0°, 180°	0°, 180°, 0°, 180°, 0°, 180°	0°, 180°, 0°, 180°, 0°, 180°	0°, 180°, 0°, 180°, 0°, 180°

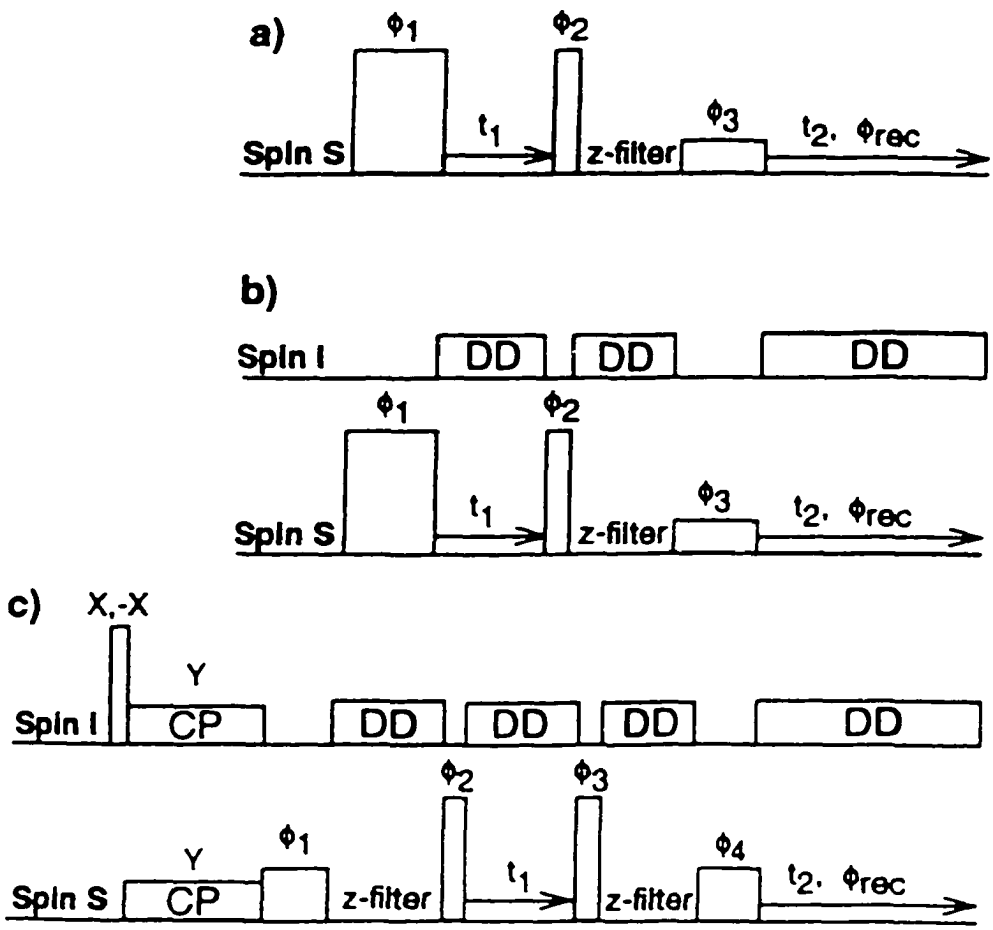
a)
ϕ_1
ϕ_2
Spin S
t_1
z-filter
ϕ_3
t_2, ϕ_{rec}
b)
Spin I
DD
DD
DD
ϕ_1
ϕ_2
Spin S
t_1
z-filter
ϕ_3
t_2, ϕ_{rec}
c)
X,-X
Y
Spin I
CP
DD
DD
DD
DD
ϕ_2
ϕ_3
Y
ϕ_1
Spin S
CP
z-filter
t_1
z-filter
ϕ_4
t_2, ϕ_{rec}

Figure 1.

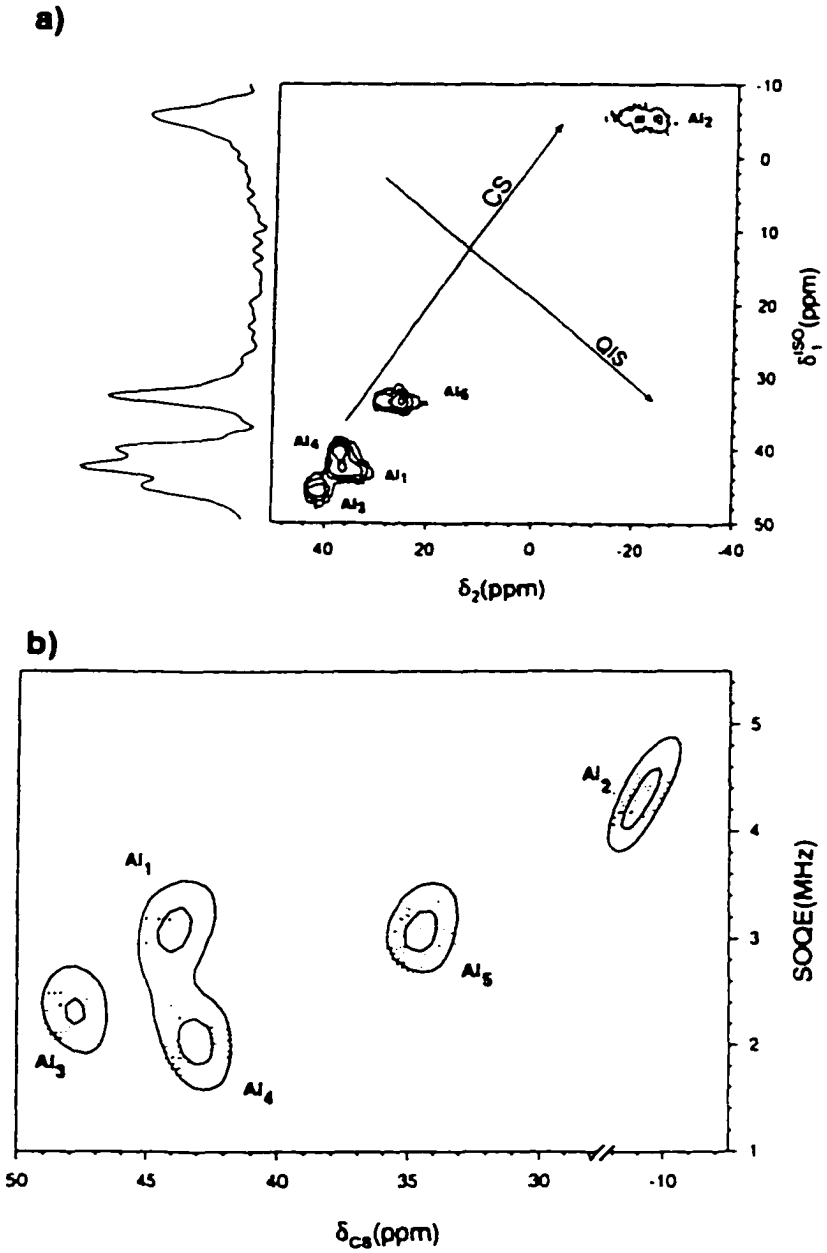
a)
CS
QIS
Al2
Al6
Al4
Al1
Al3
-10
0
10
20
30
40
50
40
20
0
-20
-40
δ2(ppm)
δ1ISO(ppm)
b)
Al2
Al1
Al5
Al3
Al4
5
4
3
2
1
50
45
40
35
30
-10
δCS(ppm)
SOQE(MHz)

Figure 2.

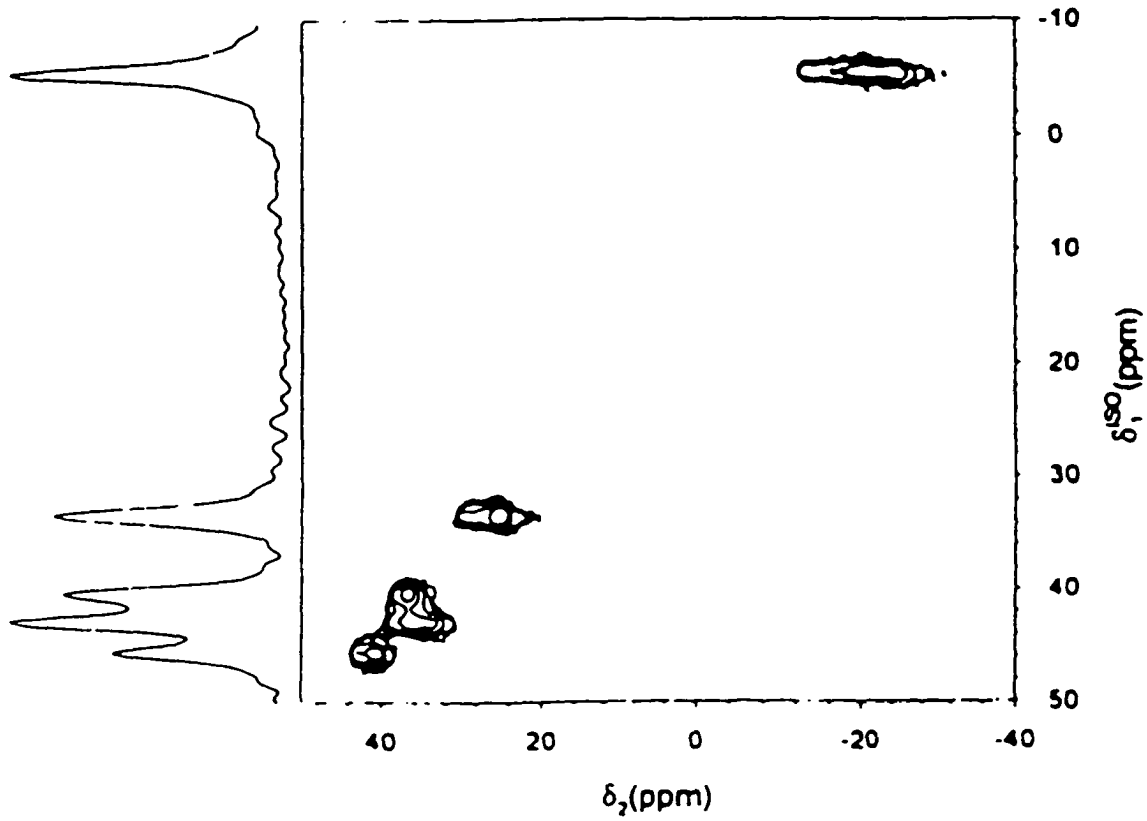

Figure 3.

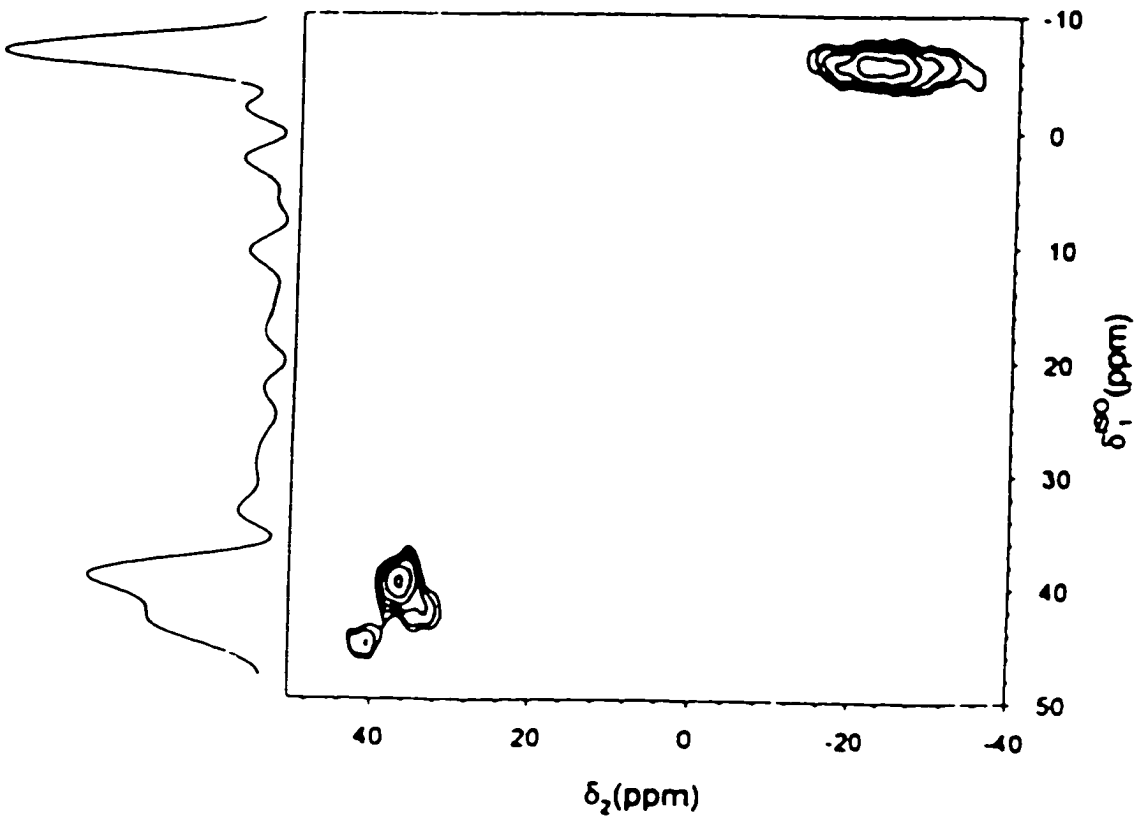

Figure 4.

GENERAL CONCLUSIONS

In this dissertation, an experiment was presented that combines the techniques of multiple-quantum magic-angle spinning (MQMAS) and cross-polarization (CP) between spin-1/2 and half-integer quadrupolar spin nuclei. Such spin systems are of technological interest as they often serve an essential role in the areas of catalysts, glasses, and semiconductors (79-84). The technique developed, referred to as CP MQMAS, allows the coordination of the spin-1/2 nuclei within a quadrupole system to be accurately determined. Knowing the structure, nature and extent of disorder in a system is often fundamental to understanding its chemical and physical attributes.. While the CP MQMAS technique is technically straightforward, it does require very specific programming in order to limit the possible coherence pathways. To this end, the radio-frequency (rf) pulse sequences, and necessary phase-cycling required are developed and examined. A novel approach of incorporating a 'z-filter' between the two techniques allowed us to optimize our new procedure, CP MQMAS, as two unique experiments prior to their coupling. The CP MQMAS technique provides additional insight into the structure of a sample, and proves to be a valuable tool for spectral editing. Experimental details concerning the manipulations necessary to produce and detect multiple-quantum (MQ) NMR spectra of half-integer quadrupole nuclei are presented. Such factors include, [1] high rf power, [2] very fast MAS, and [3] digital phase shifting capabilities on all channels and the receiver.

Additionally in this report, the matching conditions and spin dynamics of CP from a spin-1/2 nucleus to the central transition of a quadrupolar nucleus during magic-angle spinning

(MAS) are examined. An interesting discovery regarding the CP process is that it operates most efficiently using very low rf field strengths, which is markedly different than conventional CP. When low rf field strengths are used, however, no longer is the Hartmann-Hahn matching rf power necessarily the lone dominant perturbation as the Hamiltonians from the second-order quadrupolar interaction, MAS speed and carrier frequency offset(s) cannot be treated as negligible interactions. Thus, as the MQMAS technique requires the usage of very high rf field strengths, and CP very low rf field strengths, it can be seen that the CP MQMAS technique demands the usage of high-quality linear power amplifiers.

In our initial test of the CP MQMAS technique we were able to show, for the first time, how solid-state NMR could be used on a complex quadrupolar system to determine the coordination of fluorine within an $AlPO_4$ chabazite-like lattice. The steps of the experiment are, sequentially, (i) $^{19}F \rightarrow {}^{27}Al$ single-quantum cross-polarization, (ii) utilization of a z-filter to bring the CP magnetization back to zero-quantum, (iii) execution of a symmetric MQMAS experiment on the 'stored' magnetization followed by another z-filter, e.g., 'p' = $0 \rightarrow \pm 3 \rightarrow 0$, and (iv) observation of the multiple-quantum modulated signal in the p = -1 single-quantum state, e.g. $p = 0 \rightarrow -1$. The fluorinated $AlPO_4$ aluminophosphate material studied contains three equally populated crystallographic sites for aluminum: one site octahedrally coordinated to four oxygen and two fluorine atoms, and two sites that are tetrahedrally coordinated as AlO_4. The results displayed that while all three aluminum environments were resolved in the MQMAS experiment, only that Al coordinated to the fluorine atoms was resolved in the CP MQMAS experiment.

Our second CP MQMAS experiment was accomplished using $^{1}H \rightarrow {}^{27}Al$ cross-polarization to the study of a calcined and fully rehydrated $AlPO_4$-11 aluminophosphate sample. Similar experimental procedures and coherence pathways were utilized, e.g., $p = 0 \rightarrow \pm1 \rightarrow 0 \rightarrow \pm3 \rightarrow 0 \rightarrow -1$. This sample is a more complicated spin system as it involves five unique aluminum environments that can only be resolved if MQMAS NMR is employed. The application of the CP MQMAS technique allows one to determine the positions of the water molecules within the $AlPO_4$-11 framework.

REFERENCES CITED

1. B.C. Gerstein and C.R. Dybowski, "Transient Techniques in NMR of Solids", Academic Press, NewYork, 1985.

2. A. Abragam, "Principles of Nuclear Magnetism", Oxford University Press, 1961.

3. U. Haeberlen, "High Resolution NMR in Solids: Selective Averaging ", Academic Press, New York, 1976.

4. M. Mehring, "The Principles of High Resolution NMR in Solids", Springer-Verlag, Berlin, 1983.

5. E.R. Andrew, A. Bradbury and R.G. Eades, Nature (London), 182, 1659, 1958.

6. J.S. Waugh, L.M. Huber and U. Haeberlen, Phys. Lett., 20, 180, 1968.

7. A. Pines, M.G. Gibby and J.S. Waugh, J. Chem. Phys., 56, 1776, 1972.

8. B.C. Gerstein, R.G. Pembelton, R.C. Wilson and L.M. Ryan, J. Chem. Phys., 66, 362, 1977.

9. C.P. Slichter, "Principles of Magnetic Resonance", 3rd edn., Springer-Verlag, Berlin, 1990.

10. M.H. Cohen and F. Rief, in 'Solid State Physics', eds. F. Seitz and D. Turnbull, Academic Press, NewYork, 1958, Vol. 5 p. 321.

11. M.M. Maricq and J.S. Waugh, J. Chem. Phys., 70, 3300, 1979

12. J.-P. Amoureux, C. Fernandez and L. Frydman, Chem. Phys. Lett. 259, 347, 1996.

13. J.P. Amoureux, Solid State NMR, 2, 83, 1993.

14. S. Ganapathy, S. Schramm and E. Oldfield, J. Chem. Phys., 77, 4360, 1982.

15. A. Llor and J. Virlet, Chem. Phys. Lett., 152, 248, 1988.

16. `A. Samoson, E. Lipmaa and A. Pines, Mol. Phys., 65, 1013, 1988.

17. H.J. Jakobsen, in 'Encyclopedia of Magnetic Resonance', eds. D.M. Grant and R.K. Harris, John Wiley & Sons, Chichester, 1996, Vol. 4, p. 2370.

18. J. Skibsted, N.C. Nielsen, H. Bildsoe and H.J. Jakobsen, J. Magn. Reson., 95, 88, 1991.

19. A. Samoson, E. Kundla and E. Lipmaa, J. Magn. Reson., 49, 350, 1982.

20. E. Kundla, A. Samoson and E. Lipmaa, Chem. Phys. Lett., 83, 229, 1981.

21. A. Samoson and E. Lipmaa, J. Magn. Reson., 79, 255, 1988.

22. A.P.M. Kentgens, J. Magn. Reson., A 104, 302, 1993.

23. N.C. Nielsen, H. Blidsoe and H.J. Jakobsen, J. Magn. Reson., 97, 149, 1992.

24. A. Samosan, Chem. Phys. Lett., 119, 29, 1985.

25. C. Jager, J. Magn. Reson., 99, 353, 1992.

26. C. Fernandez, P. Bodart and J. P. Amoureux, Solid State NMR, 3, 79, 1994.

27. C. Marichal, J.Y. Kempf, B. Maigret and J. Hirschinger, Solid State NMR, in press.

28. Y. Dumazy, C. Fernandes, J.P. Amoureux and L. Delmotte, J. Chem. Phys., 92, 1855, 1995.

29. D. Massiot, V. Montouillout, F. Fayon, P. Florian and C. Bessada, Chem. Phys. Lett., 272, 295, 1997.

30. F. Lefebvre, J.P. Amoureux, C. Fernandez and E.G. Derouane, J. Chem. Phys., 86, 6070, 1987.

31. C.S. Blackwill and R.L. Patton, J. Phys. Chem., 88, 6135, 1984.

32. A.J. Vega, J. Magn. Reson., 96, 50, 1992.

33. A.J. Vega, Solid State NMR, 1, 17, 1992

34. T. Guillion and J. Schaefer, J. Magn. Reson., 81, 196, 1989.

35. C.A. Fyfe, K.T. Mueller, H. Grodney and K.C. Wong-Moon, Chem. Phys. Lett., 199, 198, 1992.

36. A.W. Hing, S. Vega and J. Schaefer, J. Magn. Reson., 96, 205, 1992.

37. E.R.H. van Eck, R. Jansen, W.E.J.r. Maas and W.S.Veeman, Chem Phys Lett., 174, 428, 1990.

38. C.P. Grey and A.J. Vega, J. Am. Chem. Soc.,117, 8232, 1995.

39. T. Guillion, J. Magn. Reson., A 117, 326, 1995.

40. J.R. Sachleben, V. Frydman and L. Frydman, J. Am. Chem. Soc., 118, 9786, 1996.

41. K.T. Mueller, B.Q. Sun, G.C. Chingas, J.W. Zwanziger, T. Terao and A. Pines, J. Magn. Reson., 86, 470, 1990.

42. B.F. Chmelka, K.T. Mueller, A. Pines, J. Stebbins, Y. Wu and J. Zwanziger, Nature, 339, 42, 1989.

43. L. Frydman and J.S. Harwood, J. Am. Chem. Soc., 117, 5367, 1995.

44. A. Medek, J.S. Harwood and L. Frydman, J. Am. Chem. Soc., 117, 12779, 1995.

45. D. Freude and J. Haase, in 'NMR Basic Principles and Progress', eds. P. Diehl, E. Fluck, and R. Kosfeld, Springer-Verlag, Berlin, 1993, Vol. 29, p. 1.

46. W. Sun, J.T. Stephen, L.D. Potter and Y. Wu, J. Magn. Reson. A, 116, 181, 1995.

47. R.R. Ernst, G. Bodenhausen, and A. Wokaun, *Principles of Nuclear Magnetic Resonance in One and Two Dimensions*, Clarendon Press, Oxford, U. K., 1987.

48. M. Munowitz, *Coherence and NMR*, John Wiley & Sons, New York, 1988.

49. I.I. Rabi, N.F. Ramsey, and J. Schwinger, Rev. Mod. Phys., 26, 167, 1954.

50. E. van Eck, *Solid State NMRDouble Resonance Experiments for Spectral Assignment and Structure Elucidation*, Ph.D. Thesis Katholieke Universiteit, Nijmegen 1995.

51. I.J. Lowe, Phys. Rev. Lett., 2, 285, 1959.

52. M.E. Rose, "Elementary Theory of Angular Momentum", John Wiley &Sons, Inc. London, 1957.

53. E.R. Andrew, in 'Encyclopedia of Magnetic Resonance', eds. D.M. Grant and R.K. Harris, John Wiley & Sons, Chichester, 1996, Vol. 5, p. 2900.

54. L.R. Sarles and R.M. Cotts, Phys. Rev., 111, 853, 1958.

55. W.K. Rhim, D.D. Elleman and R.W. Vaughn, J. Chem. Phys., 59, 3470, 1973.

56. D.P. Burum and W.K. Rhim, J. Chem. Phys., 71,944, 1979.

57. S.R. Hartmann and E. L. Hahn, Phys. Rev., 128, 2042, 1962.

58. A. Pines, M.G. Gibby, and J.S. Waugh, J. Chem. Phys., 56, 1176, 1972.

59. J. Schaefer and E.O. Stejskal, J. Am. Chem. Soc., 98, 1031, 1976.

60. S. Hediger, B.H. Meier, and R.R. Ernst, Chem. Phys. Lett., 213, 627, 1993.

61. R.G. Bryant, S. Ganapathy, and S.D. Kennedy, J. Magn. Reson., 72, 376, 1987.

62. T.H. Walter, G.L. Turner, and E. Oldfield, J. Magn. Reson. 76, 106, 1988.

63. J. Klinowski, Chem Rev., 91, 1459, 1991.

64. R.K. Harris and G.J. Nesbitt, J. Magn. Reson., 78, 245, 1988.

65. H.D. Morris and P.D. Ellis, J. Am. Chem. Soc., 111, 6044, 1989.

66. S. Vega, Phys. Rev. A, 23, 3152, 1981.

67. A. Wokaun and R.R. Ernst, J. Chem. Phys., 67, 1752, 1977.

68. S. Vega and Y. Naor, J. Chem. Phys., 75, 75, 1981.

69. A. Samoson and E. Lippmaa, Phys. Rev. B, 28, 6567, 1988.

70. A.P.M. Kentgens, J.J.M. lemmens, F.M.M. Geurts and W.S. Veeman, J. Magn. Reson., 71, 62, 1987.

71. M. Goldman, *Quantum Description of High-Resolution NMR in Liquids*, Clarendon Press, Oxford U. K,,1988

72. J. Keeler, in Multinuclear Magnetic Resonance in Liquids and Solids - Chemical Applications, eds. P. Granger and R.K. Harris, Kluwer Academic Publishers, 1990, p. 130.

73. J. Jeener, Ampere International Summer School, Basko Polje, Yugoslavia 1971.

74. W.P. Aue, E. Bartholdi, and R.R. Ernst, J. chem. Phys. 64, 2229, 1976.

75. S. Vega, J. Chem. Phys., 75, 75, 1978.

76. N.C. Nielsen, H. Bildsoe and H.J. Jakobsen, Chem. Phys. Lett., 191, 205, 1992.

77. J.-P. Amoureux, C. Fernandez and S. Steuernagel, J. Magn. Reson., A123, 116, 1996.

78. S.P. Brown, S.J. Heyes and S. Wimperis, J. Magn. Reson., A119, 280, 1996.

79. C. Fernandez and J.-P. Amoureux, Chem. Phys. Lett., 242, 449, 1995.

80. C. Fernandez, J.-P. Amoureux, L. Delmotte and H. Kessler, Micropor. Mater., 6, 125, 1996.

81. C. Fernandez, J.-P. Amoureux, J.M. Chezeau, L. Delmotte and H. Kessler, Micropor. Mater., 6, 331, 1996.

82. S.-J. Hwang, C. Fernandez, J.-P. Amoureux, J. Cho, S.W. Martin and M. Pruski, Solid State Nucl. Magn. Reson., in press.

83. C. Fernandez and J.-P. Amoureux, Solid State Nucl. Magn. Reson., 6, 315, 1996.

84. D. Massiot, B. Touzo, D. Trumeau, J.P. Coutures, J. Virlet, P. Florian and P.J. Grandinetti, Solid State Nucl. Magn. Reson., 6, 73, 1996.

85. U. Haeberlen and J.S. Waugh, Phys. Rev., 175, 453, 1968.

86. M. Pruski, D.P. Lang, C. Fernandez and J.-P. Amoureux, Solid State Nucl. Magn. Reson., 7, 327, 1997.

87. E.W. Wooten, K.T. Mueller and A. Pines, Acc. Chem. Res., Vol. 25, 5, 210, 1992.

88. .R. Jannsen, W.S. Veeman, J. Chem. Soc., Faraday Trans. 84, 3747, 1988.

89. J.-P. Amoureux, C. Fernandez and Y. Dumazy, J. Chim. Phys, 2, 1939, 1995.

90. J.-P. Amoureux, D.P. Lang, M.Pruski, C. Fernandez, J. Magn. Reson. 130, 544 1998.

91. L. Marinelli and L. Frydman, Chem. Phys. Lett., 275, 188,1997.

92. A.G. Redfield and S.D. Kunz, J. Magn. Reson. 19, 250, `1975.

93. D.J. States, R.A. Haberkorn and D.J. Ruben, J. Magn. Reson., 48, 286, 1982.

94. D. Marion and K. Wuhrich, Biochem, Biophys. Res. Commun., 113, 967, 1983.

95. A.P.M. Kentgens, Two-dimensional Solid State NMR, Ph.D. Thesis, Department of Chemistry, De Katholieke Universitei te Nijmegen, Belguim 1987.

96. S.P. Brown and S. Wimperis, J. Magn. Reson., 128, 42, 1997.

97. F. Engelke, in 'Encyclopedia of Magnetic Resonance', eds. D.M. Grant and R.K. Harris, John Wiley & Sons, Chichester, 1996, Vol. 3, p. 1529.

98. P.J. Grandinetti, J.H. Baltisinger, A. Llor, Y.K. Lee, U. Werner, M.A. Eastman, and A. Pines, J. Magn. Reson., A103, 72, 1993.

99. R. Benn and H. Gunter, Agnew. Chem., 95,381, 1983.

ACKNOWLEDGEMENTS

It would be virtually impossible to thank everyone who has had a hand in getting me to this point. The individuals listed are but a sampling of the people to whom I owe a tremendous debt of gratitude.

First of all, I would like to thank my research director, Dr. Marek Pruski. His guidance, patience, and instruction have been of immeasurable value to me during my tenure (not ten years) here. Dr. Pruski has a very high standard for research in the lab, and I have always been proud to be able to work for/with him. His ability to motivate and demand without saying a word inspires me daily to be a better scientist.

I also thank Dr. Bernard C. Gerstein for allowing me to join his NMR research group just as he was about to retire. Dr Gerstein's love for science and desire to better understand and explain the unknown are contagious. My appreciation for working under his and Dr. Pruski's tutelage grows deeper as time passes. They are my mentors and my friends.

I also owe a very special thanks to Dr. Sonjong Hwang. He introduced me to the area of multiple-quantum NMR, helped refine my abilities at the spectrometer, let me ride on his coattail when I needed it, and cut me loose when I had to be let go. Sonjong is my good friend first, and a gifted colleague second.

I also owe a great debt to Dr. Christian Fernandez and Dr. Jean-Paul Amoureux. Our collaboration with them has advanced our multiple-quantum research exponentially. Their understanding and love for the topic are laudable. Without their input, this thesis would not exist.

I would like to express my thanks to the members of the Thiel group. I consider them my surrogate group and am thankful for being allowed into their ranks. Hopefully they will realize someday that beauty is only skin deep, and what matters is on the inside. So when you're ready to make the transition from the 'surface' over to NMR and see the whole picture, I'll be there to hold the door for you. (Ha, ha??)

Thanks to the people who paid the bills: Ames Laboratory with the US Department of Energy, Office of Basic Energy Sciences, Division of Chemical Sciences, under contract W-7405-Eng-82

I also wish to thank my family and especially my parents for their support and love throughout these years. I cannot tell you how much you all mean to me. You are my anchor.

Finally, I would like to thank God for bringing me here, surrounding me with incredible people, giving me tremendous opportunities, and making it all possible. Thanks for making the cross I carry so bearable, and help me to always choose to do Your will.

IMAGE EVALUATION
TEST TARGET (QA-3)

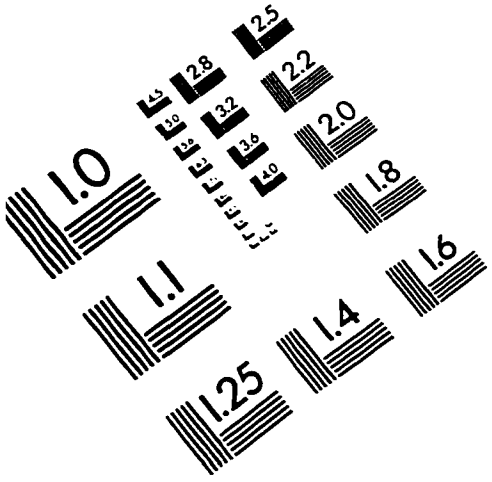

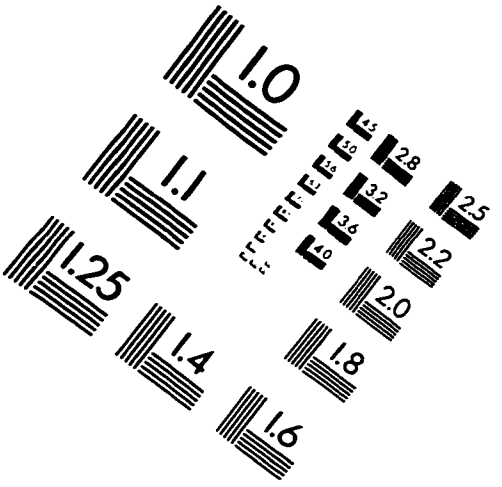

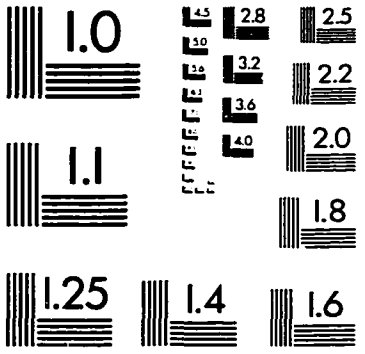

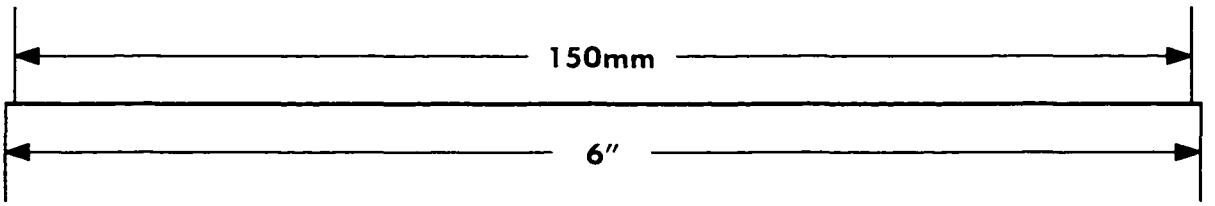

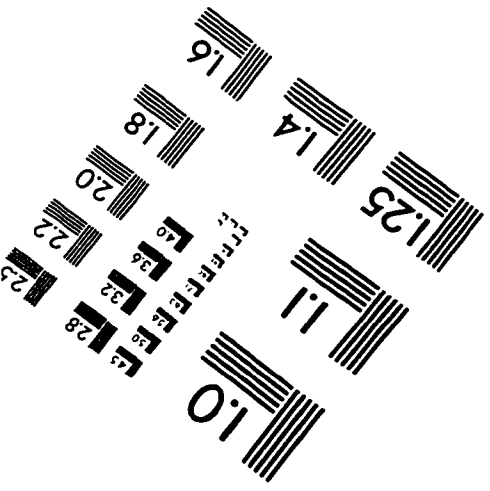

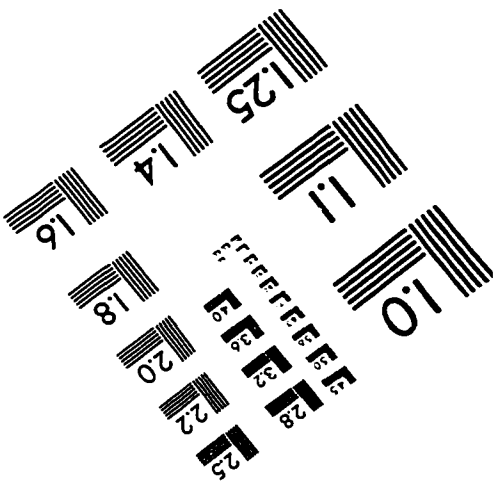

APPLIED IMAGE, Inc
1653 East Main Street
Rochester, NY 14609 USA
Phone: 716/482-0300
Fax: 716/288-5989